

AD 653069

OPTICAL INHOMOGENEITIES IN PUMPED LASERS

VOLUME I

FINAL REPORT
MAY 1967

Contract No. Nonr 4875(00)
ARPA Order No. 306
Project No. 4730

Office of Naval Research
Washington, D.C.

Prepared by

Dr. Charles J. Koester, Project Manager
Research Division
American Optical Company
Southbridge, Massachusetts

Reproduction in whole or part is permitted by the
U. S. Government.

Distribution of this document is unlimited.

ARCHIVE COPY

OPTICAL INHOMOGENEITIES
IN
PUMPED LASERS
VOLUME I

FINAL REPORT
MAY 1967

ARPA Order No. 306
Project 4730
Contract No. Nonr 4875(00)

Prepared by

Research Division
American Optical Company
Southbridge, Massachusetts

Dr. Charles J. Koester, Project Manager

This research is part of Project DEFENDER under the joint sponsorship of the Advanced Research Projects Agency, Department of Defense, and the Office of Naval Research.

Reproduction in whole or in part is permitted by the United States Government.

Distribution of this document is unlimited.

FOREWORD

This report was prepared by the Research Division of American Optical Company, Southbridge, Massachusetts, under contract Nonr 4875(00), Optical Inhomogeneities in Pumped Lasers, for the Office of Naval Research, Washington, D. C., as part of Project Defender.

Principal contributors to this report were C. J. Koester, Introduction, Review of Previous Work and overall compilation of material; E. Snitzer, Thermally Stable Cavities; L. W. Smith, Calculation of Temperature Profile; S. M. Bergmann, Effect of the Laser Field on the Index of Refraction of the Laser Rod; and D.W. Cuff, End Region Stress Analysis.

The report is published in two volumes, the first unclassified and the second, a classified supplement entitled Optical Inhomogeneities in Pumped Lasers(U), Volume II.

ABSTRACT

This report delineates efforts expended during the one year period of contract Nonr 4875(00), entitled Optical Inhomogeneities in Pumped Lasers, which required an analysis in depth of thermal distortion of wavefronts in large laser rods and discs. Two approaches for elimination of this distortion were considered: (1) Establishment of a uniform temperature throughout the laser during pumping and (2) Development of athermal glass parameters. Elements of both approaches were found necessary to solve the problem. In separate sections of the report detailed treatments are given to Thermally Stable Cavities, Temperature Profile Calculations, the Effect of the Laser Field on Index of Refraction of the Laser Rod, and finally an Analysis of End Region Stress.

A classified supplement published separately as Volume II of this report completes the research findings under this project.

CONTENTS		PAGE
VOLUME I		
1.	Introduction and Summary	1
2.	Review of Previous Work	4
3.	Thermally Stable Cavities	5
4.	Calculation of Temperature Profile	16
4.1	Assumptions and Definitions	16
4.2	Derivation of the Basic Equation	18
4.3	Polished Laser Rod with Cladding and Isotropic Radiation without Multiple Reflections	22
4.4	Spectral Radiance of the Source	34
4.5	Refractive Indices and Absorption Coefficients	35
4.6	Check Calculations	38
4.7	Results	42
5.	Effects of the Laser Field on the Index of Refraction of the Laser Rod	49
5.1	Introduction	49
5.2	Maxwell Stress, Kerr Effect and Electrostrictive Effect	49
5.3	Photoelastic Effect	66
5.4	Discussion	70
5.5	Summary	70
6.	End Region Stress Analysis	71
	References	97

ILLUSTRATIONS

FIGURE		PAGE
1	Schematic of a laser with a rectifying Faraday rotator.	10
2	Use of a 90° optically-active rotator to rectify stress-birefringence in a laser system.	10
3	Geometry of the laser rod, cladding layers and source.	22
4	Typical ray diagram for rays in the xy-plane of a polished cylinder of laser material.	26
5	Typical surface areas of a rod which can irradiate point P.	27
6	Spectral radiance N_0 from the FX-47A flashtube in watts per millimicron-cm ² -steradian divided by the number λ of kilojoules of energy in an 0.75 millisecond rectangular input voltage pulse to the flashtube.	36
7	The absorption coefficient α_1 in mm ⁻¹ of AO 3835 laser glass.	37
8	The absorption coefficient α in mm ⁻¹ of (a) AO type EOD-830 samarium glass, (b) distilled water and (c) a representative sample of pyrex #7740 glass.	39
9	The distribution of energy which causes heating in an unclad rod of laser glass with $\rho R \approx 2 \times 10^{20}$ ions/cm ² for Corning 0580 glass and AO 3835 glass.	41
10	The distribution of heat production Γ vs. the normalized radius in rods of AO 3835 laser glass with $RF = 1.9$.	43
11	Temperature rise in a laser rod of neodymium glass with $RF = 1.9$ when pumped by a xenon flashtube.	46

ILLUSTRATIONS (cont'd)

FIGURE		PAGE
12	Comparison between the temperature distribution found experimentally by Welling and Bickart and the distribution calculated from the same rod with similar pumping but neglecting internal reflections.	48
13	Maxwell stress boundary nomenclature.	56
14	Notation used by Adams and Williamson.	67
15	Point designations for relaxation grid.	76
16	Comparison of computer solution and plane strain theory for a cross section about 1.6 diameters from end of rod.	84
17	Comparison of computer solution and plane stress theory for midsection of disc.	85
18	Stress-strain distribution at 0.477 cm radial distance from axis in a 2.54 cm diameter 0835 laser rod with 11.1°C temperature difference between center and edge.	86
19	Stress-strain distribution at 0.954 cm radial distance from axis in a 2.54 cm diameter 0835 laser rod with 11.1°C temperature difference between center and edge.	87
20	Optical path variation for the end region of a 2.54 cm AO 3835 neodymium glass rod.	89
21	Experimental results for heat production in AO 3835 glass laser rods pumped in a close-coupled silver reflector wrap.	91
22	Relative temperature change, end face distortion, and optical path variation for the end region of a 2.54 cm diameter x 1 meter 3835 glass laser rod pumped at 23.5 kj input.	93
23	Relative temperature change, end face distortion, and optical path variation for the end region of an 0.9 cm diameter 3835 glass laser rod pumped at 153 j/cm ² .	95

1. INTRODUCTION and SUMMARY

The effort in this program has been a theoretical analysis of the thermal distortion problem in glass laser rods and discs. The goal has been not merely analysis, however, but rather a more thorough understanding of the causes of wavefront distortion, leading to more effective athermalization.

There are two basic approaches to eliminating wavefront distortion due to thermal effects: (1) Attempt to establish a uniform temperature throughout the laser during pumping. (2) Develop a glass in which the change in length due to thermal expansion is balanced by the (negative) change in index with temperature. The nature of the cavity must be considered in arriving at the glass specifications. Also the effects of stress-birefringence must be removed or reduced to an acceptable level.

For a number of reasons it is desirable to use both approaches. The first method by itself will probably not be sufficient since it does not appear likely that a perfectly uniform temperature distribution can be achieved. The second approach is capable in principle of athermalizing an infinitely long rod or a thin disc. But in any rod of finite length there will be end effects which depend on the magnitude of the thermal gradient. A method for calculating these end effects is developed in Section 6.

Relatively uniform temperature distribution is desirable for another reason. Both temperature distribution and distribution of inversion are governed by the distribution of absorbed pumping energy. If the latter is uniform, both of the former will be uniform or very nearly so. And uniformity of inversion is important to give a laser emission wavefront which is uniform in intensity as well as in phase. Uniformity in intensity is desirable to give the best possible far-field pattern, and to reduce non-linear effects in the laser material which in turn will cause phase distortion of the wavefront. The import of non-linear effects is discussed in Section 5.

The calculation of temperature profiles in Section 4 was originally intended to (a) develop the method of calculation, (b) show the magnitude of the temperature gradient problem, and (c) provide input data for the end effect calculations. The calculations showed that an unclad rod of radius R has a minimum temperature at or near the surface, with a substantial gradient in the vicinity of R/n , where n is the index of refraction

Water or glass clad rods have a maximum temperature just inside the surface (at 0.8 R and 0.9 R respectively). The most uniform temperature distribution is for the glass clad rod. An unexpected result of this work was that it pointed out a potential method of improving substantially the pumping uniformity. That method is to use a cladding of about the same index as that of the laser core glass but of a thickness somewhat less than that chosen for the example (0.5 R). Additional calculations would be necessary to establish the optimum cladding thickness and index.

In Section 5 the formalism is developed to allow calculation of index of refraction changes due to electrostriction, photoelastic effect, and Kerr effect when the laser field distribution in the rod is given.

End-effect studies were undertaken to establish under what conditions they are negligible, and what form they take when they are non-negligible. In a typical rod configuration, the end effects become important only when the glass has been athermalized. However, in this important case the end effects can result in several wavelengths distortion of the laser wavefront. For the unclad rod, the steep temperature gradient gives rise to an optical path distortion which is not proportional to the temperature distribution. Therefore, it does not lend itself to correction by adjusting the glass parameters. However, in cases where the temperature gradient is less severe, the calculations indicate that it would be possible to compensate for the end effects almost completely by proper choice of glass parameters. Specifically, a value of α'_n is chosen which is slightly less negative than the value α_n which is optimum for an infinitely long rod. The difference, $\alpha_n - \alpha'_n$, depends, of course, on the length of the rod.

Analysis of the limiting cases of infinitely long rods (plane strain) and thin discs (plane stress) provides insight into the athermalization problem. The analyses of Quelle¹ and of Snitzer² have been utilized to compute the thermal coefficient of optical path for several laser glasses in rod and immersed disc cavities. This work confirms that athermalization is possible for a long rod, but that it is substantially easier to accomplish for an immersed disc. The required indices for the immersion fluid are close to that of water. Methods for removing the stress-birefringence effect are given.

In all phases of the work it was assumed that essentially a single pumping pulse is to be used. That is, no considerations of cooling time, or steady state temperature distribution were

entertained. The analyses would therefore apply to cases in which the temperature of the rod returns to ambient before the next shot and in which the absorption of pumping light provides the only heating effect during the time period of interest, namely the period of lasing.

2. REVIEW OF PREVIOUS WORK

The problem of calculating optical path differences induced by temperature gradients in pumped laser rods has been formulated by Snitzer.³ The analysis indicated that there exist relations between the thermal expansion coefficient α , the index coefficient α_n , and other glass constants which will yield an athermalized condition. In the writing of a proposal⁴ for the present contract this formulation was improved and extended to include both radial and tangential polarization.

Walsh⁵ has studied the photoelastic effects in a long laser rod under the conditions of constant heat production and surface cooling. He has also estimated the distortion of the end face under these conditions. Quelle⁶ has formulated the calculation of optical path differences and has shown mathematically that the athermalization condition can be independent of the temperature distribution if a Pockels type glass is assumed. This glass has a zero value of the stress-optical coefficient.

The distribution of pumping energy in a laser rod has been considered by several authors. McKenna⁷ treated the case of an absorbing rod with a transparent sheath, the absorption coefficient having a given value for all pumping wavelengths. Sooy and Stitch⁸ also formulated the calculation of the pumping energy distribution in a laser rod with three-dimensional pumping. Skinner⁹ studied experimentally the distribution of pumping energy in a ruby rod using two-dimensional pumping. Borrelli and Charters¹⁰ calculated pumping energy distribution in unclad glass laser rods.

Experimental determination of thermal distortion of wavefronts has been accomplished by Welling, Bickert, and Andresen.¹¹ They have shown that single flashlamp pumping produces large asymmetries in the optical path, but that four flashlamp pumping produces a nearly circular symmetric pattern. They have shown experimentally the development of the path differences during the pumping pulse, and their dependence on diameter, doping concentration, and surface finish for ruby and neodymium glass.

Work at American Optical Company under contract Nonr 3835(00) has been directed in part toward the attainment of a high optical quality glass which will also have a low thermal distortion coefficient. Data for a few of the glasses studied under this contract are included in Section 3.

3. THERMALLY STABLE CAVITIES

A serious problem in large lasers is the thermal distortion of the cavity due to non-uniform pumping. Glasses can be made with an index of refraction variation of no greater than $\pm 0.8 \times 10^{-6}$ across a 25 mm section, which corresponds to 2.5 fringes in a one meter length rod. However, when the glass is pumped, substantial changes in index of refraction occur.¹¹ The result is the frequently encountered frustration in attempting to produce a high intensity, diffraction limited beam. Just above threshold narrow beams are possible, but for increased pumping the thermal distortions increase. More energy is produced but in a wider beam. If a strong mode selection scheme¹² is used the output rapidly levels off with increased pumping.

In order to obtain diffraction limited beams from the end of laser devices the cavity should not distort while pumping. If the temperature of the laser rod changes uniformly during pumping there will not be any distortion of the wavefront within the rod. By placing flashtubes symmetrically about the rod a non-uniform azimuthal heating can be avoided. A non-uniform radial heating of the rod is almost inevitable if reasonable rod sizes and neodymium concentrations are used. However, by the proper design of the total resonant cavity and with properly chosen glass compositions one can minimize the effect of non-uniform heating.

Due to pumping of the laser a temperature gradient is produced from the center to the edge. The distortion of the cavity arises because of three factors. The change in temperature leads to an elongation because of the finite coefficient of expansion of the glass. With a change in temperature the index of refraction in general also changes. Finally, thermal gradients within the glass produce stresses which result in both a change in index of refraction and birefringence. The expansion coefficient α and the thermal coefficient of index α_n are functions only of the temperature of the point under consideration, but the indices of refraction produced by the strains are dependent on the shape of the rod and the details of the temperature distribution.

For glasses, the index of refraction always increases in compression, but α_n can be positive or negative. The effects producing the index change can be made to cancel each other by an appropriate glass composition with the correct negative value of α_n .

There are two geometries with cylindrical symmetry that are of interest for which approximate solutions can readily be calculated. One is the long rod in which the length L is much larger than the radius a . The other is the disc configuration with $L \ll a$. The description is similar to that given by F. W. Quelle.¹

For the solid rod, the total optical pathlength $P_r(r)$ for a typical ray parallel to the axis and displaced a distance r from the center and with its plane of polarization in the radial direction is given by

$$P_r(r) = nL \left\{ 1 + \left[\alpha_n T - \left(\frac{p}{v} (\epsilon_z + \epsilon_\theta) + \frac{q}{v} \epsilon_r \right) \right] \right\}, \quad (1)$$

where T is the difference in temperature between the center and a point at a distance r from the center. A cylindrical coordinate system is used with the z direction along the rod axis. The ϵ 's are the strains. The quantities q/v and p/v are the strain-optic coefficients which relate the change in index of refraction to the strains in the directions parallel and perpendicular, respectively to the plane of polarization of the light. The notation is the same as used by Morey.^{1,3} The corresponding expression for tangential polarization is

$$P_\theta(r) = nL \left\{ 1 + \left[\alpha_n T - \left(\frac{p}{v} (\epsilon_z + \epsilon_r) + \frac{q}{v} \epsilon_\theta \right) \right] \right\}. \quad (2)$$

For an isotropic medium the principal strains are related to the stresses σ by^{1,4}

$$\begin{aligned} \epsilon_r &= E^{-1} [\sigma_r - s(\sigma_\theta + \sigma_z)] \\ \epsilon_\theta &= E^{-1} [\sigma_\theta - s(\sigma_r + \sigma_z)] \\ \epsilon_z &= E^{-1} [\sigma_z - s(\sigma_r + \sigma_\theta)] \end{aligned} \quad (3)$$

where E is Young's modulus and s Poisson's ratio.

For a long rod with the end effects neglected, the problem is one of plane strain. If the ends are free of traction so that they can move in response to the heating, the condition that applies is^{1,5}

$$\sigma_z = \sigma_r + \sigma_\theta. \quad (4)$$

In arriving at Eqs. (7) - (9) for the long rod end effects were neglected. If the rod is very long the end effects are small and the problem reasonably approximates that of plane strain. On the other hand, if the length is much shorter than the diameter the "end effects" predominate and the constraints correspond fairly closely to plane stress.

Analysis of these equations shows that there are three ways to achieve simultaneously athermalization and freedom from stress-birefringence. They are:

(1) Athermalize for either the radial or tangential polarization. This would also require mode selection so that only one polarization is able to oscillate.

Conditions	Long Rod	Disc
Radial Polarization	$\Delta P_r(r) = 0$ (Eq. 7)	$\Delta P_r'(r) = 0$ (Eq. 12)
Tangential Polarization	$\Delta P_\theta(r) = 0$ (Eq. 8)	$\Delta P_\theta'(r) = 0$ (Eq. 13)

(15)

(2) Obtain a Pockels glass, i.e., a glass for which $p = q$. Quelle¹ has shown that the condition for athermalization for a long rod is then

$$n \left\{ \alpha_n + \frac{2\alpha}{1-s} (1-2s) \frac{p}{v} \right\} = 0 \quad (\text{rod}) \quad (16)$$

This expression is obtained from Quelle's equation by noting that

$$B_1 = \frac{n}{E} \left[(1-s) \frac{p}{v} - s \frac{q}{v} \right] = \frac{n}{E} (1-2s) \frac{p}{v} \quad \text{for a Pockels glass.}$$

Equation (16) can also be derived from Eq. (9) by letting $p = q$.

For the stacked disc case, athermalization of a Pockels glass dictates the following relation

$$\alpha_n + \alpha \left\{ \frac{n-n'}{n} (1+s) + \frac{p}{v} (1-2s) \right\} = 0 \quad (\text{disc}) \quad (17)$$

(3) Rectify the stress-birefringence effect.

On passing once through a rod with a radial temperature distribution a phase difference $[\Delta P_r(r) - \Delta P_\theta(r)]$ is introduced between the radially polarized ray and the tangentially polarized ray at the same radius r . Now if the two rays pass through a 90°

polarization rotator, the radially polarized ray will be converted to tangential polarization, and vice-versa. If the two rays are passed again through the same rod, or through an identical rod, the phase difference between the two rays will be removed.

For a single rod the cavity is shown in Fig. 1. On each round trip, the light passes through the 45° Faraday rotator, thereby undergoing a 90° rotation of the plane of polarization.

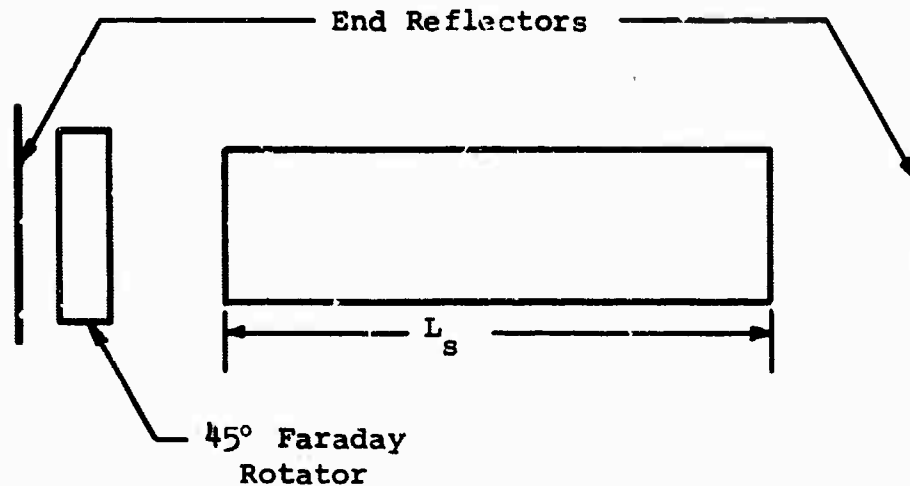


Figure 1. Schematic of a laser with a rectifying Faraday rotator.

Another method can be used when there are two identical laser rods in either an oscillator or an amplifier. It employs a 90° optical rotator between the two laser rods, as shown in Fig. 2.

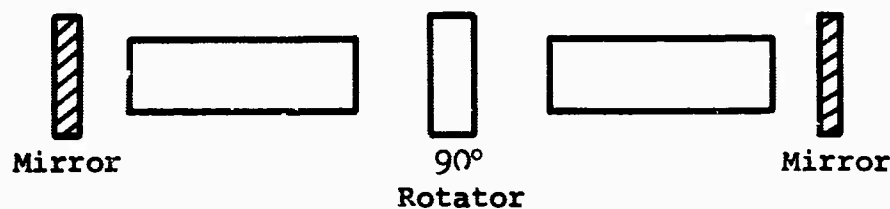


Figure 2. Use of a 90° optically-active rotator to rectify stress-birefringence in a laser system.

This rotator can be of crystalline quartz, for example, cut perpendicular to the optic axis. Other optically active materials can be used.

In these cases, the birefringence is automatically cancelled, and the athermalization conditions are found from Eqs. (9) and (14):

$$\text{rod} \quad \alpha_n + \frac{\alpha}{1-s} \left[\frac{3-5s}{2} \frac{p}{v} - \frac{1-3s}{2} \frac{q}{v} \right] = 0 \quad (18)$$

$$\text{disc} \quad \alpha_n + \alpha \left[\frac{n-n'}{n} (1+s) + \frac{1-3s}{2} \frac{p}{v} + \frac{1-s}{2} \frac{q}{v} \right] = 0 \quad (19)$$

The possibilities of achieving athermalization by these approaches are explored more fully below. At this point some general comments are in order.

The conditions for athermalization, Eqs. (15) - (19), can be regarded as requirements on the ratio α_n/α . This is because s , p/v , and q/v do not depend strongly on the glass composition. Bridgman¹⁸ measured several glasses, including lead silicates, borosilicates, and alkali earth silicates and found that Poisson's ratios, varies from 0.19 to 0.26. Furthermore, the quantities in braces in Eqs. (7) - (9), (12) - (14) are not sensitively dependent on s . A number of references on the strain-optic coefficients are given in Morey.¹⁴ Pockel's measurements indicate $p/v = q/v = 0.42$ for a silicate glass containing approximately 75% by weight of PbO .¹⁷ For the more common glasses the strain-optic coefficients are smaller; q/v decreases more rapidly than p/v . A light flint silicate (54.3 wt % SiO_2 , 33 PbO , 1.5 B_2O_3 , 3 Na_2O , 8 K_2O) has the values $p/v = 0.306$ and $q/v = 0.213$, and for a borosilicate crown (68.2 wt % SiO_2 , 10 B_2O_3 , 10 Na_2O , 9.5 K_2O , 2 Al_2O_3) $p/v = 0.269$ and $q/v = 0.147$.¹⁹

To obtain an estimate of the required α_n to reduce the various ΔP 's to zero, typical values for the parameters are assumed. The strain-optic parameters are taken as $p/v = 0.3$ and $q/v = 0.21$ and Poisson's ratio as $s = 0.25$. A linear expansion coefficient of $\alpha = 10^{-5}/^\circ\text{C}$ is assumed. If the temperature T varies as r^p , then $R/T = 1/(p+2)$; for a quadratic dependence of T on the radius, $p = 2$ and $R/T = 1/4$. With these values for the parameters the braces in Eqs. (7) - (9) are equal to zero for $\alpha_n = -42 \times 10^{-7}/^\circ\text{C}$, $-34 \times 10^{-7}/^\circ\text{C}$, $-38 \times 10^{-7}/^\circ\text{C}$, respectively. For the stacked discs in air, the braces in Eqs. (12) - (14) are equal to zero for $\alpha_n = -56 \times 10^{-7}/^\circ\text{C}$, $-50 \times 10^{-7}/^\circ\text{C}$, $-53 \times 10^{-7}/^\circ\text{C}$, respectively. Note that the required values of α_n are all negative. In most silicate glasses α_n is not sufficiently negative to satisfy any of the conditions for zero pathlength difference between rays at the center and at the edge of the rod. If the temperature is higher at the edge than at the center the pathlength is greater

at the edge and furthermore, radially polarized light propagates more slowly than light with tangential polarization. If the quantity in the braces is not zero but is reduced to $10^{-7}/^{\circ}\text{C}$, three fringes at $1.06\ \mu$ would appear between center and edge if $T = 10^{\circ}\text{C}$ for a meter length rod made from a material of index $n = 1.5$.

At low temperature α_n is negative because expansion of the glass reduces the amount of polarizable material per unit volume; at high temperatures, this is more than offset by the increased thermal population of higher vibration states of the ground electronic state, which appears to shift the fundamental absorption band of the material to longer wavelengths and thereby increases the index of refraction. The temperature T_0 at which $\alpha_n = 0$ is a function of the glass composition and wavelength. It increases with increasing λ through the visible and near infrared. For most glasses T_0 is less than room temperature at $1\ \mu$, but it is above 300°K for a few, such as the silicates with high barium content.

Molby²⁰ and Prod'homme²¹ give values of α_n in the visible region of the spectrum for various glasses. Measurements were made in this laboratory at $1.06\ \mu$ by using a thin plate of the glass to be measured as the end reflector of the laser cavity.²² Laser emission occurs at those wavelengths at which the plate thickness and index give an odd number of $\lambda/4$. From the shift in wavelength of the laser lines as a function of temperature of the plate and by independent measurements of the expansion coefficient of the glass, α_n was determined. Room temperature values for various glasses were between $29 \times 10^{-7}/^{\circ}\text{C}$ and $-41 \times 10^{-7}/^{\circ}\text{C}$. The positive values were for dense lead silicates. High barium content silicates gave the large negative values.

DISCUSSION

(1) Athermalization for radial or tangential polarization. It is necessary to mode-select a field distribution with axially symmetric polarization, such as the TE_{01} or TM_{01} modes. For example, the TM_{01} mode is radially polarized in the electric vector.

Its intensity distribution is $[J_1(u_1 r/a)]^2$, where u_1 is the first zero at 3.832 of the first order Bessel function J_1 . If one end of the glass rod is cut in the form of a Brewster angle cone and a plane mirror placed at the proper distance, all the modes except the family TM_{0m} ($m \geq 1$) are discriminated against. The lowest order member of this family could then be selected

by other means, such as a limited aperture at the other reflector. This approach has several disadvantages. First, it is difficult to make cones with good optical quality. Second, the beam is a hollow cone, which is not as desirable as the lowest order HE_{11} mode. Third, the requirements on α_n depend on R and hence on the details of the temperature distribution.

(2) For a Pockels glass, the required values of α_n are calculated as follows. In Eqs. (16) and (17) substitute the typical values $p/v = 0.45$ and $s = .25$, $n = 1.5$, $n' = 1.33$.

$$\text{From Eq. (16): } \alpha_n = -0.6 \alpha \quad (\text{rod})$$

$$\text{From Eq. (17): } \alpha_n = -.367 \alpha \quad (\text{disc})$$

The original Pockels glass has a positive value of α_n . Efforts to obtain a negative value for α_n in a Pockels glass will be reported under contract Nonr 3835(00).

(3) Rectification of the stress-birefringence effect appears at present to be the most promising approach. In order to compare the various possible configurations and available glasses, the thermal coefficient of optical pathlength, $\frac{1}{nL} \frac{d\bar{P}}{dT}$, is

tabulated below. The expressions are obtained from Eqs. (9) and (14) for the average optical path \bar{P} , for the rod and immersed disc cases respectively.

$$\begin{aligned} (\text{rod}) \quad \frac{1}{nL} \frac{d\bar{P}}{dT} &= \alpha_n + \frac{\alpha}{2(1-s)} \left[(3-5s) \frac{p}{v} + (1-3s) \frac{q}{v} \right] \\ &\approx \alpha_n + .383 \alpha \end{aligned}$$

$$\begin{aligned} (\text{disc}) \quad \frac{1}{nL} \frac{d\bar{P}'}{dT} &= \alpha_n + \alpha \left[\frac{n-n'}{n} (1-s) + \frac{1-3s}{2} \frac{p}{v} + \frac{1-s}{2} \frac{q}{v} \right] \\ &\approx \alpha_n + \alpha \left[\frac{n-n'}{n} .125 + .1162 \right] \end{aligned}$$

TABLE I

Thermal Coefficient of Optical Path for a Long Rod, a Disc in Air ($n' = 1.0$), and a Disc Immersed in Water ($n' = 1.33$)

Glass	n	α	α_n	(Rod)	(Disc)	
				$\frac{1}{nL} \frac{d\bar{P}}{dT}$	$\frac{1}{nL} \frac{d\bar{P}'}{dT}$	$\frac{1}{nL} \frac{d\bar{P}'}{dT}$
					$n'=1.0$	$n'=1.33$
3835*	1.51	$103 \cdot 10^{-7}$	$-22 \cdot 10^{-7}$	$11.8 \cdot 10^{-7}$	$14 \cdot 10^{-7}$	$-3.1 \cdot 10^{-7}$
1203	1.52	122	-28	18.8	38.2	5.3
1204	1.57	119	-41	4.6	26.8	-4.4
1263	1.52	112	-32	11	28.8	-1.5
1270	1.53	114	-36	7.7	26.3	-4.2
1276	1.62	111	-28	14.6	38	9.9

Constants used: $\frac{p}{v} = .30$, $\frac{q}{v} = .21$, $s = .25$, except 3835.

*For 3835 $\frac{p}{v} = .25$, $\frac{q}{v} = .13$, $s = .225$.

Several conclusions are apparent from this table. For the rod case a number of experimental glasses have a lower thermal coefficient than the standard 3835 glass, number 1204 being a factor of three lower. The disc in air is considerably poorer than the long rod. But the disc immersed in water ($n' = 1.33$) appears very attractive. The value $-1.5 \cdot 10^{-7}$ for glass number 1263 means that for a 1 m length of glass, $nL = 1.52$ m, a 20°C temperature differential between center and edge of the discs would produce an optical path difference of

$$\Delta\bar{P}' = nL \frac{d\bar{P}'}{dT} \Delta T = 1.52 \cdot 10^3 (-1.5 \cdot 10^{-7})$$

$$= -2.28 \cdot 10^{-4} \text{ cm} = -228 \text{ nm}$$

Furthermore, the numbers in the last column of the table suggest that it may be possible to find either (a) a glass composition which is precisely athermalized

$$\left(\frac{1}{nL} \frac{d\bar{P}'}{dT} = 0 \right)$$

for the water immersed disc, or (b) an immersion liquid with index n' which will exactly athermalize an existing glass.

For the constants p/v , q/v , and s assumed above, the required index n_L for the immersion liquid is given by

$$n' = n \left[1 + \frac{\alpha_n + .116 \alpha}{1.25 \alpha} \right]$$

The required indices for a few glasses are listed below

Glass	Required n'
3835	1.36
1203	1.38
1263	1.34

The required indices are all within the range attainable with water solutions of inorganic materials.

The general expression of the required index, n' , is obtained from Eq. (19)

$$(Disc) \quad n' = \frac{n}{1+s} \left[\frac{\alpha_n}{\alpha} + 1+s + \frac{1-3s}{2} \frac{p}{v} + \frac{1-s}{2} \frac{q}{v} \right] \quad (20)$$

The assumption has been made that the index of the liquid does not change during the pumping cycle. Since there can be very little heat transfer to the liquid from the laser glass during the pumping period, the assumption implies that the liquid is non-absorbing to the pumping radiation.

4. CALCULATION OF TEMPERATURE PROFILE

4.1 ASSUMPTIONS AND DEFINITIONS

If we may assume that the temperature change in a laser rod is proportional to the radiation-heating effect due to absorption of radiation from an adjacent flashtube, then the calculation of the temperature profile reduces to a calculation of the distribution of heat production in the laser rod. Measurements on a large variety of glasses^{23,24} show that the specific heat capacity is sufficiently constant over the temperature range expected in the laser rod so that the proportionality may be assumed.

A computer program has been written by which to calculate the distribution of heat production. The program, written in the FORTRAN language for an IBM-360-30 computer, allows for three different homogeneous media to be placed between the flashtube and the laser rod. Cylindrical geometry and polished refracting surfaces are assumed so that all boundaries between media form infinitely long, cylindrical surfaces concentric with an infinitely long, cylindrical laser rod.

It is assumed that the flashtube and reflector produce a volume of isotropic radiation (called the source hereafter) in which the rod and its cladding media are immersed (no variation with azimuth about the axis of the laser rod).

It is assumed that the radiant flux absorbed by the laser material goes entirely into exciting the doping ions to higher energy levels plus a radiative decay that produces the laser radiation.

It is assumed that each photon absorbed results in a photon of laser radiation while the rest of the energy is converted to heat.

It is assumed that the transmissivity of the laser material does not change significantly with change in population density of excited states of any of the ions.

The effect of multiple passes of the radiation through the rod are not taken into account by the program. This effect will be most noticeable for weakly absorbing and/or small diameter rods. Partial compensation for this omission can be carried out by (1) increasing the overall energy content of the flashtube

spectrum and (2) adjusting the spectrum to favor the weakly absorbed wavelengths.

Parameters which affect the distribution of heat production, and which must be specified at the time the program is run, are: (1) the product of the radius times the absorption coefficient for the laser rod and each layer of its cladding, (2) the refractive indices of the media, and (3) the spectral radiance of the source.

The following definitions have been adapted from references (25, 26):

radiant flux - rate of transfer of radiant energy, specified in watts

radiant transmittance - or simply transmittance, is the ratio W_t/W_i of the transmitted flux to the incident radiant flux.

spectral transmittance - the radiant transmittance evaluated for a particular wavelength of the incident energy.

transmissivity - the value of the internal transmittance for a unit thickness of a non-diffusing substance.

absorption coefficient - Bouguer's law states that equal layers of an imperfectly transparent material will absorb equal fractions of the radiant energy entering them. If this law is applied to infinitesimal layers and if the losses are integrated, the radiant flux at a distance x within the medium, for the wavelength λ , is found to be $P = P_0 \exp(-\alpha(\lambda)x)$, where P_0 is the flux of wavelength λ entering the first layer and $\alpha(\lambda)$ is the absorption coefficient.

radiance - the radiant flux or power per unit solid-angle-in-the-direction-of-a-ray per unit projected-area-perpendicular-to-the-ray. It has the same value at any point along the ray within an isotropic medium in the absence of losses by absorption, scattering, or reflection. (It may be helpful to note that radiance is analogous to the photometric quantity luminance or photometric brightness).

spectral radiance - the radiance at any specific wavelength. Typical units are watts/cm²-steradian per millimicron.

spectral irradiance - radiant flux incident per unit area of a surface at any specific wavelength. Typical units are watts/cm² per millimicron.

4.2

DERIVATION OF THE BASIC EQUATION

Optical pumping of laser rods subjects the laser material to a distribution of energy density; power is extracted from the radiation field in the form of heat and laser radiation. Consider, then, the simple one-dimensional case of an elemental volume of cross section dA and length dl . Let the energy density due to radiation in the wavelength interval $d\lambda$ centered on the wavelength λ be uniform and of strength dE in the volume $dA \cdot dl$. Let it arise from collimated radiation propagating along the direction dl . Then the radiation in the volume $dA \cdot dl$ will move a distance $\Delta t \cdot c/n_1$ in time Δt , where n_1 is the refractive index of the medium and c is the velocity of light in vacuum. If the medium is absorbing with a linear absorption coefficient $\alpha_1(\lambda)$, the energy $W = dE \cdot dA \cdot dl$ will be diminished to

$$W' = W e^{-\alpha_1 c \Delta t / n_1} \quad (21)$$

in its passage through the medium. The energy absorbed will be

$$W - W' = W \left(1 - e^{-\alpha_1 c \Delta t / n_1} \right), \quad (22)$$

or, for a short time interval

$$W \approx W \alpha_1 \frac{c}{n_1} \Delta t. \quad (23)$$

That is, the energy absorbed per unit of time, or the power loss will be

$$w / \Delta t = W \alpha_1 c / n_1. \quad (24)$$

This power loss occurs in the volume $dA \cdot dl$, so the power loss per unit volume is

$$dp' = w / \Delta t / (dA \cdot dl) = \alpha_1 c dE / n_1. \quad (25)$$

Of this loss, only the fraction $(1 - \lambda / \lambda_e)$ goes into thermal agitation of the medium, where λ_e is the wavelength of the laser radiation. The heat production per unit volume due to the radiation in the wavelength interval $d\lambda$ is

$$dp = \alpha_1 \frac{c}{n_1} dE (1 - \lambda / \lambda_e) \quad \text{watts/cm}^3 \quad (26)$$

where dE is termed the spectral energy density.

The spectral energy density at a point M can be found as follows: Let the point be contained in a surface element dA through which the spectral irradiance is $H_M(\lambda)$. The partial energy density due to that radiation is

$$dE(\lambda) = H_M(\lambda) n_1(\lambda)/c \quad (27)$$

The total spectral energy density for incoherent radiation would be found by adding up all such contributions at the point M. Suppose, however, that the spectral irradiance $H_M(\lambda)$ is due to radiation contained in a solid angle $d\omega$ centered around the normal σ to the surface element dA . Then the spectral irradiance $H_M(\lambda)$ at M, being the flux dF passing through dA could be expressed as

$$H_M(\lambda) = dF/dA = N_M(\lambda, \sigma) d\omega, \quad (28)$$

where $N_M(\lambda, \sigma)$ is the spectral irradiance at M due to radiation in the wavelength interval $d\lambda$. That is, $N_M(\lambda, \sigma)$ is the radiant flux per unit solid angle in the direction of the normal per unit projected area perpendicular to the normal. The summation of all such contributions at the wavelength λ becomes

$$dE_M(\lambda) = \frac{n_1}{c} \int N_M(\lambda, \sigma) d\omega. \quad (29)$$

Now, $N_M(\lambda, \sigma)$ is the spectral radiance at the point M within the laser rod and is not known directly. But, in the homogeneous medium of the rod with index $n_1(\lambda)$ and absorption coefficient $\alpha_1(\lambda)$ the spectral radiance along a given ray diminishes according to the exponential decay law $\exp(-\alpha_1 l)$. Thus, the spectral radiance N_M in a given direction at M must be a diminution of the spectral radiance N_1 in the same direction just inside the surface of the laser rod;

$$N_M(\lambda, \sigma) = N_1(\lambda, \sigma) \exp[-\alpha_1(\lambda) d_1(\sigma)], \quad (30)$$

where $d_1(\sigma)$ is the pathlength of the ray from the surface to the point M.

In the absence of reflection losses, the spectral radiance N_1 would be²³

$$N_1 = N_2 (n_1/n_2)^2, \quad (31)$$

where N_2 is the spectral radiance in the direction specified by σ and Snell's law, and n_2 is the refractive index of the material

surrounding the laser rod. N_1 is diminished from this value by the Fresnel coefficient of transmission $T(\sigma)$.

$$N_M(\lambda, \sigma) = T(\sigma) N_2(\lambda, \sigma) \frac{n_1^2}{n_2^2} e^{-\alpha_1(\lambda) d_1(\sigma)}. \quad (32)$$

The ray may be traced back through the various cladding media, in this way, to the isotropic source volume. Such a source, by definition, has a spectral radiance $N_0(\lambda)$ which is independent of the angle of exit from the source.

For a general j th ray,

$$N_M(\lambda, \sigma) = T_j(\lambda) N_0(\lambda) n_1^2 \exp \left[- \sum_m \alpha_m(\lambda) d(m, j) \right], \quad (33)$$

where $T_j(\lambda)$ is the product of the transmission coefficients at the interfaces encountered by the j th ray, $\alpha_m(\lambda)$ is the absorption coefficient of the m th medium along the ray, and $d(m, j)$ is the pathlength in that medium for that ray.

Equations (29) and (33) yield

$$dE_M(\lambda) = \frac{n_1^3}{c} \int T_j(\lambda) N_0(\lambda) \exp \left[- \sum_m \alpha_m(\lambda) d(m, j) \right] d\omega. \quad (34)$$

The integration indicated in Eq. (34) was done numerically by dividing the angular space about M into angular intervals and summing the contributions from all the intervals. Because of symmetry we need integrate over only one quarter of the space so it becomes convenient to express $d\omega$ in terms of the polar angles γ and α , where γ is measured from the axis of the laser rod and α is measured in a plane normal to the axis. Thus,

$$d\omega = \sin \gamma d\alpha d\gamma. \quad (35)$$

Let α be incremented in the fashion

$$1/2 \Delta\alpha (\Delta\alpha) 180^\circ - 1/2 \Delta\alpha, \quad (36)$$

and let γ be decremented in the fashion

$$90^\circ - 1/2 \Delta\gamma (\Delta\gamma) 1/2 \Delta\gamma. \quad (37)$$

Then no ray with polar angles (α, γ) lies in any of the planes xy , yz or xz , (α measured from the x -axis, γ measured from the z -axis),

yet the intervals are regularly spaced about M. Equation (34) becomes

$$dE_M = \frac{n_1^3(\lambda)}{c} \sum_j T_j(\lambda) N_0(\lambda) \sin \gamma_j \Delta \alpha \Delta \gamma \cdot \exp \left[- \sum_m \alpha_m(\lambda) d(m, j) \right] \quad (38)$$

The total heat production per unit volume in the laser rod can be found by substituting Eq. (38) into Eq. (26) and integrating over the wavelength range of the radiation from the source contributing to the energy density E_M .

$$E_M = \int \alpha_1(\lambda) (1 - \lambda/\lambda_e) n_1^2(\lambda) \Delta \alpha \Delta \gamma \cdot \sum_j T_j(\lambda) N_0(\lambda) \exp \left[- \sum_m \alpha_m(\lambda) d(m, j) \right] \sin \gamma_j d\lambda. \quad (39)$$

Equation (39) is the basic equation for the computation of the distribution of heat production in the laser rod. The integration over wavelength was done numerically using Simpson's rule. The operations required to apply the equation form a four-fold nest of loops:

1. Trace the selected ray from the point $M(x, 0, 0)$ in the laser rod back to the source for a chosen wavelength. Compute the transmission coefficients at each of the interfaces, and evaluate the contribution of the flux arriving at P from the selected direction (innermost loop).
2. Change the angles specifying the ray and do (1) again. Keep repeating these operations until all the flux in the interval $d\lambda$ arriving at M has been accounted for.
3. Add the energy from this wavelength interval to the energy contributed by other intervals according to Simpson's rule for numerical integration. Repeat the entire loop for each of the wavelength intervals required to cover the operative spectrum of the source.
4. Repeat the entire calculation for various points $M(x, 0, 0)$ along the radius of the laser rod selected to best show the distribution of heat production.

Basic Ray-Tracing Equations

Let the laser rod of index n_1 be immersed in a medium of index n_2 . Let the infinitely long rod be a cylinder of radius R_1 . Let the flashtube be approximated by a uniformly radiant gas volume separated from the laser rod cladding by a transparent envelope forming an infinitely long cylindrical cavity concentric with the laser rod. The cavity has radius R_2 and index n_2 . This geometry is illustrated in Fig. 3, which includes a rectangular coordinate system with z -axis coincident with the axis of the laser rod. We wish to consider a typical point P in the laser rod and trace rays from it to the surface of the surrounding gas volume.

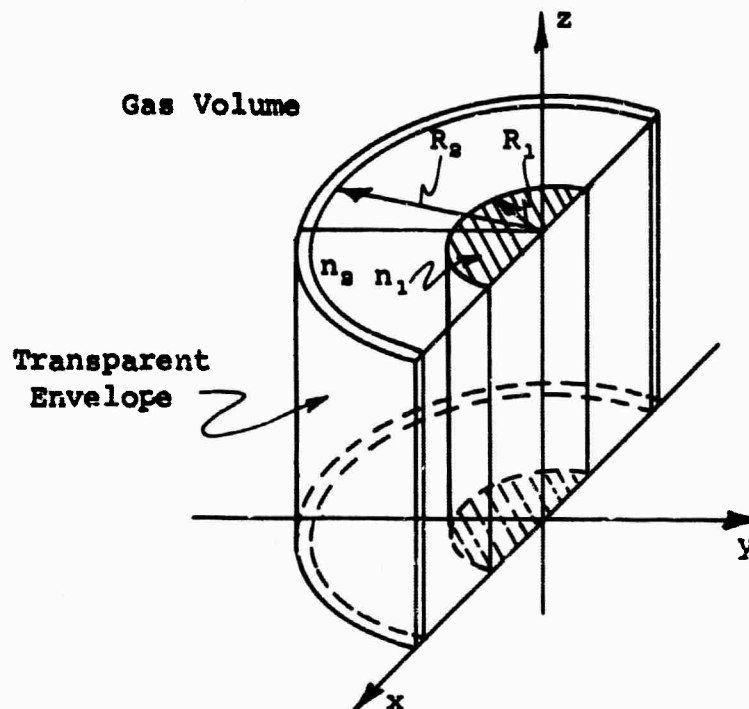


Figure 3. Geometry of the laser rod, cladding layers and source.

The point P of observation can be taken on the positive x -axis without loss of generality; $P = P(x, 0, 0)$. The xz -plane and the xy -plane are planes of symmetry. The total radiation arriving at P can be obtained by ray tracing in the sector $y \leq 0, z \geq 0$ only, as long as we neglect reflected rays. An arbitrary point on the surface of the laser rod, in this sector, will be called

$P_1(x_1, y_1, z_1)$, where the equation of the surface of the rod is

$$F_1(x_1, y_1, z_1) = 0 = x_1^2 + y_1^2 - R_1^2. \quad (40)$$

The geometrical distance from P_1 to P is

$$d_1 = \left[(x-x_1)^2 + y_1^2 + z_1^2 \right]^{\frac{1}{2}} \quad (41)$$

The optical direction cosines of the ray proceeding from P_1 to P are

$$p_1 = n_1 \frac{x-x_1}{d_1}; \quad q_1 = -n_1 \frac{y_1}{d_1}; \quad r_1 = -n_1 \frac{z_1}{d_1}. \quad (42)$$

The ray which is bent along this direction by refraction at the surface has optical direction cosines (p_2, q_2, r_2) related to (p_1, q_1, r_1) by Snell's law:

$$p_2 - p_1 = \zeta \frac{\partial F_1}{\partial x_1}; \quad q_2 - q_1 = \zeta \frac{\partial F_1}{\partial y_1}; \quad r_2 - r_1 = \zeta \frac{\partial F_1}{\partial z_1}, \quad (43)$$

where ζ is an (as yet) undetermined multiplier. Such a ray proceeds from the source point $P_2(x_2, y_2, z_2)$ with

$$p_2 = n_2 \frac{x_1 - x_2}{d_2}; \quad q_2 = n_2 \frac{y_1 - y_2}{d_2}; \quad r_2 = n_2 \frac{z_1 - z_2}{d_2}, \quad (44)$$

where

$$d_2 = \left[(x_1 - x_2)^2 + (y_1 - y_2)^2 + (z_1 - z_2)^2 \right]^{\frac{1}{2}}. \quad (45)$$

Finally, we add the conditions that

$$p_1^2 + q_1^2 + r_1^2 = n_1^2 \quad (46)$$

$$p_2^2 + q_2^2 + r_2^2 = n_2^2$$

in order to complete the system of equations. We will solve the system in the sense that -- given the parameters x, n_1, n_2, R_1, R_2 , find p_2, q_2, r_2, d_1 and d_2 as functions of p_1, q_1, r_1 .

We find x_1, y_1, z_1 by solving Eqs. (40) and (42) simultaneously. Thus,

$$x_1 = x + y_1 p_1 / q_1 \quad (47)$$

so that

$$R_1^2 = x^2 + y_1^2 (p_1/q_1)^2 + 2 x y_1 (p_1/q_1) + y_1^2 \quad (48)$$

$$y_1^2 [1 + (p_1/q_1)^2] + 2 x p_1/q_1 y_1 + x^2 - R_1^2 = 0 \quad (49)$$

$$y_1 = - \frac{p_1/q_1}{1 + (p_1/q_1)^2} x - \left[\left\{ \frac{p_1/q_1}{1 + (p_1/q_1)^2} x \right\}^2 + \frac{R_1^2 - x^2}{1 + (p_1/q_1)^2} \right]^{\frac{1}{2}} \quad (50)$$

The negative root is chosen in order to work only with the radiation coming toward p from the negative half space $y \leq 0$. It is desirable to use Eq. (50) whenever $|p_1| < |q_1|$, obtaining x_1 from the relation

$$x_1 = x - (y - y_1) p_1/q_1 \quad (51)$$

and obtaining z_1 from the relation

$$z_1 = + y_1 r_1/q_1. \quad (52)$$

When $|p_1| > |q_1|$, Eqs. (40) and (42) may be solved to yield

$$x_1 = \frac{(q_1/p_1)^2}{1 + (q_1/p_1)^2} x + \left[\left\{ \frac{(q_1/p_1)^2 x}{1 + (q_1/p_1)^2} \right\}^2 + \frac{R_1^2 - x^2 (q_1/p_1)^2}{1 + (q_1/p_1)^2} \right]^{\frac{1}{2}} \quad (53)$$

if $\text{sgn}(pn) = \text{sgn}(x - x_1)$

$$x_1 = \frac{(q_1/p_1)^2}{1 + (q_1/p_1)^2} x - \left[\left\{ \frac{(q_1/p_1)^2 x}{1 + (q_1/p_1)^2} \right\}^2 + \frac{R_1^2 - x^2 (q_1/p_1)^2}{1 + (q_1/p_1)^2} \right]^{\frac{1}{2}} \quad (54)$$

if the sign condition is not met by Eq. (53).

In both of these cases one obtains y_1 and z_1 from the equations

$$y_1 = y - (x - x_1) q_1/p_1 \quad (55a)$$

$$z_1 = (x_1 - x) r_1/p_1 \quad (55b)$$

Next we find ζ in terms of x_1, y_1, z_1 ,

$$\frac{\partial F_1}{\partial x_1} = 2x_1; \quad \frac{\partial F_1}{\partial y_1} = 2y_1; \quad \frac{\partial F_1}{\partial z_1} = 0 \quad (56)$$

$$p_2 = 2\zeta x_1 + p_1; q_2 = 2\zeta y_1 + q_1; r_2 = r_1 \quad (57)$$

By squaring each of the relations in Eq. (57) and adding, we obtain by Eq. (46),

$$n_2^2 = n_1^2 + 4\zeta^2(x_1^2 + y_1^2) + 4\zeta(p_1 x_1 + q_1 y_1) \quad (58)$$

or,

$$\zeta = - \frac{p_1 x_1 + q_1 y_1}{2R_1^2} \pm \left[\left\{ \frac{p_1 x_1 + q_1 y_1}{2R_1^2} \right\}^2 - \frac{n_1^2 - n_2^2}{4R_1^2} \right]^{\frac{1}{2}}. \quad (59)$$

In Eq. (59), that root must be chosen which makes ζ approach the physically correct limit $\zeta \rightarrow 0$ as $n_1 \rightarrow n_2$; i.e., plus if $(p_1 x_1 + q_1 y_1) > 0$ and negative otherwise.

Equations (41), (45), (57) and (59) allow us to calculate p_2 , q_2 , r_2 , d_1 and d_2 as functions of p_1 , q_1 , r_1 , which is the solution we sought.

Forbidden Rays

Equations (50), (53), (54) and (59) all contain radicals which must be real for a physically acceptable solution to the ray-tracing. The radicals of Eqs. (50), (53) and (54) become imaginary only if x exceeds R_1 , a condition which will not occur. On the other hand, the limitation that the radical in Eq. (59) be real delineates the angular region in which the rays must lie in order to be refracted into the laser rod toward P rather than be totally reflected by the interface. The condition is that

$$(p_1 x_1 + q_1 y_1)^2 \geq R_1^2 (n_1^2 - n_2^2). \quad (60)$$

An instructive example is the case already investigated by W. R. Sooy and M. L. Stitch, wherein $n_2 = 1$. ["Energy Density Distribution in a Polished Cylinder of Laser Material," J. Appl. Phys. 34, 1719 (1963).] In particular, for rays in the xy -plane, we may construct the typical ray diagram of Fig. 4. By the law of sines,

$$\sin \alpha_1 = \frac{R_1 \sin \theta}{x}, \quad (61)$$

or,

$$p_1 = n_1 \cos \alpha_1$$

$$p_1 = \pm n_1 \left[1 - \frac{R_1^2 \sin^2 \theta}{x^2} \right]^{\frac{1}{2}} \quad (62)$$

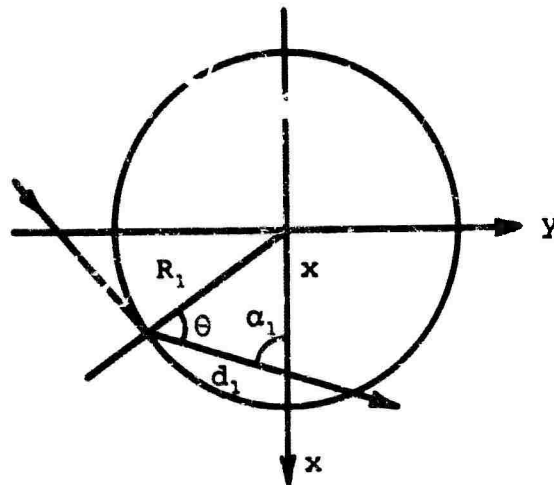


Figure 4. Typical ray diagram for rays in the xy-plane of a polished cylinder of laser material.

A ray in the xy-plane will be "forbidden" if $[(R_1/x)\sin\theta]^2 > 1$. For small values of x the inequality always can be satisfied by an appropriate value of θ . However, the maximum value for $\sin\theta$ is $1/n_1$ (critical refraction) so that the largest value x can have and still allow the relation to be satisfied for all p_1 is $x = R_1/n_1$. When x is larger than R_1/n_1 the region for which

$$|p_1| < n_1 \left[1 - \left(\frac{R_1}{n_1 x} \right)^2 \right]^{1/2} \quad (63)$$

is a region which contains no rays headed towards the point $P(x,0,0)$. Relation (60) is a more general form of relation (63) since it applies to the three-dimensional case with arbitrary $n_2 < n_1$.

Figure 5 attempts to display typical surface areas of the rod which can irradiate the point P . Figure 5a is sketched for $x < R_1 n_2/n_1$, while Fig. 5b is sketched for $x > R_1 n_2/n_1$.

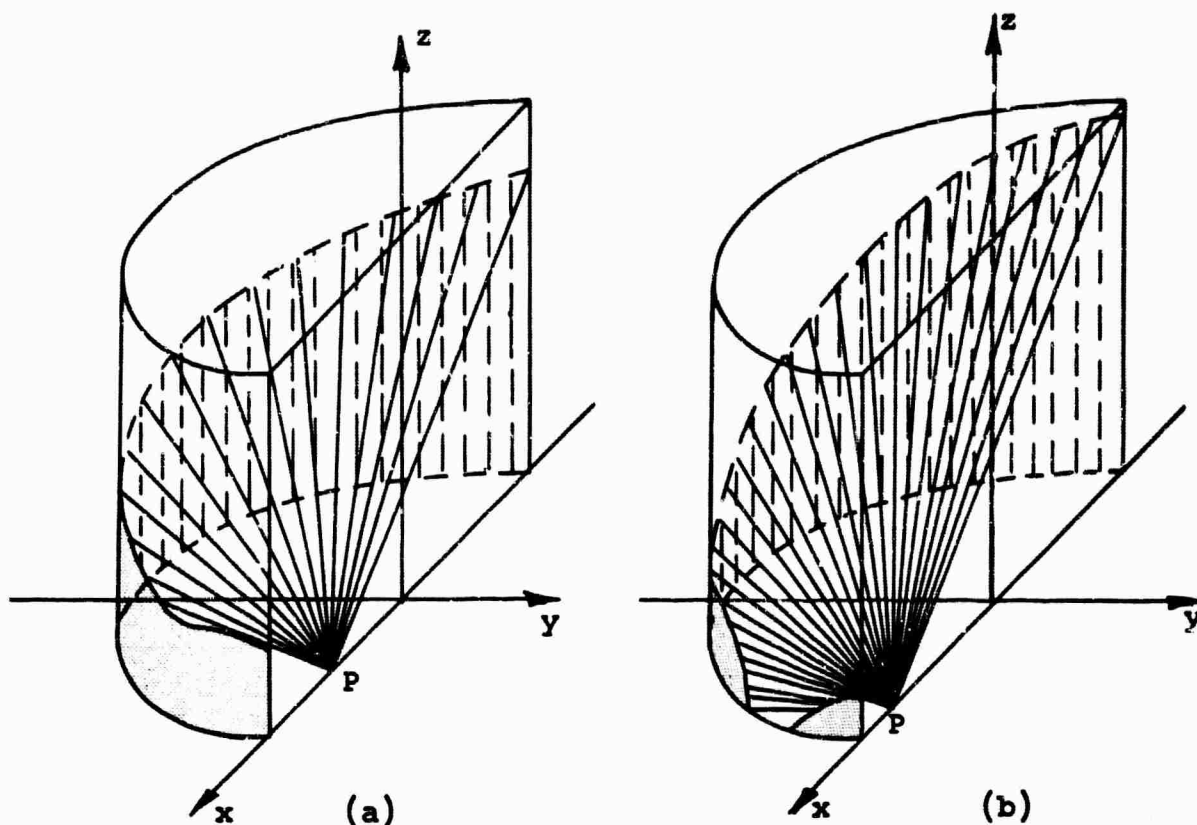


Figure 5. Typical surface areas of a rod which can irradiate point P.

Transmission Coefficients

We follow the notation of Born and Wolf, "Principles of Optics," and use the average coefficients for unpolarized radiation. Thus, from Born and Wolf, § 1.5.3, Eqs. (61), (60) and (51) in that order,

$$T = 1 - R; R = 1/2 (R_{\parallel} + R_{\perp}) \quad (64)$$

$$R_{\parallel} = \frac{\tan^2(\theta_i - \theta_t)}{\tan^2(\theta_i + \theta_t)} ; R_{\perp} = \frac{\sin^2(\theta_i - \theta_t)}{\sin^2(\theta_i + \theta_t)} \quad (65)$$

So,

$$R = \frac{1}{2} \left[\frac{\cos^2(\theta_i + \theta_t)}{\cos^2(\theta_i - \theta_t)} + 1 \right] \left[\frac{\sin(\theta_i - \theta_t)}{\sin(\theta_i + \theta_t)} \right]^2 \quad (66)$$

$$= \frac{1}{2} \left[\frac{[\cos\theta_i \cos\theta_t - \sin\theta_i \sin\theta_t]^2 + [\cos\theta_i \cos\theta_t + \sin\theta_i \sin\theta_t]^2}{[\cos\theta_i \cos\theta_t + \sin\theta_i \sin\theta_t]^2} \right] \cdot \left[\frac{\sin\theta_i \cos\theta_t - \cos\theta_i \sin\theta_t}{\sin\theta_i \cos\theta_t + \cos\theta_i \sin\theta_t} \right]^2 \quad (67)$$

But by Snell's law, $n_i \sin\theta_i = n_t \sin\theta_t$, so

$$R = \left[\frac{\cos^2\theta_t [1 - (n_t/n_i)^2 \sin^2\theta_t] + \sin^2\theta_t \cdot (n_t/n_i)^2 \sin^2\theta_t}{[\cos\theta_t \sqrt{1 - (n_t/n_i)^2 \sin^2\theta_t} + \sin\theta_t \cdot (n_t/n_i) \sin\theta_t]^2} \right] \cdot \left[\frac{\cos\theta_t \cdot (n_t/n_i) \sin\theta_t - \sin\theta_t \sqrt{1 - (n_t/n_i)^2 \sin^2\theta_t}}{\cos\theta_t \cdot (n_t/n_i) \sin\theta_t + \sin\theta_t \sqrt{1 - (n_t/n_i)^2 \sin^2\theta_t}} \right]^2 \quad (68)$$

Therefore,

$$T = 1 - \left\{ \frac{\cos^2\theta_t [1 - (n_t/n_i)^2 \sin^2\theta_t] + (n_t/n_i)^2 \sin^4\theta_t}{[\cos\theta_t \sqrt{1 - (n_t/n_i)^2 \sin^2\theta_t} + (n_t/n_i) \sin^2\theta_t]^2} \cdot \left[\frac{\sqrt{1 - (n_t/n_i)^2 \sin^2\theta_t} - (n_t/n_i) \cos\theta_t}{\sqrt{1 - (n_t/n_i)^2 \sin^2\theta_t} + (n_t/n_i) \cos\theta_t} \right]^2 \right\} \quad (69)$$

The angle θ_t in Eq. (69) is the angle between the normal \hat{N} to the (cylindrical) surface between medium n_i and medium n_t and the vector \hat{p}_t along the ray with direction cosines $(p_t/n_t, q_t/n_t, r_t/n_t)$. That is,

$$\cos\theta_t = \cos(\hat{N}, \hat{p}_t) = \frac{\hat{N} \cdot \hat{p}_t}{|\hat{N}| |\hat{p}_t|} \quad (70)$$

For example, by Eq. (40) for the surface of the laser rod, the angle of refraction for the ray passing from (x_1, y_1, z_1) to $P(x, 0, 0)$ is such that

$$\cos \phi_1 = \cos \theta_{t1} = \frac{\frac{p_1}{n_1} \frac{\partial F}{\partial x_1} + \frac{q_1}{n_1} \frac{\partial F}{\partial y_1} + \frac{r_1}{n_1} \frac{\partial F}{\partial z_1}}{\sqrt{\left(\frac{\partial F}{\partial x_1}\right)^2 + \left(\frac{\partial F}{\partial y_1}\right)^2 + \left(\frac{\partial F}{\partial z_1}\right)^2}} \quad (71)$$

$$= \frac{2x_1 p_1 / n_1 + 2y_1 q_1 / n_1}{2\sqrt{x_1^2 + y_1^2}} = \frac{x_1 p_1 + y_1 q_1}{R_1 n_1} \quad (72)$$

The angle ϕ_1 must lie in the range $0 \leq \phi_1 \leq \pi/2$, so we may take

$$\phi_1 = \arccos \left\{ |(x_1 p_1 + y_1 q_1) / (n_1 R_1)| \right\} \quad (73)$$

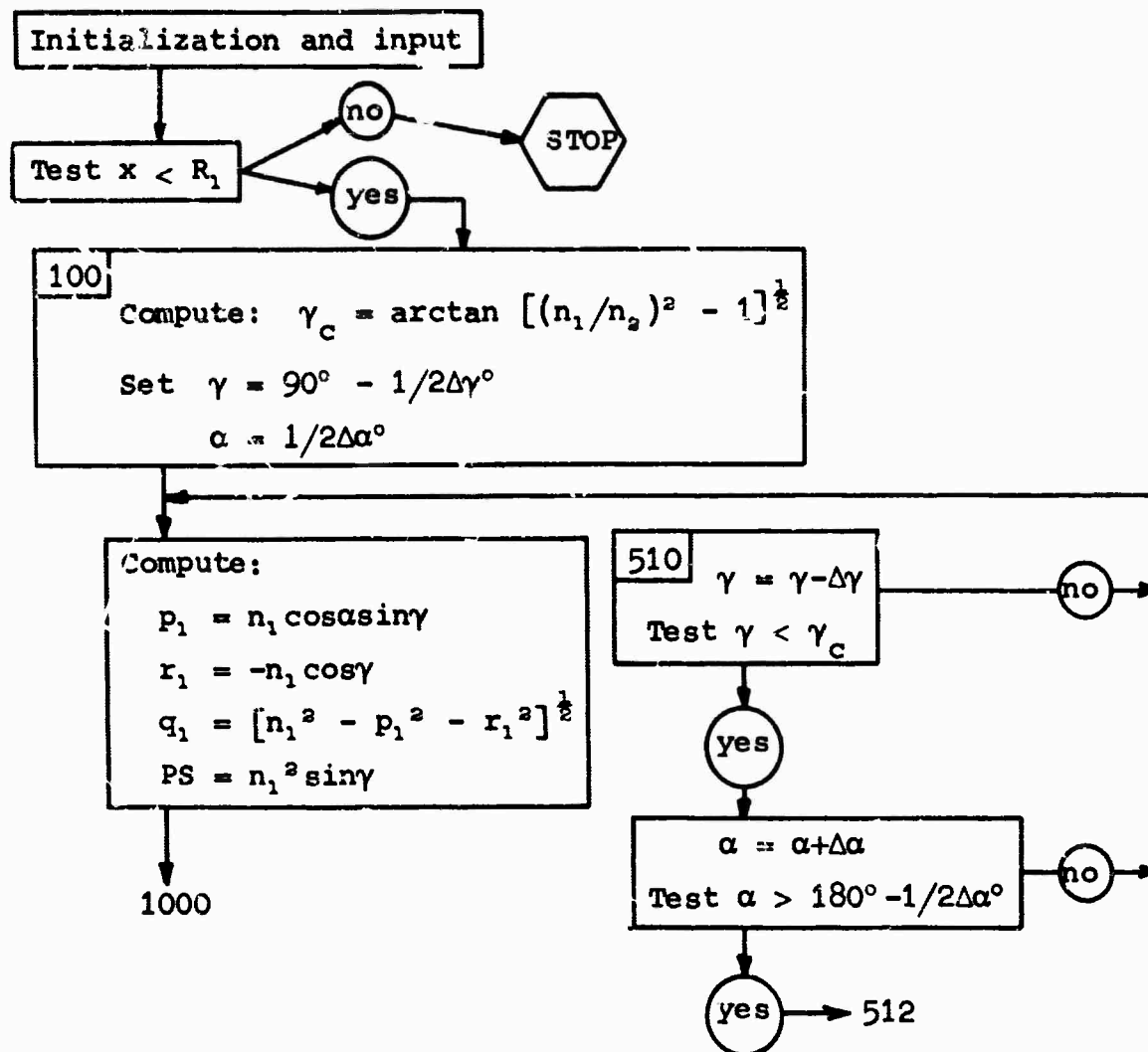
without ambiguity due to positive or negative arguments.

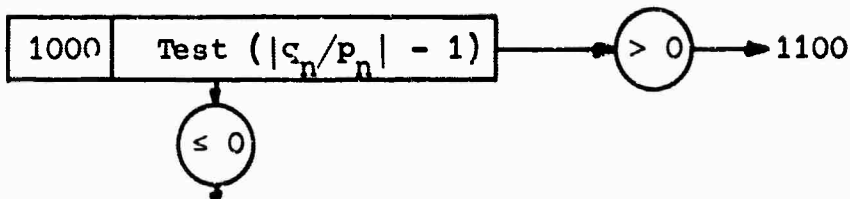
Similarly, the angle of refraction ϕ_2 into the medium n_2 from a surrounding medium must be

$$\phi_2 = \arccos \left\{ |(x_2 p_2 + y_2 q_2) / (n_2 R_2)| \right\}, \quad (74)$$

where x_2, y_2, p_2 and q_2 are determined by the equations in section 4.2, Basic Ray-Tracing Equations.

Flow Diagram of the Computer Program (polished rod)





Compute:

$$x_n = + \frac{[q_n/p_n] [(q_n/p_n) x_{n-1} - y_{n-1}]}{1 + (q_n/p_n)^2}$$

$$\pm \left[\frac{\left(\frac{(q_n/p_n) [(q_n/p_n) x_{n-1} - y_{n-1}]}{1 + (q_n/p_n)^2} \right)^2}{1 + (q_n/p_n)^2} \right]^{\frac{1}{2}}$$

$$+ \frac{R_n^2 - (y_{n-1} - x_{n-1} q_n/p_n)^2}{1 + (q_n/p_n)^2}$$

Choose the + sign if $\text{sgn}(p_n) = \text{sgn}(x_{n-1} - x_n)$

Choose the - sign if $\text{sgn}(p_n) \neq \text{sgn}(x_{n-1} - x_n)$

$$y_n = y_{n-1} - (x_{n-1} - x_n) q_n/p_n; z_n = z_{n-1} - (x_{n-1} - x_n) r_n/p_n \rightarrow 1103$$

1100 Compute:

$$y_n = \frac{[p_n/q_n] [(p_n/q_n) y_{n-1} - x_{n-1}]}{1 + (p_n/q_n)^2}$$

$$\pm \left[\frac{\left(\frac{(p_n/q_n) [(p_n/q_n) y_{n-1} - x_{n-1}]}{1 + (p_n/q_n)^2} \right)^2}{1 + (p_n/q_n)^2} \right]^{\frac{1}{2}}$$

$$+ \frac{R_n^2 - (x_{n-1} - y_{n-1} p_n/q_n)^2}{1 + (p_n/q_n)^2}$$

Choose the + sign if $\text{sgn}(q_n) = \text{sgn}(y_{n-1} - y_n)$

Choose the - sign if $\text{sgn}(q_n) \neq \text{sgn}(y_{n-1} - y_n)$

$$x_n = x_{n-1} - (y_{n-1} - y_n) p_n/q_n; z_n = z_{n-1} - (y_{n-1} - y_n) r_n/q_n \rightarrow 1103$$

1103	Test $\left[\frac{(p_n x_n + q_n y_n)^2}{2R_n^2} \right] \geq \left[\frac{n_n^2 - n_{n+1}^2}{4R_n^2} \right]$
------	---

yes

no → 510

Compute:

$$\zeta_n = - \frac{p_n x_n + q_n y_n}{2R_n^2} \pm \left[\left(\frac{p_n x_n + q_n y_n}{2R_n^2} \right)^2 - \frac{n_n^2 - n_{n+1}^2}{4R_n^2} \right]^{\frac{1}{2}}$$

Choose the \pm sign according as $(p_n x_n + q_n y_n)$ is positive or negative.

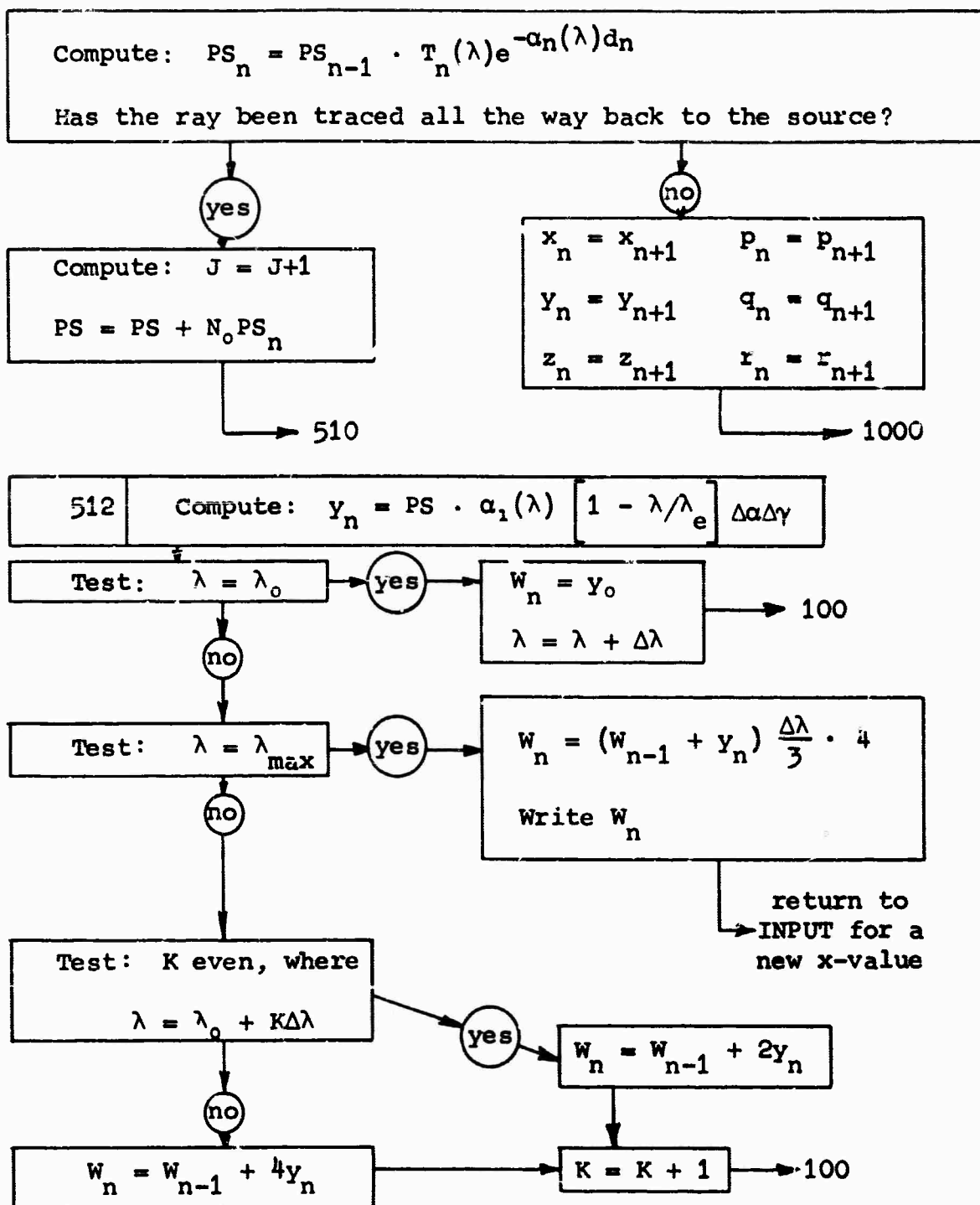
$$p_{n+1} = p_n + 2\zeta_n x_n ; q_{n+1} = q_n + 2\zeta_n y_n ; r_{n+1} = r_n$$

$$d_n = \left[(x_{n-1} - x_n)^2 + (y_{n-1} - y_n)^2 + (z_{n-1} - z_n)^2 \right]^{\frac{1}{2}}$$

Compute:

$$\cos \phi_n = \left| \frac{p_n x_n + q_n y_n}{n_n R_n} \right| ; \quad \sin^2 \phi_n = 1 - \cos^2 \phi_n$$

$$T_n = 1 - \left\{ \frac{\cos^2 \phi_n \left[1 - (n_n/n_{n+1})^2 \sin^2 \phi_n \right] + \left(\frac{n_n}{n_{n+1}} \right)^2 \sin^4 \phi_n}{\left[\cos \phi_n \sqrt{1 - (n_n/n_{n+1})^2 \sin^2 \phi_n} + \left(\frac{n_n}{n_{n+1}} \right) \sin^2 \phi_n \right]^2} \right. \\ \left. \cdot \left[\frac{\sqrt{1 - (n_n/n_{n+1})^2 \sin^2 \phi_n} - (n_n/n_{n+1}) \cos \phi_n}{\sqrt{1 - (n_n/n_{n+1})^2 \sin^2 \phi_n} + (n_n/n_{n+1}) \cos \phi_n} \right]^2 \right\}$$



"Isotropic radiation" is realized when the spectral radiance N_0 is the same for all points on the surface and for all directions of emission from the surface of the source (gas volume plus transparent envelope of Fig. 3). Such a source is known as a Lambertian radiator because the flux emitted per unit solid angle (radiant intensity) must be proportional to the cosine of the angle measured from the normal to the surface in order that the radiance be independent of the viewing angle.

Goncuz and Newell²⁷ have made measurements on xenon discharge tubes using an EG&G model 585 spectroradiometer. In particular, for an FX-47A flashtube (16.5 cm arc length, 1.3 cm bore, 0.4 atm Xe fill pressure) they report the ratio G of the total light energy emitted per millimicron by the lamp to the total electrical energy supplied to the lamp per discharge. Two different curves of spectral output are given corresponding to two current densities (1700 and 5300 amp/cm²) in the flashtube. We shall assume that the radiant energy comes out uniformly over the surface of the tube and thereby calculate values of spectral radiant emittance E_0 for the lamp. Thus, if the measured relative energy output of the lamp is G joules per millimicron per joule input, and the energy input is in the form of a nearly rectangular 0.75 millisecond voltage pulse containing f kilojoules, the energy output per unit area, or spectral radiant emittance E_0 is

$$E_0 = G \frac{\text{joules}}{\mu\text{m} \cdot \text{joules input}} \cdot \frac{f \times 10^3 \text{ joules input}}{(16.5)\pi(1.3)\text{cm}^2} \cdot \frac{1}{0.75 \text{ msec}} \quad (75)$$

The next step toward obtaining numerical values for the spectral radiance N_0 is somewhat arbitrary; the spectral radiance I_0 at the outermost surface of the cladding materials around the laser rod is taken numerically equal to the spectral radiant emittance E_0 of Eq. (75). This equality does not imply that a flashtube with a spectral radiant emittance E_0 will produce, with the help of a reflecting enclosure, such as spectral irradiance, but only that it is possible (by employing several flashtubes if necessary) to produce an irradiance of the magnitude calculated from reference (27) by using Eq. (75). Since the radiation field is to be isotropic, the connection between I_0 and N_0 is

$$I_0 = \int_{\text{hemisphere}} N_0 \cos\theta d\omega = N_0(\lambda) \int \cos\theta d\omega, \quad (76)$$

where θ is measured from the normal to the element of surface area. It is easy to verify that for the case of isotropic radiation,

$$I_0 = \pi N_0. \quad (77)$$

Thus, finally,

$$N_0(\lambda) = \frac{4f \times 10^6}{64.35 \pi^2} \text{ G } \frac{\text{watts}}{\text{m}\mu\text{-cm}^2\text{-steradian}} \quad (78)$$

The curves of N_0/f which, under the enumerated assumptions, correspond to the spectral output curves for the FX-47A flashtube as reported by Goncz and Newell are shown in Fig. 6. Values of N_0 for every 5 millimicrons from 300 to 1000 millimicrons were used in the computer program.

4.5 REFRACTIVE INDICES AND ABSORPTION COEFFICIENTS

A neodymium-doped laser glass (#3835 barium crown glass) containing 4.3 wt% of Nd^{3+} ions made by American Optical Company) was selected for the laser material of this study. The required refractive index values were computed to five significant figures from the equation

$$n_1^2 = 1 + 1.27245 [1 - 0.01/\lambda^2]^{-1} - 0.0047655\lambda^4, \quad (79)$$

where λ is in microns. Measured values used to obtain Eq. (79) were the index values 1.5259, 1.5219, 1.5198, 1.5171, 1.5098 and 1.5093 at the wavelengths 0.486, 0.546, 0.589, 0.656, 1.014 and 1.060 microns respectively. The absorption coefficient $\alpha_1(\lambda)$, see Fig. 7, was obtained from transmission measurements made on plane parallel samples with a Cary Model 14 recording spectrophotometer.

Transmission measurements were made with the same instrument on a samarium cladding glass, EOD-830, containing 9½% Sm_2O_3 . The absorption coefficient derived from the measurements is shown in Fig. 8a.

The condition of an exact index match between the samarium glass used as a cladding and the neodymium glass of the rod itself (to suppress whispering modes) was not duplicated in the computer program because of possible program halts. Instead, the samarium glass was given an index $n_2 = n_1 - 0.0001$.

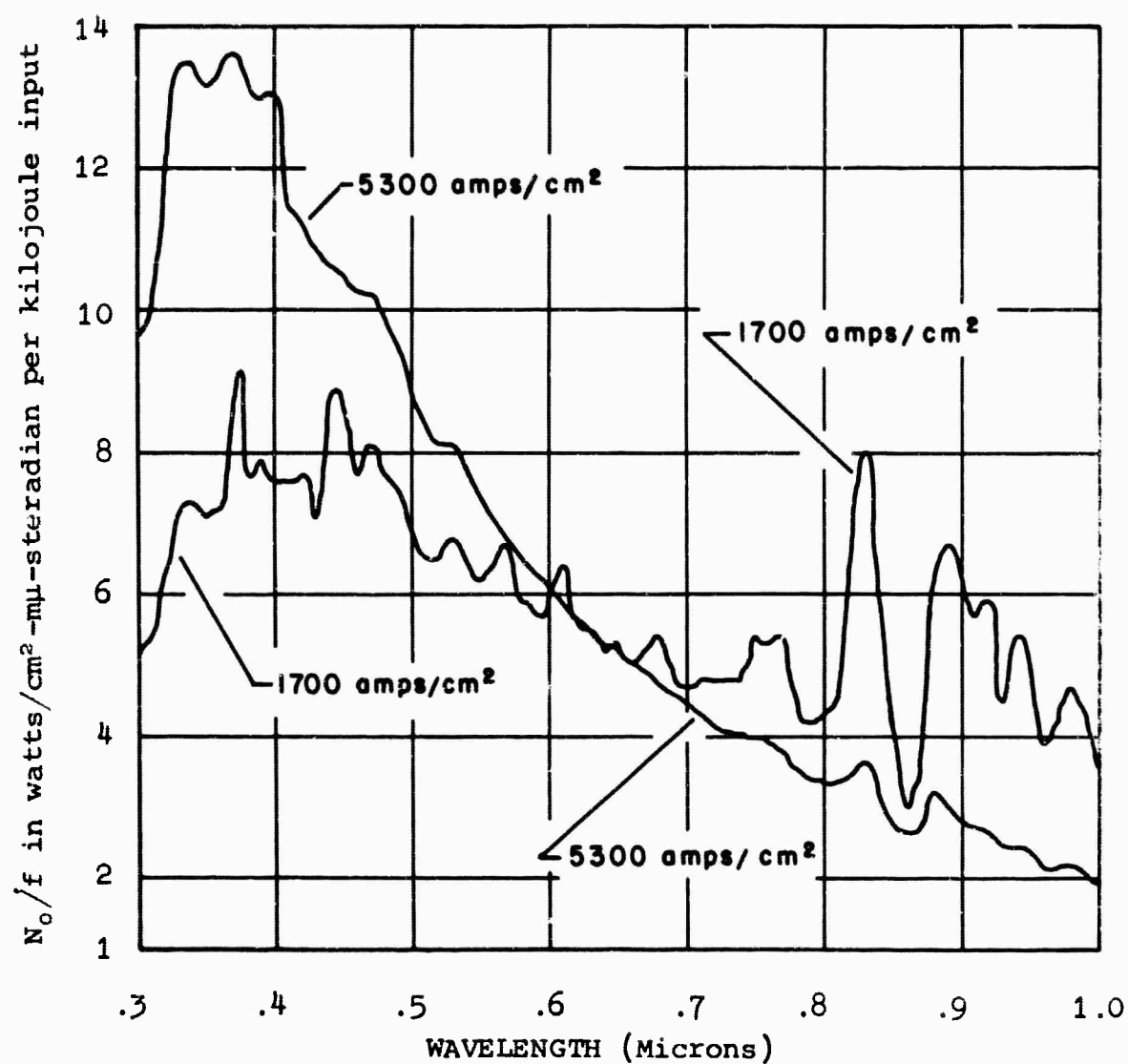


Figure 6. Spectral radiance N_0 from the FX-47A flashtube in watts per millimicron-cm²-steradian divided by the number f of kilojoules of energy in an 0.75 millisecond rectangular input voltage pulse to the flashtube. (After Goncz and Newell)

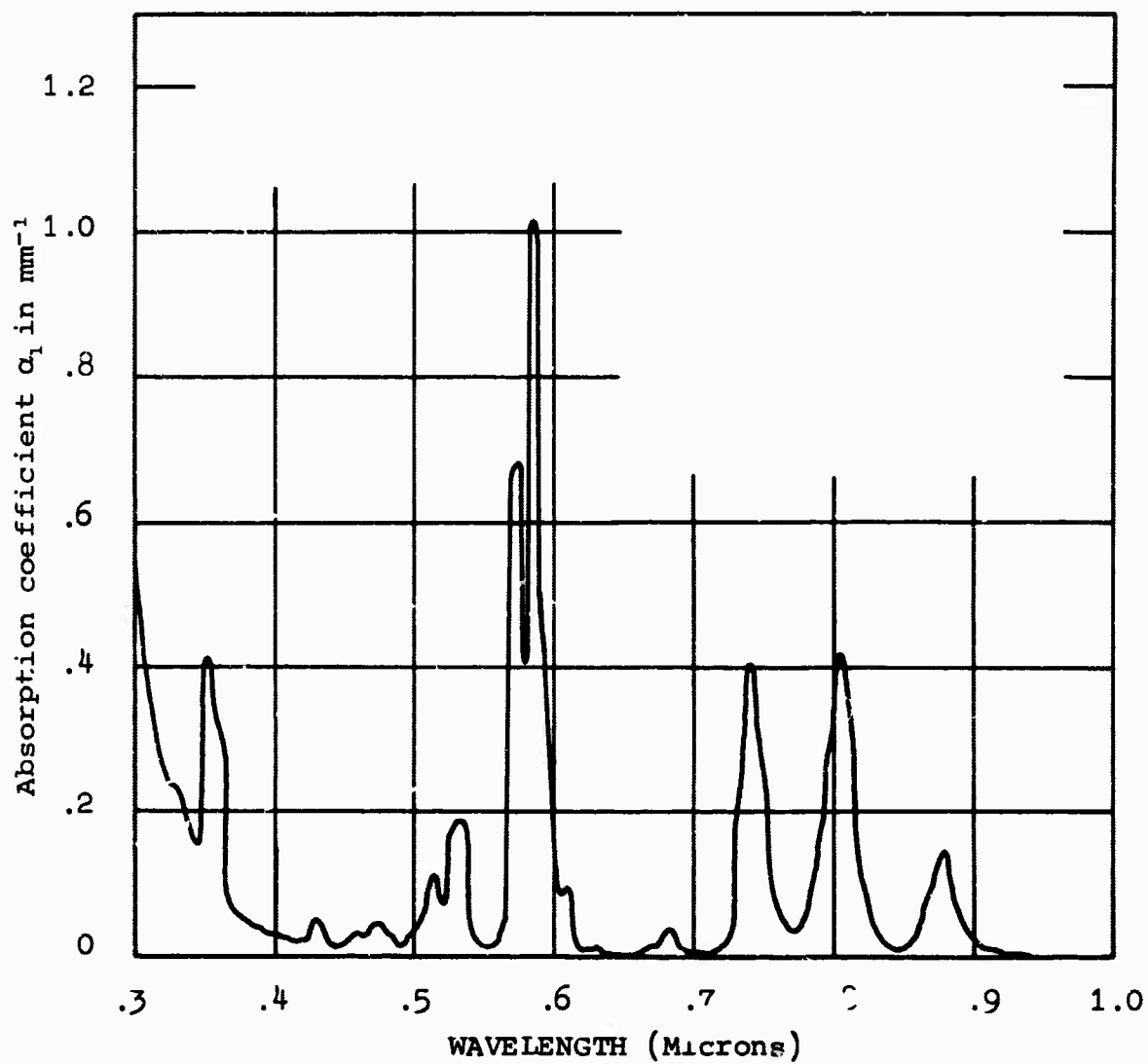


Figure 7. The absorption coefficient α_1 in mm^{-1} of AO 3835 laser glass.

The refractive index of the water cladding used in another of the calculations was taken from published tables;^{28,29} the absorption coefficient, see Fig. 8b, was found from transmission measurements made with a Cary Model 14 spectrophotometer.

Pyrex tubing was chosen as typical envelope material for the water cladding. Refractive index values were taken from the relation

$$n = 1.46815 - 0.0080515\lambda^2 + 0.0021134(\lambda^2 - 0.035)^{-1} + 0.000022788(\lambda^2 - 0.035)^{-2}, \quad (80)$$

which was adjusted to fit measurements made on a Corning Pyrex #7740 plate. Transmission measurements also were taken. No significant absorption was found except near 300 millimicrons, see Fig. 8c. Pyrex #7740 is not an optical glass and transmission characteristics are not controlled, so Eq. (80) and the curve of Fig. 8c must be considered only as representative.

4.6 CHECK CALCULATIONS

The first two of the program loops stated at the end of section 4.2 give an approximation to the monochromatic energy density at a chosen point M in the laser rod. The larger the number of rays traced, the better is the approximation up to the point where machine round-off errors begin to interfere. However, the more rays the machine has to trace, the longer the computing time. It is necessary, then, in starting the program, to estimate the number of rays to be traced to the point M for any given wavelength. Ideally, one would select values for the angular increments $\Delta\alpha$ and $\Delta\gamma$, compute an answer, then select smaller values and compute again -- continuing the process until the answer remained constant to the necessary number of significant figures.

An abbreviated version of this process was carried out for the monochromatic calculations of Sooy and Stitch³⁰ on an unclad ruby rod. Their curves were duplicated to within $\pm 3\%$ by taking $\Delta\alpha = \Delta\gamma = 5^\circ$. An extended printout of the computation for a point near the surface of the rod showed the "forbidden ray" phenomenon explained in section 4.3 and sketched in Fig. 5. The minimum number of rays traced per quadrant was 100, while 252 rays were traced when the point M was at the center of the rod. The greatest difference from the result of Sooy and Stitch occurred for $\alpha_1 R_1 = 0.003$, the least absorbing case, and $x = 0$. The calculations were repeated for that point with $\Delta\alpha = \Delta\gamma = 2.5^\circ$,

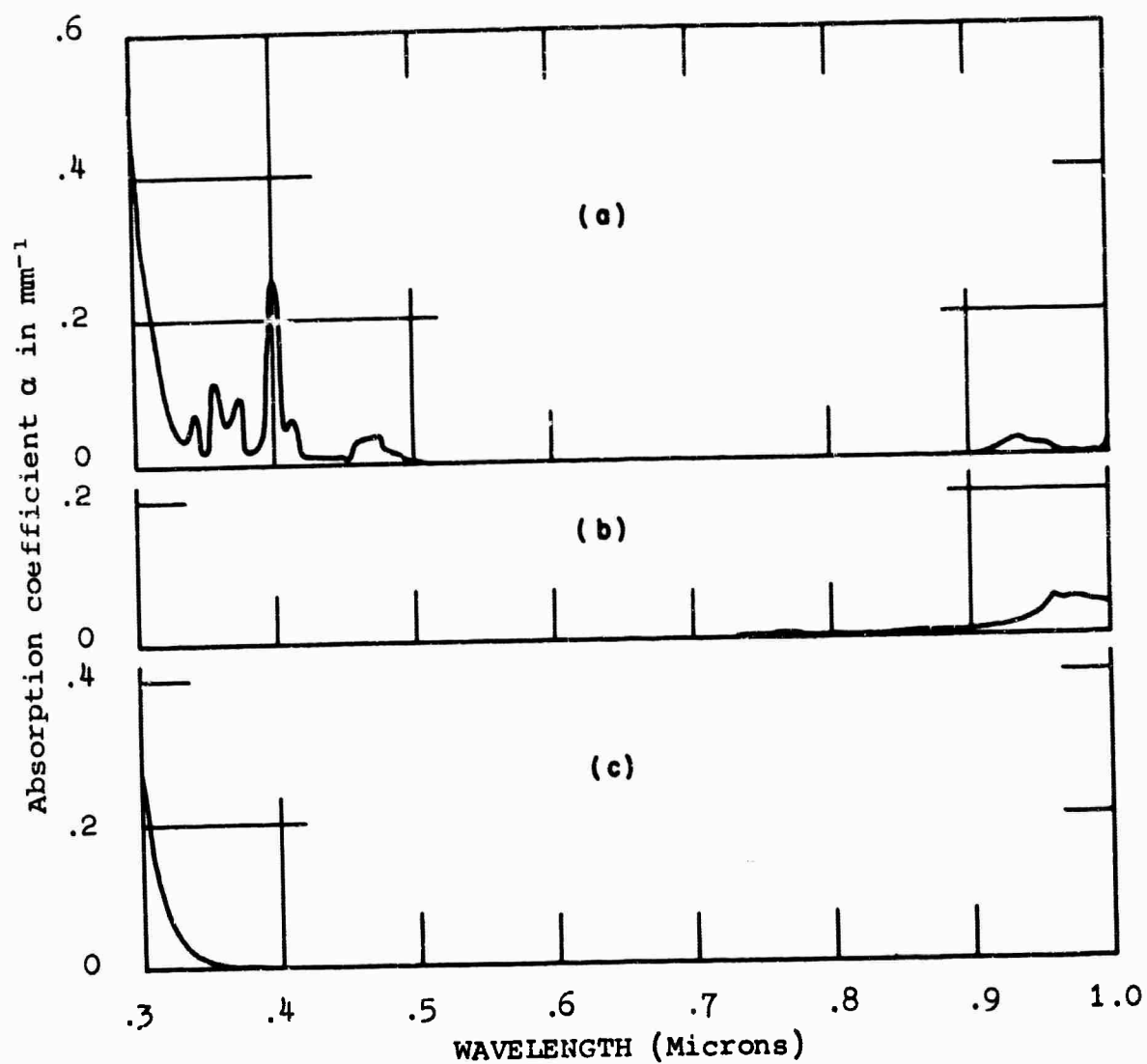


Figure 8. The absorption coefficient α in mm^{-1} of (a) AO type EOD-830 samarium glass, (b) distilled water, and (c) a representative sample of Pyrex #7740 glass.

and $\Delta\alpha = 5^\circ$, $\Delta\gamma = 0.625^\circ$ which reduced the difference to 2% and 0.5% respectively. The computing time for this case and the two repetitions were in the ratio 1:4:8. Estimates of the overall computing time (a minimum of 10 hours on an IBM-360-30 for ten points within an unclad rod using $\Delta\alpha = \Delta\gamma = 2.5^\circ$ for $x < 0.4R$ and $\Delta\alpha = \Delta\gamma = 5^\circ$ for $x \geq 0.4R$, with $\lambda = 0.3$ (0.005) 1.0 micron) made any further refinement of the calculation inadvisable.

It is believed that the close agreement with the results of Sooy and Stitch verifies the computational method of the first two loops of this program, particularly in view of the considerable difference between this method of approximation and the method of approximation used by Sooy and Stitch.

The third and fourth loops of the computer program were verified step by step from an extended printout of an actual computation (as were the steps of the first and second loops). The logic of the computational method was given an overall check by computing the distribution of heat production in an unclad rod and comparing the result to similar calculations by Borrelli and Charters.³¹ They calculated energy distributions in Nd^{3+} doped rods of Corning 0580 laser glass using the spectrum between 0.3 and 0.9 microns obtained from an FT-524 flashtube operated at 4.4 kv from a 400 μF condenser bank. The spectrum was arbitrarily normalized against its peak value. Results are presented for several values of the parameter ρR , where ρ is the concentration of doping ions in ions/cm^3 and R is the radius of the rod in centimeters. The curve of energy which causes heating vs. the normalized radius interval when $\rho R = 2 \times 10^{20}$ ions/cm^2 has been replotted in Fig. 9.

The parameters of the check calculation verifying the agreement between the method of Borrelli and Charters and the method of this report were chosen with an eye on some of the values used by Welling and Bickart³² in their experimental work on laser rods. Thus, the FX-47A flashtube spectrum corresponding to 5300 amp/cm^2 was chosen as more nearly equivalent to the output obtained by Borrelli and Charters for their FT-524 flashtube. The AO 3835 laser glass has an ion concentration of 4.7×10^{20} ions/cm^3 so that for a rod 0.45 cm in radius the product ρR is 2.1×10^{20} ions/cm^2 .

The heating energy released per unit volume in such a rod was calculated for 11 points along the radius. For comparison, normalization at $x = 0$ to the value reported by Borrelli and Charters for $\rho R = 2 \times 10^{20}$ ions/cm^2 was carried out. The agreement seen in Fig. 9 is considered good evidence that the methods of calcu-

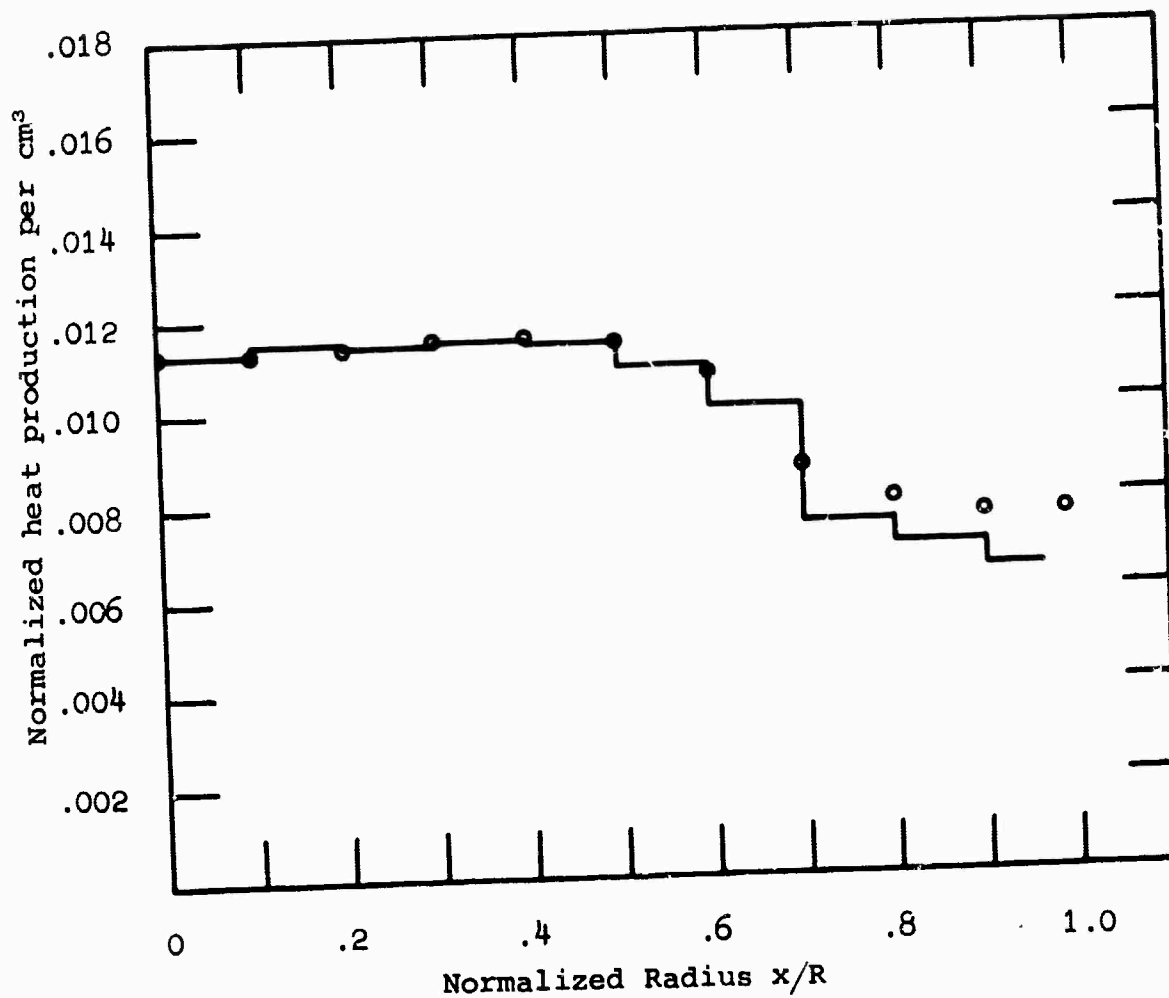


Figure 9. The distribution of energy which causes heating in an unclad rod of laser glass with $\rho R \approx 2 \times 10^{20}$ ions/cm²; (—) Corning 0580 glass (after Borrelli and Charters), (○) Ao 3835 glass.

lation agree because the physical properties of the materials described in each case are quite similar. The slightly higher production of heat energy in the outer layers of the rod relative to that in the central region as ρP is increased is predicted by Borrelli and Charters.

4.7 RESULTS - Profiles of Heat Production and of Temperature

The spectral irradiance at the outer surface of the laser rod and cladding assembly, as explained in section 4.4, has been taken equal to the spectral radiant emittance of the FX-47A flashtube as computed from data reported by Goncz and Newell. These authors also calculated the spectral efficiency of the lamp for the two current densities, 1700 amp/cm² and 5300 amp/cm², and the spectral range, 0.35 to 1.1 microns, investigated. By taking the spectral efficiency to be the same for the range 0.3 to 1.0 microns, it is possible to assign specific values not only for the spectral irradiance, but also for the irradiance itself. A current density of 1700 amp/cm² is produced by a square-wave, 3/4 millisecond electrical pulse of 1 kilojoule. Assuming that the flashtube is 64.6% efficient, 646 joules of radiant energy appear in the light pulse. This is emitted uniformly (by assumption) through a surface area of $\pi(1.3)(16.5) = 21.45 \pi$ cm², so the radiant emittance and hence the irradiance corresponding to the 1700 amp/cm² discharge is about 12.8 kilowatts/cm² over the wavelength range 0.3 to 1.0 microns. The irradiance corresponding to 5300 amp/cm² current density is about 64.1 kilowatts/cm² = $(5)(648)/(21.45 \pi)(0.75)$.

Four profiles were computed, all for a ρR value of 2.1×10^{20} ions/cm², or if one prefers, $RF = 1.9$, where ρ is the concentration of doping ions in ions/cm³, F is the ion concentration in weight percent, and R is the radius of the laser rod in cm. The profiles of Fig. 10 shows the distribution of heat production in a Nd³⁺ doped, polished, laser rod with optical pumping through the side, (1), (2) without cladding, (3) with water cladding and (4) with samarium glass cladding. The curves have been normalized against the irradiance occurring at the outer surface of the laser rod and cladding assembly. Curves (1), (3) and (4) were computed for the spectrum produced when the current density in the flashtube is 1700 amp/cm², while curve (2) was computed for a current density of 5300 amp/cm².

Figure 10 has the immediate experimental interpretation that if one were to set up a pumping enclosure which could fill a volume of space with an isotropic energy density of light flux having the spectral distribution of the FX-47A flashtube or its

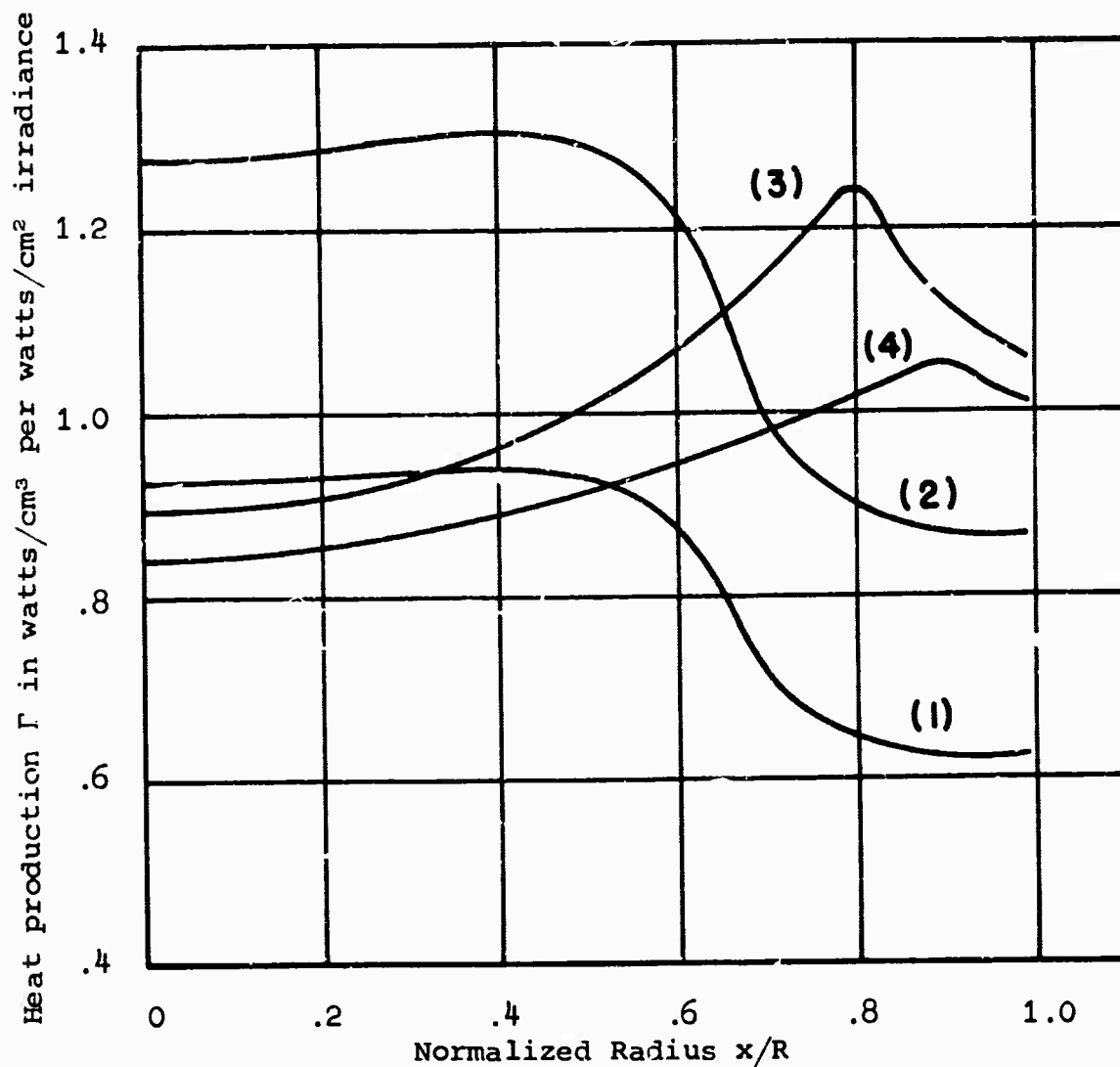


Figure 10. The distribution of heat production Γ vs the normalized radius in rods of AO 3835 laser glass with $RF = 1.9$. The ordinate Γ is measured in watts/cm³ per watts/cm² irradiance at the surface of the laser rod and cladding assembly: (1) unclad rod, 1700 amp/cm² lamp spectrum; (2) unclad rod, 5300 amp/cm² lamp spectrum; (3) rod clad with water 4.17R thick (held in place by an outer shell of Pyrex tubing 0.39R thick), 1700 amp/cm² lamp spectrum; (4) rod clad with samarium glass 0.5R thick, 1700 amp/cm² lamp spectrum

equivalent, then the relative power dissipation as heat in a laser rod with $RF = 1.9$, (a) unclad, (b) clad with water of thickness $4.17 R$, and (c) clad with samarium glass of thickness $0.5 R$ would follow the curves (1) or (2), (3) and (4) respectively.

The normalization for the distribution of heat production was adopted because it leads quickly to numbers of direct use in laser pumping. For example, if the surface of an unclad rod of AO 3835 laser glass with $RF = 1.9$ is irradiated by 1 kilowatt/cm^2 of light power distributed in the spectral range 0.3 to 1.0 microns according to the spectrum of the FX-47A flash-tube operated at 1700 amp/cm^2 current density, then the rate of release of heat energy at the center of the rod will be, according to curve (1) of Fig. 10, 920 watts/cm^3 . By the same arithmetic, if the light pulse from the lamp contained 1 kilojoule/cm^2 , 920 joules/cm^3 of heat energy would be released.

It can be inferred from curves (1) and (2) that the change in lamp spectrum produces very little change in the shape of the curve, a result which is expected since the changes in the lamp spectrum do not coincide with the major absorption regions of the laser glass. (Compare Figs. 5 and 7). The higher concentration of heat energy in the central region of the unclad rod, due to the focusing effect, is the predominant feature of curves (1) and (2). When the rod is clad with a material of index between that of air and that of the rod, the focusing effect is altered significantly, curve (3), so that an annular region in the rod becomes the site of the maximum heat production per unit volume. Such a ring structure can occur in an unclad rod for higher concentrations of doping ion as shown by Borrelli and Charters and suggested by the calculations of Cooke, McKenna and Skinner.³³ A hint that the ring structure might occur in the clad rod for a lower concentration of doping ions can be gleaned from the paper by Borrelli and Charters, the one by Cooke et al, and one by McKenna.³⁴ The reasoning, which is admittedly somewhat nugatory, is as follows: Curves by Borrelli and Charters indicate that the distribution of heat production is closely tied to the distribution of absorbed energy. Curves by Cooke et al indicate that the distributions of absorbed energy for "two- and three-dimensional" pumping are quite similar. Curves by McKenna for two-dimensional pumping show that the ring structure can be made to appear in a clad rod for a much smaller concentration of doping ion than is required in the unclad rod. Be that as it may, the phenomenon is undesirable when one is trying to produce a uniform distribution. McKenna does find, however, that the thickness of the cladding affects the size and shape of the annular region, a fact which suggests that the thickness of

the cladding should be chosen as a function of the doping ion concentration or, more likely, the product ρR in order to produce the most nearly uniform distribution.

Specifically, in Fig. 10, let us compare curve (1) for a polished unclad rod to curve (4) for a rod with cladding thickness $0.5 R$. If we now imagine the cladding thickness reduced toward zero, we expect the curve representing temperature distribution to deform smoothly from the shape of curve (4) into that of curve (1). At some cladding thickness the curve will show a minimum temperature excursion, i.e., there should be a cladding thickness which is optimum for producing a uniform temperature distribution.

The temperature rise in the laser rod is nearly proportional to the heat production per unit volume. The constant of proportionality for AO 3835 laser glass, with a density of 2.63 gm/cm^3 and a specific heat capacity $C_p \approx 0.14 \text{ gm-cal/gm-C}^\circ$, is

$$\Delta T(\text{C}^\circ) \approx 0.65 E_M (\text{joules/cm}^3). \quad (81)$$

We turn again to the FX-47A flashtube and a rod of AO 3835 laser glass such that $RF = 1.9$ for a concrete example of the temperature rise which can occur in a laser rod. Suppose an assembly of such tubes operating at a current density of 1700 amp/cm^2 produces $12.8 \text{ kilowatts/cm}^2$ irradiance at the surface of the laser rod and cladding assembly. Let the duration of the flash be $3/4 \text{ ms}$. Then 9.6 joules/cm^2 are incident on the laser rod and cladding assembly per flash. According to curve (1) of Fig. 10, $(9.6)(0.92) = 8.8 \text{ joules/cm}^3$ of heat will be generated at the center of the unclad rod with corresponding values outward to the edge. Curve (1) of Fig. 11 shows the magnitude and the distribution of temperature rise one flash of the pump assembly will produce. Curves (3) and (4) show the temperature rise for the same pumping when the rod is clad with water $4.17R$ thick and samarium glass $0.5R$ thick respectively. Curve (2) was computed for the unclad rod irradiated by a flashlamp assembly working at 5300 amp/cm^2 current density and producing 48.1 joules/cm^2 per flash at the surface of the laser rod.

Experiments carried out by Welling and Bickart on rods of AO 3835 laser glass provide a comparison between the experimentally observed distribution of temperature rise caused by pumping and that predicted by the theory presented in this report. For $RF = 1.9$, $R = 0.45 \text{ cm}$, they report a temperature rise of about 7°C at the center of an unclad rod after one flash, wherein the

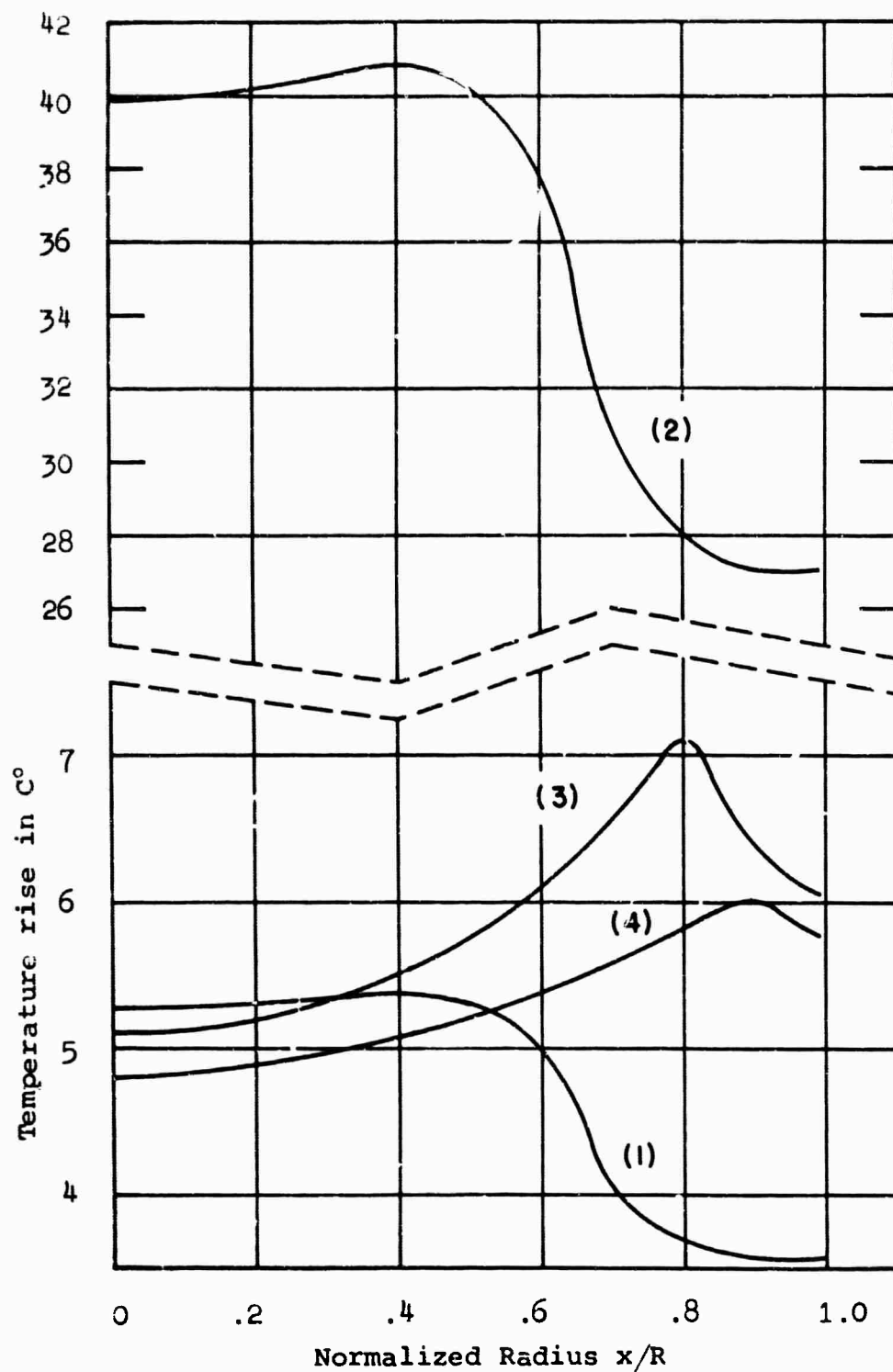


Figure 11. Temperature rise in a laser rod of neodymium glass with $RF = 1.9$ when pumped by a xenon flashtube: (1) unclad rod, 9.6 j/cm^2 incident energy, (2) unclad rod, 48.1 j/cm^2 incident energy, (3) rod clad with water $4.17R$ thick, 9.6 j/cm^2 incident energy, (4) rod clad with samarium glass $0.5R$ thick, 9.6 j/cm^2 incident energy.

flashlamp input energy to laser rod cross section ratio is 1000 j/cm^2 . Since the 7.5 cm long rod had a cross section of 0.636 cm^2 , the flashlamp, probably of about 65% efficiency, was supplied with 636 joules, and radiated 413 joules per flash. If the coupling between lamp and rod were 73% efficient, 301 joules reached the rod, or the surface density of energy was $301/(\pi)(0.9)(7.5) = 14.2 \text{ j/cm}^2$. By curve (1) of Fig. 10 and Eq. (81), the predicted temperature rise at the center of the rod is $(14.2)(0.92)(0.65) = 8.5^\circ\text{C}$.

A comparison between the experimental and the calculated distributions is shown in Fig. 12. The value of 73% chosen for the coupling efficiency in the preceding paragraph was used to obtain the broken curve of Fig. 12 and represents a normalization of the curve such that the total energy released as heat is the same for the theoretical distribution as it was for the experimental one.

Figure 12 shows a noticeable difference between the experimental and theoretical distributions of temperature near the surface of the rod. This same phenomenon has been observed and discussed by Welling and Bickart for unclad ruby rods. No satisfactory explanation of the phenomenon is known.

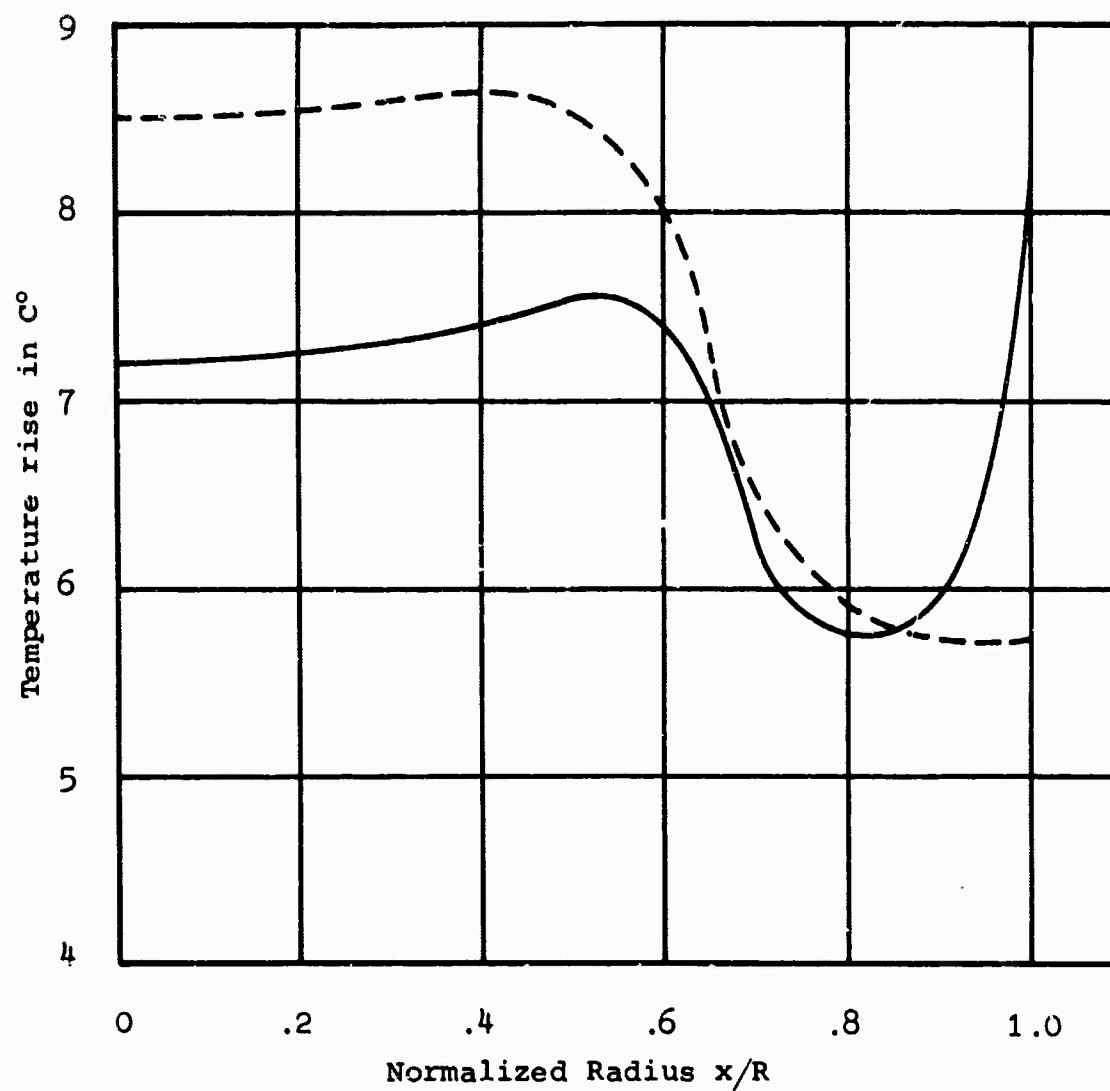


Figure 12. Comparison between the temperature distribution found experimentally by Welling and Bickart (solid curve) and the distribution calculated from the same rod with similar pumping but neglecting internal reflections (broken curve).

5. EFFECTS OF THE LASER FIELD ON THE INDEX OF REFRACTION OF THE LASER ROD

5.1 INTRODUCTION

In the following we shall consider the effect of the laser field on the distribution across the laser rod of changes in index of refraction caused by the field itself. In section 5.2 we shall treat the Maxwell stress in the rod and at the boundary, the Kerr effect, and the electrostrictive effect. In section 5.3 we shall discuss the photoelastic effect and take as the applied mechanical pressure the Maxwell stress computed in section 5.2. In section 5.4 we shall attempt to justify the assumptions made in the analysis and suggest a method (valid in principle) of achieving greater laser beam uniformity.

5.2 MAXWELL STRESS, KERR EFFECT AND ELECTROSTRICTIVE EFFECT

A. Mechanical Force

The mechanical force f per unit volume due to the presence of an electric field in a material of dielectric constant ϵ and density ρ is given by³⁵

$$f = -\frac{1}{8\pi} E^2 \text{ grad } \epsilon + \frac{1}{8\pi} \text{ grad } \left(E^2 \rho \frac{d\epsilon}{d\rho} \right) \quad (82)$$

It will be our task to find explicit expressions for ϵ and $\rho \frac{d\epsilon}{d\rho}$ in the presence of electrostriction and any quadratic effect in the field.

B. Electrostriction

We wish to calculate the change in density $\Delta\rho$ owing to the presence of an electrostrictive force. From the Helmholtz-Lippman law³⁶ the change of volume δv for an initial volume v_0 is given by

$$\delta v = - \left(\frac{\partial v}{\partial p} \right) \frac{v_0 E^2}{8\pi} \frac{\partial \epsilon}{\partial v} = - \kappa v \frac{v_0 E^2}{8\pi} \frac{\partial \epsilon}{\partial v} = - \frac{v_0 E^2}{8\pi} \left(\frac{\partial \epsilon}{\partial p} \right)_{E=0} \quad (83)$$

$T = \text{Const.}$

where p is the pressure

E the electric field strength

ϵ the dielectric constant of the material

κ the compressibility.

The change in density $\Delta\rho$ and the density ρ lead, using Eq. (83), to the relation

$$-\frac{\delta v}{v_0} = \frac{\Delta\rho}{\rho} = \frac{E^2}{8\pi} \left(\frac{\partial\epsilon}{\partial p} \right)_{E=0, T=\text{Const.}} \quad (84)$$

So that we have

$$\Delta\rho = \rho \frac{E^2}{8\pi} \left(\frac{\partial\epsilon}{\partial p} \right)_{E=0, T=\text{Const.}} \equiv \rho \frac{E^2}{8\pi} a. \quad (85)$$

Equation (85) expresses the electrostrictive effect due to the presence of the field E .

C. Optical Kerr Effect

Owing to the presence of the electric field E the medium becomes birefringent. The respective dielectric constants become³⁷

$$\epsilon_e = \epsilon + E^2 N (a - b)\alpha \quad (86)$$

$$\epsilon_o = \epsilon + E^2 N (a + 2b)\alpha \quad (87)$$

where ϵ_e is the dielectric constant \perp to E

ϵ_o is the dielectric constant \parallel to E

and N, a, b, α are constants of the medium.

The corresponding indices of refraction are

$$n_e = \sqrt{\epsilon_e} = \sqrt{\epsilon} \left[1 + E^2 N (a-b) \frac{\alpha}{2\epsilon} \right] \equiv n_1 \quad (88)$$

$$n_o = \sqrt{\epsilon_o} = \sqrt{\epsilon} \left[1 + E^2 N (a+2b) \frac{\alpha}{2\epsilon} \right] \equiv n_2 \quad (89)$$

In the Kerr effect measurements, both DC and optical, one measures the quantity

$$n_o - n_e = 3b E^2 N \frac{\alpha}{2n} = B_1 \lambda E^2 \quad (90)$$

where B_1 is the Kerr constant.

In our case and for our purpose we are interested in the absolute change of index

$$n_o - n = n E^2 N (a + 2b) \frac{\alpha}{2\epsilon} \quad (91)$$

It will be noticed that in the measurement of B_1 only the coefficient b in Eq. (90) is determined. In the case of Eq. (91) the coefficient a has to be determined independently. Using Eq. (87) we can write

$$\epsilon_o - \epsilon = E^2 N (a + 2b) \alpha \equiv B \frac{E^2}{8\pi} \quad (92)$$

where we have defined another constant B which we shall subsequently use.

D. Conditions at the Boundary

(1) Surface Force per Unit Area

In this section we wish to calculate the Maxwell stresses at the boundary of the laser rod. We shall have to transform the force per unit volume of Eq. (82) into a force per unit area. The first term in Eq. (82) becomes (omitting the cumbersome factor of $1/8\pi$ for the moment)

$$- E^2 \text{grad } \epsilon = \text{grad } (-\epsilon E^2) - \epsilon \text{grad } (-E^2) \quad (93)$$

The second term on the right-hand side will mostly concern us since it is not readily amenable to the desired transformation. From vector analysis³⁵ we have

$$\text{grad } (A \cdot B) = (A \cdot \nabla) B + (B \cdot \nabla) A + A \times (\nabla \times B) + B \times (\nabla \times A) \quad (94)$$

We shall henceforth only handle the electrostatic case (see justification in section 5.4), hence

$$\nabla \times E = 0.$$

Then we have,

$$\epsilon \text{grad } E^2 = 2\epsilon (E \cdot \nabla) E = 2(D \cdot \nabla) E \quad (95)$$

where $D = \epsilon E$ is the electric displacement vector. In order to make headway with the term $D \cdot \nabla$ in general (as opposed to cartesian coordinates) we shall have to draw more heavily on vector analysis. We define the indefinite or dyadic product of two vectors A and B as $A;B$. Taking a third vector C we define the scalar product of the dyad $A;B$ by

$$(A;B) \cdot C = A(B \cdot C) \quad (96)$$

and

$$C \cdot (A;B) = B(C \cdot A) \quad (97)$$

Thus the product is a vector, and is different depending on whether C follows or precedes the dyad. For the operator nabla ∇ we define for a given vector F

$$\nabla;F = \lim_{V \rightarrow 0} \frac{1}{V} \int_{(S)} n;F \, dS \quad (98)$$

where n is the normal vector to a closed surface S enclosing a volume V . This definition is analogous to the definition of the gradient of a function ϕ , which looks as follows

$$\nabla\phi = \lim_{V \rightarrow 0} \frac{1}{V} \int_{(S)} n \phi \, dS \equiv \text{grad } \phi \quad (99)$$

Similarly for the divergence of an operator we have the definition

$$\nabla \cdot F = \lim_{V \rightarrow 0} \frac{1}{V} \int_{(S)} n \cdot F \, dS = \text{div } F \quad (100)$$

We can now find a clearer meaning to the operator $A \cdot \nabla$ as given in Eq. (94).

Let A be a vector which is not to be varied in the limiting process given by Eq. (98), then

$$\lim_{V \rightarrow 0} \frac{1}{V} \int_{(S)} (A \cdot n) F \, dS = A \cdot \left[\lim_{V \rightarrow 0} \frac{1}{V} \int_{(S)} (n;F) \, dS \right] = A \cdot (\nabla;F) \quad (101)$$

and from Eq. (97) we get for the last term in Eq. (101)

$$A \cdot (\nabla;F) = (A \cdot \nabla) F \quad (102)$$

Given two vectors a and b we wish to calculate the divergence of the dyad $a;b$. We have

$$\nabla \cdot (a;b) = \nabla \cdot (a;b_0) + \nabla \cdot (a_0;b) \quad (103)$$

where the suffix zero indicates that the corresponding quantity is not to be varied when applying the operator ∇ .

Applying Eq. (100) to the first term on the right of Eq. (103) yields

$$\nabla \cdot (a;b_0) = \lim_{V \rightarrow 0} \frac{1}{V} \int_{(S)} n \cdot (a;b_0) dS \quad (104)$$

Using Eq. (97) this is equal to

$$\lim_{V \rightarrow 0} \frac{1}{V} \int_{(S)} (n \cdot a) b_0 dS = \left[\lim_{V \rightarrow 0} \frac{1}{V} \int_{(S)} (n \cdot a) dS \right] b_0 = (\nabla \cdot a) b \quad (105)$$

This follows from Eq. (100) and we have dropped the suffix zero on the extreme right hand side.

So that we have

$$\nabla \cdot (a;b_0) = (\nabla \cdot a) b \quad (106)$$

Let us do the same thing for the second term on the right of Eq. (103). Using Eq. (100) and Eq. (97) we have

$$\nabla \cdot (a_0;b) = \lim_{V \rightarrow 0} \frac{1}{V} \int_{(S)} n \cdot (a_0;b) = \lim_{V \rightarrow 0} \frac{1}{V} \int_{(S)} n \cdot (a_0) b dS \quad (107)$$

This last expression on the right leads by Eq. (101) and Eq. (102) to

$$\lim_{V \rightarrow 0} \frac{1}{V} \int_{(S)} (n \cdot a_0) b dS = (a \cdot \nabla) b \quad (108)$$

So that we have

$$\nabla \cdot (a_0;b) = (a \cdot \nabla) b \quad (109)$$

Assembling Eqs. (109) and (106) we get the final result for Eq. (103)

$$\nabla \cdot (a;b) = (\nabla \cdot a) b + (a \cdot \nabla) b \quad (110)$$

We now derive what may be called the tensor form of Gauss' Theorem.

$$\int_{(V)} \nabla \cdot (a; b) d\tau = \int_{(S)} n \cdot (a; b) dS \quad (111)$$

Using Eq. (110) the left hand side of Eq. (111) can be written

$$\int_{(V)} \nabla \cdot (a; b) d\tau = \int_{(V)} (\nabla \cdot a) b d\tau + \int_{(V)} (a \cdot \nabla) b d\tau \quad (112)$$

Using Eq. (97) the right hand side of Eq. (111) can be written

$$\int_{(S)} n \cdot (a; b) dS = \int_{(S)} (n \cdot a) b dS \quad (113)$$

So that the tensor form of Gauss' Theorem becomes, using Eqs. (112) and (113)

$$\int_{(V)} (\nabla \cdot a) b d\tau + \int_{(V)} (a \cdot \nabla) b d\tau = \int_{(S)} (n \cdot a) b dS \quad (114)$$

By invoking Eq. (114) we can now write

$$\int_{(V)} [E(\nabla \cdot D) + (D \cdot \nabla)E] d\tau = \int_{(S)} E(n \cdot D) dS \quad (115)$$

In our case, since we do not have any free charges in the laser rod we have $\nabla \cdot D = 0$, hence Eq. (115) becomes,

$$\int_{(V)} (D \cdot \nabla)E d\tau = \int_{(S)} E(n \cdot D) dS \quad (116)$$

Equation (116) provides us with the sought for relation enabling us to pass from a volume integral of Eq. (95) to a surface integral. Integrating Eq. (99) over a volume V we have

$$\int_{(V)} \nabla \phi d\tau = \int_{(V)} \text{grad } \phi d\tau = \int_{(S)} n \phi dS \quad (117)$$

We are now in a position to transform the volume integral $\int_{(V)} f d\tau$ of Eq. (82) into a surface integral. Using Eq. (117), the volume integral of the second term of Eq. (82) becomes

$$\frac{1}{8\pi} \int_{(V)} \text{grad} \left(E^2 \rho \frac{d\epsilon}{d\rho} \right) d\tau = \frac{1}{8\pi} \int_{(S)} n E^2 \rho \frac{d\epsilon}{d\rho} dS \quad (118)$$

Similarly, the volume integral of the first term on the right hand side of Eq. (93) becomes

$$-\frac{1}{8\pi} \int_{(V)} \text{grad} (\epsilon E^2) d\tau = -\frac{1}{8\pi} \int_{(S)} n \epsilon E^2 dS \quad (119)$$

The volume integral of Eq. (95) becomes

$$\frac{1}{8\pi} \int_{(V)} \epsilon \text{grad} E^2 d\tau = \frac{1}{4\pi} \int_{(S)} E(n \cdot D) dS \quad (120)$$

where use has been made of Eq. (116).

Assembling Eqs. (118), (119) and (120), the volume integral of Eq. (82) becomes

$$\int_{(V)} f d\tau = \frac{1}{4\pi} \int_{(S)} E(n \cdot D) dS - \frac{1}{8\pi} \int_{(S)} n E^2 \left(\epsilon - \rho \frac{d\epsilon}{d\rho} \right) dS \quad (121)$$

So that we have a surface force t

$$t = \frac{1}{4\pi} D(E \cdot n) - \frac{n}{8\pi} E^2 \left(\epsilon - \rho \frac{d\epsilon}{d\rho} \right) \quad (122)$$

This is the Maxwell stress.

(2) Maxwell Stress at the Boundary

Since we wish to calculate the Maxwell stress at the boundary, we shall use Eq. (121) and integrate over a surface given by Fig. 13. The boundary separating medium 1 and 2 is given by BB'. We assume an area dS perpendicular to the plane of the figure and indicated by $\alpha'\beta'$ for medium 2 and our area dS indicated by $\alpha\beta$ for medium 1. The area which shows in the plane of the figure as $\alpha'\alpha$ and $\beta'\beta$ will be chosen so small that its contribution to the surface integral will be neglected. Hence, we have

$$\begin{aligned} \int_{(V)} f d\tau = dS \left\{ \frac{1}{4\pi} \left[\epsilon_2 E_2 (E_2 \cdot n) - \epsilon_1 E_1 (E_1 \cdot n) \right] \right. \\ \left. - \frac{n}{8\pi} \left[E_2^2 \left(\epsilon - \frac{d\epsilon}{d\rho} \rho \right)_2 - E_1^2 \left(\epsilon - \frac{d\epsilon}{d\rho} \rho \right)_1 \right] \right\} \quad (123) \end{aligned}$$

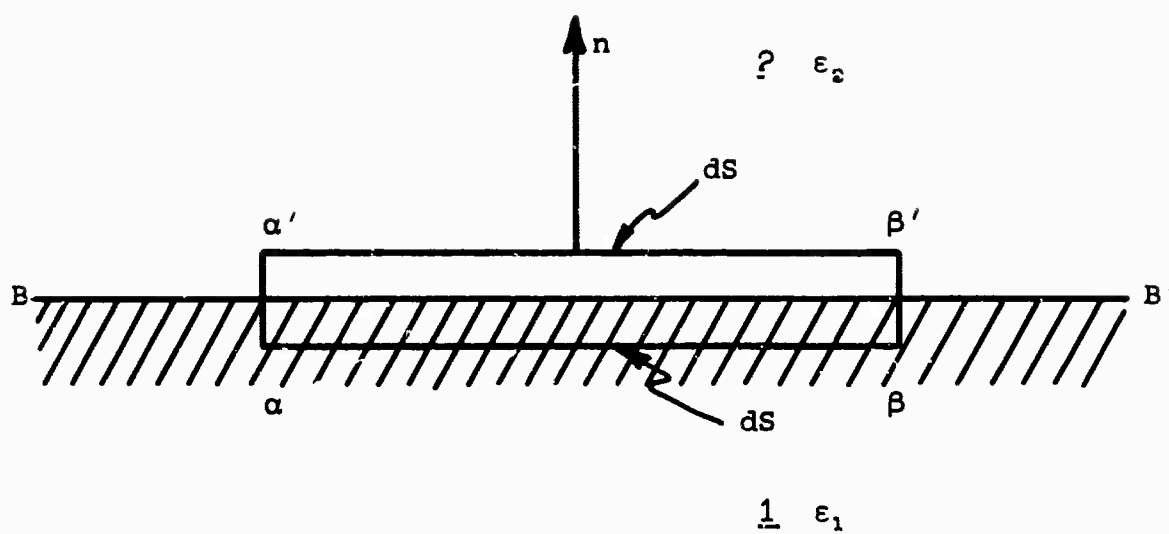


Figure 13. Maxwell stress boundary nomenclature.

We shall assume that medium 2 is the vacuum. Hence, the pressure p at the boundary is given by

$$p = \frac{1}{4\pi} [E_2 (E_2 \cdot n) - \epsilon_1 E_1 (E_1 \cdot n)] - \frac{n}{8\pi} [E_2^2 - E_1^2 \alpha] \quad (124)$$

$$\text{where we have put } \left(\epsilon - \frac{d\epsilon}{d\rho} \rho \right)_1 \equiv \alpha. \quad (125)$$

Let us set up a coordinate system where the field E is decomposed into two components: E_n parallel to the vector n , and E_p parallel to the boundary. Then we have

$$E_2 \cdot n = E_{2n} ; E_1 \cdot n = E_{1n} \quad (126a)$$

$$E_2^2 = E_{2n}^2 + E_{2p}^2 ; E_1^2 = E_{1n}^2 + E_{1p}^2 \quad (126b)$$

$$E = 1_n E_n + 1_p E_p \quad (126c)$$

where 1_n and 1_p are unit vectors respectively parallel and perpendicular to the vector normal n . Inserting Eqs. (126a), (126b) and (126c) into Eq. (125) yields,

$$p = \frac{1}{4\pi} \left[\left(1_n E_{2n} + 1_p E_{2p} \right) E_{2n} - \epsilon_1 \left(1_n E_{1n} + 1_p E_{1p} \right) E_{1n} \right] - \frac{n}{8\pi} \left(E_{2n}^2 + E_{2p}^2 \right) + \frac{n}{8\pi} \alpha \left(E_{1n}^2 + E_{1p}^2 \right) \quad (127)$$

The boundary values of the field are

$$\epsilon_1 E_{1n} = E_{2n} \quad (128a)$$

$$E_{2p} = E_{1p} \quad (128b)$$

Inserting Eqs. (128a) and (128b) into Eq. (127) yields,

$$p = \frac{1}{4\pi} \left[\left(1_n \epsilon_1 E_{1n} + 1_p E_{1p} \right) \epsilon_1 E_{1n} - \epsilon_1 \left(1_n E_{1n} + 1_p E_{1p} \right) E_{1n} \right] - \frac{n}{8\pi} \left(\epsilon_1^2 E_{1n}^2 + E_{1p}^2 \right) + \frac{n}{8\pi} \alpha \left(E_{1n}^2 + E_{1p}^2 \right) \quad (129)$$

We note that the terms

$$1_p \left[\epsilon_1 E_{1p} E_{1n} - \epsilon_1 E_{1p} E_{1n} \right] \text{ in Eq. (129) cancel.}$$

We are thus left with normal stresses only. Rewriting Eq. (129) yields

$$p = \frac{1}{4\pi} \left[1_n \epsilon_1^2 E_{1n}^2 - \epsilon_1 1_n E_{1n}^2 \right] - \frac{n}{8\pi} \left(\epsilon_1^2 E_{1n}^2 + E_{1p}^2 \right) + \frac{n}{8\pi} \alpha \left(E_{1n}^2 + E_{1p}^2 \right)$$

or finally

$$p = \frac{1}{8\pi} n \left[E_{1n}^2 (\epsilon_1^2 - 2\epsilon_1 + \alpha) + E_{1p}^2 (\alpha - 1) \right] \quad (130)$$

Depending on the sign of p , we shall have a surface pressure or tension at the boundary.

E. Calculation of f

We shall derive an expression for f as given by Eq. (82) taking electrostriction and Kerr effect into account. Using Eq. (85) which yields the expression for the change in density due to electrostriction, the total density ρ is given by

$$\rho = \rho_0 + \Delta\rho = \rho_0 + \rho_0 \frac{E^2}{8\pi} a = \rho_0 \left(1 + \frac{E^2}{8\pi} a \right) \quad (131)$$

Using Eqs. (92) and (85), the total dielectric constant resulting from electrostriction and Kerr effect becomes,

$$\epsilon = \epsilon_0 + \Delta\epsilon = \epsilon_0 + \left(\frac{d\epsilon}{d\rho} \right) \Delta\rho + B \frac{E^2}{8\pi} \quad (132)$$

It should be noted that B in Eq. (132) can also be made to include any quadratic contribution to the dielectric constant other than the Kerr effect.

It will be our task now to use Eqs. (131) and (132) to find a more explicit form for Eq. (82). We start with the second term on the right hand side of Eq. (82) first.

Putting

$$x \equiv \rho_0 \quad (133a)$$

$$y \equiv \frac{E^2}{8\pi} a \quad (133b)$$

$$u \equiv \rho \equiv x + xy \quad (133c)$$

We have

$$\frac{\partial \epsilon}{\partial x} = \frac{\partial \epsilon}{\partial u} \cdot \frac{\partial u}{\partial x} = \frac{\partial \epsilon}{\partial u} \cdot 1 + y \quad (134)$$

Hence

$$\frac{\partial \epsilon}{\partial u} = \frac{1}{1 + y} \cdot \frac{\partial \epsilon}{\partial x} \quad (135)$$

Thus

$$u \frac{\partial \epsilon}{\partial u} = \frac{u}{1 + y} \frac{\partial \epsilon}{\partial x} = \left(\frac{x + xy}{1 + y} \right) \frac{\partial \epsilon}{\partial x} = x \frac{\partial \epsilon}{\partial x} \quad (136)$$

Reverting back to the physical values as given by Eqs. (133a), (133b), (133c), Eq. (136) becomes,

$$\rho \frac{\partial \epsilon}{\partial \rho} = \rho_0 \frac{\partial \epsilon}{\partial \rho_0} \quad (137)$$

Now

$$\rho_0 \frac{\partial \epsilon}{\partial \rho_0} \equiv \gamma \quad (138)$$

is a quantity which can be determined from photoelastic measurements as will be seen below. In our case γ is the value of $\rho \frac{\partial \epsilon}{\partial \rho}$ before

the application of the electric field. In this work we shall henceforth assume that γ is constant in the laser material and does not vary with position in the medium.

Before turning to the first term on the right hand side of Eq. (82), we wish to rewrite Eq. (132) after substituting Eq. (131) for $\Delta \rho$. Then Eq. (132) becomes,

$$\begin{aligned} \epsilon &= \epsilon_0 + \frac{d\epsilon}{d\rho_0} \rho_0 \frac{E^2}{8\pi} a + B \frac{E^2}{8\pi} + \gamma \frac{E^2}{8\pi} a + B \frac{E^2}{8\pi} \\ &= \epsilon_0 + \frac{E^2}{8\pi} (\gamma a + B) \end{aligned} \quad (139)$$

And after putting

$$b = \gamma a + B \quad (140)$$

Eq. (139) can be written as

$$\epsilon = \epsilon_0 + b \frac{E^2}{8\pi} \quad (141)$$

Then the first term on the right hand side of Eq. (82) becomes, assuming ϵ_0 uniform throughout the laser rod, and using Eq. (141)

$$-\frac{1}{8\pi} E^2 \text{ grad } \epsilon = -\frac{1}{8\pi} E^2 \text{ grad } \left[\frac{E^2}{8\pi} (\gamma a + B) \right] = -\frac{1}{2} b \text{ grad } \left(\frac{E^2}{8\pi} \right)^2 \quad (142)$$

The second term on the right hand side of Eq. (82) becomes, using Eq. (137)

$$\frac{1}{8\pi} \text{ grad } \left(E^2 \rho \frac{d\epsilon}{d\rho} \right) = \sigma \text{ grad } \left(\gamma \frac{E^2}{8\pi} \right) \quad (143)$$

Now, since we have assumed γ uniform throughout the laser rod we can take out γ from under the grad operation on the right hand side. Hence, Eq. (143) yields

$$\frac{1}{8\pi} \text{ grad } \left(E^2 \rho \frac{d\epsilon}{d\rho} \right) = \gamma \text{ grad } \frac{E^2}{8\pi} \quad (144)$$

Assembling Eqs. (142) and (144), we get the final form for Eq. (82), namely

$$f = -\frac{1}{2} b \text{ grad } \left(\frac{E^2}{8\pi} \right)^2 + \gamma \text{ grad } \frac{E^2}{8\pi} \quad (145)$$

F. Calculation of γ in the Clausius-Mossotti Case

Since for a large class of glasses it is reasonable to assume that the Clausius-Mossotti relation applies, it will prove useful to calculate $\gamma = \rho \frac{d\epsilon}{d\rho}$ for this case. The Clausius-Mossotti relation*

*See, for example, M. Born, Optik (Springer, Berlin, 1933) p. 339 or Born and Wolf, Principles of Optics (Pergamon Press, 1959) p. 86.

can be written for our purposes as

$$\frac{\epsilon - 1}{\epsilon + 2} = C \rho \quad (146)$$

where C is a constant and ρ is the density.

By ordinary differentiation

$$\frac{d\epsilon}{d\rho} = \frac{1}{3\rho} [\epsilon - 1] [\epsilon + 2] \quad (147)$$

Hence, we get the desired relation

$$\rho \frac{d\epsilon}{d\rho} = \frac{1}{3} [\epsilon - 1] [\epsilon + 2] \equiv \gamma \quad (148)$$

The change $\Delta\epsilon$ in ϵ due to electrostriction or changes in density $\Delta\rho$ becomes

$$(\Delta\epsilon)_{\rho} = \frac{d\epsilon}{d\rho} \Delta\rho = \frac{1}{3} [\epsilon - 1] [\epsilon + 2] \frac{\Delta\rho}{\rho} \quad (149)$$

The change $\Delta\epsilon$ in ϵ due to the Kerr effect or any other change in polarizability $\Delta\alpha$ becomes

$$(\Delta\epsilon)_{\alpha} = \frac{d\epsilon}{d\alpha} \Delta\alpha = \frac{1}{3} [\epsilon - 1] [\epsilon + 2] \frac{\Delta\alpha}{\alpha} \quad (150)$$

When the Clausius-Mossotti law applies, we get the interesting relation

$$\rho \frac{d\epsilon}{d\rho} = \alpha \frac{d\epsilon}{d\alpha} = \frac{1}{3} [\epsilon - 1] [\epsilon + 2] \quad (151)$$

Here α is buried in the constant C which itself becomes a variable. The constant C is proportional to the polarizability α .

Since the index of refraction n is related to the dielectric constant ϵ by the relation $\epsilon = n^2$ we can also express γ in terms of n as

$$\gamma = \rho \frac{d\epsilon}{d\rho} = 2n \rho \frac{dn}{d\rho} \quad (152)$$

$$\text{or } \rho \frac{dn}{d\rho} = \frac{\gamma}{2n} \quad (153)$$

G. Maxwell Stress at the Boundary

(a) In the case for which the Clausius-Mossotti relation holds.

We shall evaluate the coefficients E_{1n}^2 and E_{1p}^2 in Eq. (130). Using Eq. (151) we have

$$\begin{aligned}\epsilon_1^2 - 2\epsilon_1 + \alpha &= \epsilon_1^2 - 2\epsilon_1 + \epsilon_1 - \frac{1}{6} (2\epsilon_1^2 + 2\epsilon_1 - 4) \\ &= \frac{1}{6} [4\epsilon_1^2 - 8\epsilon_1 + 4] = \frac{4}{6} [\epsilon_1^2 - 2\epsilon_1 + 1] = \frac{2}{3} [\epsilon_1 - 1]^2\end{aligned}\quad (154)$$

Similarly for the coefficient of E_{1p}^2 we have

$$\begin{aligned}\alpha - 1 &= \epsilon_1 - \frac{1}{6} [2\epsilon_1^2 + 2\epsilon_1 - 4] - 1 = [-2\epsilon_1^2 + 4\epsilon_1 - 2] \frac{1}{6} \\ &= -\frac{2}{6} [\epsilon_1^2 - 2\epsilon_1 + 1] = -\frac{2}{6} (\epsilon_1 - 1)^2\end{aligned}\quad (155)$$

Assembling both terms Eq. (130) becomes

$$p = \frac{1}{8\pi} (\epsilon_1 - 1)^2 \frac{1}{3} [2 E_{1n}^2 - E_{1p}^2]. \quad (156)$$

We notice that the first term is a tension force and the second term a pressure force.

As an illustration, we shall calculate the pressure at the edge of the cylinder in the case of a normal component E_{1n} only being present. From Eq. (156) we then have

$$p = \frac{2}{3} [n^2 - 1]^2 \frac{1}{8\pi} E_{1n}^2 \quad (157)$$

which is a tension.

For 1 Mw per cm^2 power we have

$$p = \frac{2}{3} \frac{(1.5^2 - 1)^2 \cdot 10^6 \cdot 10^7}{3 \cdot 10^{10}} = 350 \text{ dyn/cm}^2 = 0.36 \text{ gm/cm}^2 \quad (157a)$$

since $\frac{E^2}{8\pi} = \frac{W}{c}$

where $W = \text{power/cm}^2$
 $c = \text{velocity of light.}$

For 200 Mw/cm² power we have

$$p = 7 \cdot 10^4 \text{ dyn/cm}^2 \quad (157b)$$

This indicates that there is a mechanical force being applied on the cylinder as a result of the presence of the E field. This force will contribute to a change in index due to the photoelastic effect as we shall see in section 5.3.

(b) In the general case.

We look first at the coefficients $\delta \equiv \epsilon_1^2 - 2\epsilon_1 + \alpha$ and $\alpha - 1$ of Eq. (130). Using Eqs. (139) and (140) we have for ϵ_1

$$\epsilon_1 \equiv \epsilon = \epsilon_0 + \frac{E^2}{8\pi} b \quad (158)$$

$$\text{and } \alpha = \epsilon_0 - \gamma + \frac{E^2}{8\pi} b \quad (159)$$

For ease of notation let us put

$$\frac{E^2}{8\pi} b \equiv \Delta\epsilon \quad (160)$$

Then we shall lead up to the evaluation of δ

$$\epsilon_1^2 = (\epsilon_0 + \Delta\epsilon)^2 = \epsilon_0^2 + 2\Delta\epsilon \epsilon_0 \quad (161)$$

where we have neglected the term $(\Delta\epsilon)^2$.

We now have for δ

$$\epsilon_1^2 - 2\epsilon_1 + \alpha = \epsilon_0^2 - \epsilon_0 + \Delta\epsilon (2\epsilon_0 - 1) - \gamma \quad (162)$$

If we assume the largest value for γ to be 3.40 as computed in Table II for the Pockels' glasses and putting $n = 1.5$, we get for Eq. (162)

$$\delta = -0.60 + 3.5 \frac{E^2}{8\pi} b. \quad (163)$$

TABLE II

Values of γ for Various Glasses

	s205	0428	0658	02154	01571	0500	s57
Observed $\rho \frac{\partial n}{\partial \rho}$	0.358	(0.106)	0.392	0.485	0.512	0.600	0.865
n	1.508	1.512	1.545	1.570	1.644	1.751	1.96
2n	3.016	3.024	3.090	3.14	3.288	3.502	3.92
$\gamma = \rho \frac{\partial \epsilon}{\partial \rho}$	1.08		1.21	1.55	1.62	2.1	3.40

Before proceeding in the evaluation of $\alpha - 1$ we wish to get an idea of the magnitude of b . From Eq. (140) we know that $b = \gamma a + B$. Let us start with the evaluation of a . We have

$$a = \gamma \kappa \quad (164)$$

where

$$\kappa = \frac{1}{\rho} \frac{d\rho}{dp} = \frac{1}{B} \quad (165)$$

is the compressibility and B the bulk modulus.

Now since

$$\gamma = \rho \frac{d\epsilon}{d\rho} \quad (166)$$

$$a = \gamma \kappa = \frac{d\epsilon}{d\rho} \quad (167)$$

From Morey,³⁹ the bulk modulus is 370 kilobars = 3.7×10^{11} dynes/cm². We shall take $\gamma = 1$. Hence

$$a = \frac{1}{3.70 \times 10^{11}} \approx 2.7 \cdot 10^{-12} \quad (168)$$

For a laser power of 200 Mw/cm² we have a change of dielectric constant $\Delta\epsilon$

$$\Delta\epsilon = \gamma a \frac{E^2}{8\pi} = \frac{200 \cdot 10^6 \cdot 10^7}{3 \cdot 10^{10} \times 370 \cdot 10^9} = 1.8 \cdot 10^{-6} \quad (169)$$

This corresponds to a change in index of refraction

$$\Delta n = \frac{\Delta \epsilon}{2n}, \text{ so that } \Delta n \text{ due to } \gamma \text{ is } \frac{E^2}{8\pi} \text{ is, } (n = 1.5)$$

$$\Delta n = \frac{\Delta \epsilon}{2n} = \frac{1.8 \cdot 10^{-6}}{3.0} = 6 \cdot 10^{-7} \quad (170)$$

For the constant B in Eq. (140), we shall assume that it is of the same order of magnitude as the Kerr constant. In Tauern³⁹ we find for the absolute Kerr constant in glass, the values

$$\begin{aligned} 1.7 \cdot 10^{-13} \\ 3.9 \cdot 10^{-13} \\ 5.8 \cdot 10^{-13} \\ 8.1 \cdot 10^{-13} \end{aligned}$$

The coefficient $\alpha - 1$, becomes

$$\alpha - 1 = \epsilon_0 - \gamma - 1 + \frac{E^2}{8\pi} b \quad (171)$$

Using $\gamma = 1.21$ as given in Table II

$$\alpha - 1 = 0.04 + \frac{E^2}{8\pi} b \quad (172)$$

We therefore note that only if

$$\left. \begin{aligned} \epsilon_0^2 - \epsilon_0 + \gamma \\ \epsilon_0 - \gamma - 1 \end{aligned} \right\} \text{ is close to zero}$$

the term $\frac{E^2}{8\pi} b$ can be important.

However, let us assume $\delta = 0(1)$, and a laser power of 200 Mw/cm². Then

$$p = n \delta \frac{E_{in}^2}{8\pi} = \frac{200 \cdot 10^8 \cdot 10^7}{3 \cdot 10^{10}} = 6.6 \cdot 10^4 \text{ dynes/cm}^2 \quad (173)$$

This pressure at the boundary will produce later a change in index due to the photoelastic effect.

The value of Eq. (173) should be compared to that of Eq. (157b). It is of the same order of magnitude.

We terminate this section with Table II where we have calculated the values of γ for several glasses as given by Pockels⁴⁰ from his observed values of $\rho \frac{\partial n}{\partial \rho}$.

We have simply used Eq. (153) and from some inferences in the text, we have found the corresponding indices of refraction which we are taking as given by Pockels.

5.3 PHOTOELASTIC EFFECT

In this section, we wish to apply the results of our previous work. From the Maxwell stresses calculated in the previous sections it is now possible to evaluate their effect on the index of refraction. We shall not redo here the theory of the photoelastic effect. Instead we shall refer the reader to Adams and Williamson⁴¹ (A & W). We shall use their notation. We use A & W's Fig. 3, which becomes our Fig. 14. The mechanical stress is applied along OY. We are interested in the absolute changes of index $n_y - n$ for light polarized in the y direction, and in $n_z - n$ for light polarized in the z direction. We reproduce in Table III, A & W's Table 3. We reproduce here the formulas of interest for this section. They are

$$\frac{n_y - n_z}{n} = \frac{P}{2R} \left(\frac{q}{v} - \frac{p}{v} \right) \quad (\text{A \& W Eq. 5}) \quad (174)$$

$$\frac{n_y - n}{n_y} = \frac{P}{E} \left(-2 \sigma \frac{q}{v} + \frac{p}{v} \right) \quad (\text{A \& W Eq. 3B})$$

which we approximate to

$$n_y - n = \frac{P}{E} \left(-2 \sigma \frac{p}{v} + \frac{q}{v} \right) \quad (175)$$

and finally

$$\frac{n_z - n}{n_z} = \frac{P}{E} \left[(1 - \sigma) \frac{p}{v} - \sigma \frac{q}{v} \right] \quad (\text{A \& W Eq. 3C})$$

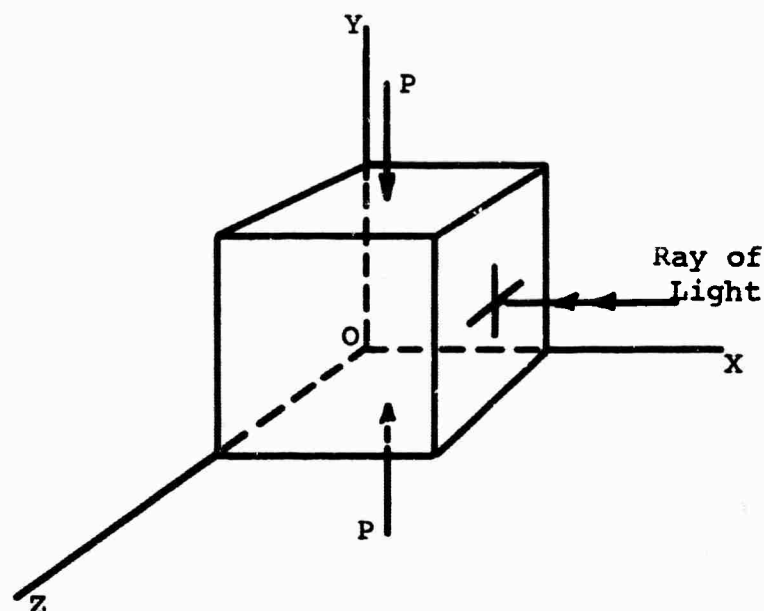


Figure 14. Notation used by Adams and Williamson — drawing to accompany elementary discussion of optical effects of stress. The thrust P is applied in the direction OY . The ray of light enters the cube of glass in the direction OX , becomes elliptically polarized and is treated as two rays vibrating, respectively, in the directions OY and OZ . Ordinarily the ray vibrating along OY travels with the higher velocity, that is, ordinary glass under unidirectional compression behaves like an optically negative uniaxial crystal.

TABLE III

Results of Pockels' Measurements on Optical Effects of Stress*

Kind of glass	Winkelmann's No.	Young's modulus kg per sq cm	Poisson's ratio σ	Refrac. index n	Percentage of PbO in glass	Coefficients of Eq. (1)		Firefiring due to 1kg per sq cm calc. from Eq. (4)	Pockels sample No.
						$\frac{p}{a}$	$\frac{b}{a}$		
Sodium Alumino- borate	2	$0.480 \cdot 10^8$	0.274	1.508	--	0.274	0.166	$-4.32 \cdot 10^{-7}$	205
Lead Alumino- borate	42	0.472	0.268	1.512	32.	0.0908	0.0228	-2.76	428
Lead Alumino- borate	21	0.547	0.250	1.545	25.	0.289	0.182	-3.78	658
Light Flint	47	0.610	0.222	1.570	33.	0.306	0.213	-2.93	2154
Heavy Flint	26	0.547	0.224	1.644	51.7	0.335	0.264	-2.61	1571
Extra Heavy Flint	33	0.550	0.239	1.751	67.5	0.354	0.319	-1.38	500
Heaviest Flint	20	0.503	0.261	1.963	80.	0.427	0.466	1.92	57

*from L. H. Adams and E. D. Williamson, J. Wash. Acad. Sci. 2, 609 (1919).

which we approximate to

$$n_z - n = n \frac{P}{E} \left[(1 - \sigma) \frac{P}{V} - \sigma \frac{q}{V} \right] \quad (176)$$

The birefringence quoted in Table III corresponds to Eq. (174). We have computed for the same glasses (identified by their Pockels number) the values as given by Eqs. (175) and (176) respectively, for $P = 1 \text{ kg/cm}^2$. This is indicated in Table IV.

TABLE IV
Index Changes for 1 kg/cm² Pressure

Pockels Sample No.	$n_y^{(0)} - n$	$n_z - n$
205	$5.06 \cdot 10^{-8}$	$48.30 \cdot 10^{-8}$
428	$-8.38 \cdot 10^{-8}$	$19.30 \cdot 10^{-8}$
658	$1.06 \cdot 10^{-7}$	$4.83 \cdot 10^{-7}$
2154	$1.99 \cdot 10^{-7}$	$4.89 \cdot 10^{-7}$
1571	$3.44 \cdot 10^{-7}$	$6.08 \cdot 10^{-7}$
500	$4.76 \cdot 10^{-7}$	$6.13 \cdot 10^{-7}$
57	$9.45 \cdot 10^{-7}$	$7.52 \cdot 10^{-7}$

It is interesting to note that although the composition of all glasses listed (except sample 57 which is positively birefringent) are negatively birefringent, glass sample 428 exhibits a negative value for $n_y - n$. For boundary pressures of $6.6 \cdot 10^4 \text{ dynes/cm}^2$ as given by Eq. (173) the change in index Δn will be

$$\Delta n = \frac{6.6 \cdot 10^4}{9.80 \cdot 10^5} \cdot \left[\begin{array}{c} n_y^{(0)} - n \\ \text{or} \\ n_z^{(0)} - n \end{array} \right] \quad (177)$$

(1 kg weight = $9.80 \cdot 10^5 \text{ dynes}$)

which would correspond for glass sample 57 and $n_y - n = 9.45 \cdot 10^{-7}$ to

$$\Delta n = \frac{6.6 \cdot 10^4 \cdot 9.45 \cdot 10^{-7}}{9.80 \cdot 10^5} = 6.38 \cdot 10^{-8} \quad (178)$$

which is small. The question of the variation of Δn across the laser rod can be dealt with adequately from the foregoing work, once the field distribution across the rod is given.

We wish to terminate this section by pointing out that it is possible to express $\rho \frac{\partial n}{\partial \rho}$ (and thus γ) in terms of the

photoelastic constants p and q , as follows,

$$\rho \frac{\partial n}{\partial \rho} = \frac{n}{3} \left(\frac{q}{v} + 2 \frac{p}{v} \right) \quad (179)$$

This was first derived by Pockels.⁴⁰

5.4 DISCUSSION

In all the foregoing we have treated the electrostatic case only. The physical justification resides in the fact that ρ cannot follow the field at optical frequencies. The DC component, however, will be present and exercise the influence we have described. If the description is adequate it would follow that it ought to be possible in principle to compensate index changes across the laser rod (leading either to convergent or divergent beams) by applying an electrostatic field with the proper field distribution (which can also be made to vary in time). We have also assumed equivalence between optical and DC Kerr effect, which is reasonable for glass.

5.5 SUMMARY

In sections 5.2 to 5.5 we have treated the problem of the influence of the laser field itself on the index of refraction of the laser rod (with special interest in a glass rod). We have developed the inter-relationship between Maxwell stresses (both in the bulk material and at the boundary), electrostriction, photoelastic effect and Kerr effect (both optical and DC in the case of glass). We have developed the formalism to a point where the distribution across the laser rod of changes in index of refraction can be readily computed provided one is given the distribution of the laser field in the rod.

6. END REGION STRESS ANALYSIS

The presence of a non-uniform temperature distribution in a circular laser cavity gives rise to two significant effects which will modify the optical path of light passing through. First, the strain patterns which accompany a temperature gradient serve to alter the optical pathlength for different radial positions within the rod. Where the material shows a stress-optic behavior, the index for the two polarizations of light will also be different. Second, as there is also a finite curvature of the end surface which accompanies a non-uniform distribution, there will be a discrete bending or refraction of the ray as it passes through the surface.

In the present effort, a program was initiated to evaluate the stresses and the optical distortion they produce in a finite length cavity under axially symmetrical temperature distribution. Both temperature and stress fields thus are assumed to exhibit no dependence on the azimuthal coordinate, θ . In practice, these conditions can be closely approximated with isotropic pumping. For a laser rod, then, in which pumping intensity is uniform along its length, and temperature variation within the rod is an arbitrary function of radius, the stress field may be resolved exactly over the major portion using plane strain theory. The region in which the plane strain formulation will not be valid is at the extreme ends, where according to St. Venant's principle, self-equilibrating mechanisms will be set up in order that specific boundary requirements are met. Since measurable changes occur in the stress field within one or two diameters of the rod end, giving rise as well to surface deformation, one would expect related changes in optical path differing from a plane strain analysis based on total length. A detailed study of the end region stress field, therefore, was undertaken.

Treatments of the end problem in cylinders reported in the literature are meager because the solution long withstood attempts even for an approximate development. In principle, however, a solution can be formulated exactly by relating stresses and displacements to the Love displacement function, $L(r,z)$ as described in Ref. 42. Now, if one sets the condition that $L(r,z)$ be biharmonic, i.e., satisfies the equation

$$\nabla^4(L) = \nabla^2 \nabla^2(L) = 0 \quad (180)$$

where $\nabla^2 = \frac{\partial^2}{\partial r^2} + \frac{1}{r} \frac{\partial}{\partial r} + \frac{\partial^2}{\partial z^2}$

r and z being cylindrical coordinates, the equations of equilibrium and compatibility for axially symmetric systems will then be satisfied. Further, if the boundary conditions to be satisfied are no forces exerted on the curved surface, and self-equilibrating symmetric normal and shear tractions on the end corresponding to

$$\sigma_r = 0, \tau = 0 \quad \text{at } r = a$$

$$\int_0^a \sigma_z(r) r dr = 0 \quad \text{at } z = 0$$

the (L) function will take the form

$$L(r, z) = e^{-\gamma z} J_0(\gamma r) + \frac{1}{2(1-\nu) + \gamma J_0(\gamma)/J_1(\gamma)} e^{-\gamma z} \gamma r J_1(\gamma r) \quad (181)$$

where here γ becomes a solution to the eigenvalue equation

$$\frac{J_0^2(\gamma)}{J_1^2(\gamma)} = -1 + \frac{2(1-\nu)}{\gamma^2} \quad (182)$$

In the absence of external forces but where loading is caused by thermal expansions, the derivations hold if the temperature function can be reduced to a symmetrical system of forces distributed at the end.

While the above equations do constitute a system of functions for the exact solution of the problem, a difficulty in use arises from the fact that the roots of Eq. (182) consist of real and imaginary parts. The task of calculating these complex roots has been found to be exceedingly great, and the real and imaginary parts of Eq. (181) give rise to increased mathematical difficulty at the boundary. Therefore, the expressions described do not provide practical workable solutions.

In an attempt to circumvent some of these difficulties, Horvay¹³ has introduced an approximate variational method of solution in which two Sadowsky-Sternberg¹⁴ stress functions, given a product representation, $\phi(r, z) = f(r)g(z)$, and $\Phi(r, z) = F(r)G(z)$, are utilized to determine the stress

distribution. Briefly, by introducing the stress functions in terms of stresses into the expression for complementary strain energy and taking the variation, δU , equal to zero there will result Euler equations with constant coefficients from which the axial functions $g(z)$ and $G(z)$ can be determined. $g(z)$ and $G(z)$ will be established as exponentially decaying sinusoidal functions of the form,

$$e^{-\alpha z} \left(\cos \beta z + \frac{\alpha}{\beta} \sin \beta z \right).$$

The α 's and β 's are real and imaginary components to the complex root $\gamma = \alpha + i\beta$ of the eigenvalue equation

$$A\gamma^4 - B\gamma^2 + C = 0$$

where A, B, and C are constants taken from the Euler equations resulting above.

The functions $f(r)$ and $F(r)$ are radial polynomials which must satisfy certain boundary conditions and rule of orthogonalization. They must be selected so that with their appropriate derivatives, they will constitute a system of boundary tractions, σ_r , σ_θ , σ_z and τ_{rz} at $z = 0$, which will closely approximate the set of end tractions imposed by the problem. The variational method permits the end tractions to be expanded employing conventional Fourier expansion techniques which alleviates much of the mathematical difficulty incurred at the boundary with the exact method. Once successful in determining matching polynomials and their derivatives, one may evaluate the Euler constants A, B, and C from which axial functions $g(z)$ and $G(z)$ will follow. To calculate the product stress functions and resultant principal stresses which they represent then becomes straightforward using available Sadowsky-Sternberg relationships. While primary obstacles inherent with an exact formulation can be removed by this approach, it does remain that considerable mathematical involvement and judgment is still required for execution of the method.

Additional papers (though more distantly related to the present problem) dealing with analytical solutions to the axial symmetrical loading of the cylinders of finite length have appeared. In Refs. 45 and 46, stress analyses have been conducted on the isothermal cylinder where prescribed tractions and displacements on the lateral surface together with the ends was investigated. The problem of thermal stresses in hollow cylinders with fairly small length to radius ratios is taken up by Bellamy.⁴⁷

The method of analysis here is based on a complementary strain energy theorem for thermoelasticity and approximate solutions for a cylinder of particular proportions have been worked out.

In our present work, we have undertaken to handle the thermal stress problem, initially at least, by way of a numerical method of solution. There appeared to be these special advantages in this approach over the analytical method outlined above:

(1) The governing equations for a numerical relaxation stress analysis could be developed with minimum difficulty and application to the end region of a cylinder seemed straightforward.

(2) The equations could be programmed for solution on a high speed computer allowing investigation of many different temperature distributions, including axial temperature variation, without constituting a new boundary value problem.

For such axially symmetrical systems, we have equations by Hoyle^{4,6}

$$I^2 x = 0$$

$$\frac{\partial^2 x}{\partial z^2} = I^2 \psi - \frac{E\alpha}{1-\nu} r \frac{\partial T}{\partial r} \quad (183)$$

which have been found suited to relaxation solutions. The stress variables $\psi(r,z)$ and $x(r,z)$ take the form

$$\psi = r \frac{\partial \phi}{\partial r}$$

$$x = \frac{r}{1-\nu} \frac{\partial \Omega}{\partial r}$$

where ϕ and Ω are arbitrary functions of the coordinates, r and z . E , α , ν and $T(r,z)$ above are Young's modulus, thermal expansion coefficients, Poisson's ratio and temperature at a specific coordinate location, respectively. I^2 is the differential operator:

$$\frac{\partial^2}{\partial r^2} - \frac{1}{r} \frac{\partial}{\partial r} + \frac{\partial^2}{\partial z^2} .$$

The principal stresses, σ_r , σ_θ , etc. can be expressed in terms of the functions ψ and x as

$$\sigma_r = \frac{\psi + (1-\nu)x}{r^2} - \frac{1}{r} \frac{\partial}{\partial r} (\psi + x) - \frac{E\alpha T}{1-\nu} \quad (184a)$$

$$\sigma_z = \frac{1}{r} \frac{\partial \psi}{\partial r}; \quad \tau_{rz} = -\frac{1}{r} \frac{\partial \psi}{\partial z} \quad (184b,c)$$

$$\sigma_\theta = -\frac{\psi + (1-\nu)x}{r^2} - \frac{\nu}{r} \frac{\partial x}{\partial r} - \frac{E\alpha T}{1-\nu} \quad (184d)$$

where it may be verified by substitution that the equilibrium equations given by

$$\frac{\partial \sigma_r}{\partial r} + \frac{\partial \tau_{rz}}{\partial z} + \frac{\sigma_r - \sigma_\theta}{r} = 0 \quad (185)$$

$$\frac{\partial \sigma_z}{\partial z} + \frac{\partial \tau_{rz}}{\partial r} + \frac{\tau_{rz}}{r} = 0$$

are identically satisfied.

The bounds of the system impose certain other requirements on the equations as well. Since the surfaces of a laser rod will remain essentially free of external force, the boundary conditions to be applied take the form

$$\sigma_r l + \tau_{rz} m = 0 \quad (186)$$

$$\sigma_z m + \tau_{rz} l = 0$$

where here 'l' and 'm' are direction cosines of the normal, N, at boundary points under examination. It may be observed that on the horizontal surface, these expressions reduce to

$$\sigma_r = 0, \quad \tau_{rz} = 0$$

where $l = \cos(Nr) = 1$

$m = \cos(Nz) = 0$

And on the vertical surface

$$\sigma_z = 0, \tau_{rz} = 0$$

where $l = 0$

$m = 1$

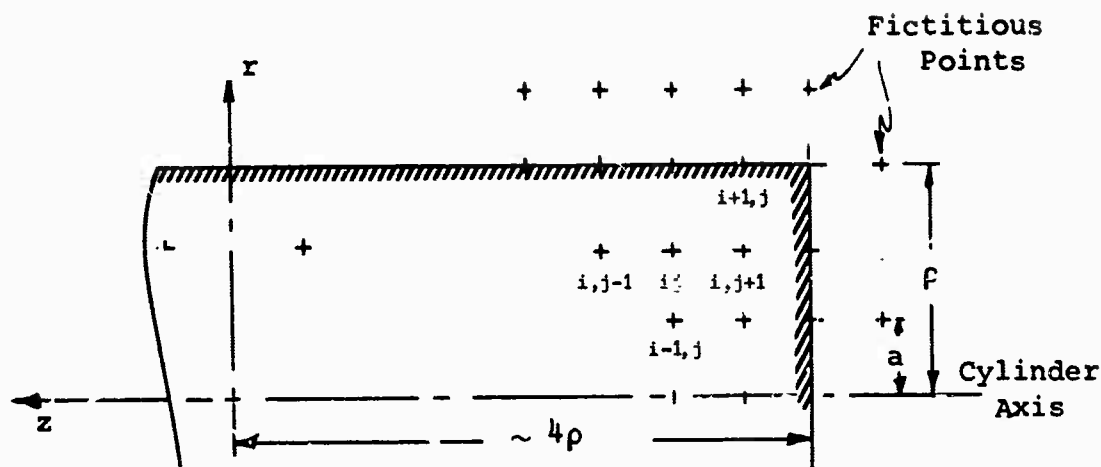


Figure 15. Point designations for relaxation grid.

Figure 15 represents a schematic representation of the axial cross-sectional portion of a laser rod used for analysis. The cylinder axis becomes a bound of symmetry; also, at the left, about 1.5 diameters from the end, another arbitrary bound of symmetry is established along a section where stress patterns no longer exhibit dependence on the axial coordinate, z . The end region so defined between these bounds and the free surfaces is then subdivided into a convenient number of zones or points to form the relaxation grid. A general point in this array is assigned the designation ij , referring to the row and column number. In conventional notation, a neighbor to the left becomes: $i, j-1$; one to the right: $i, j+1$; and so on.

Appropriate dependence between points in the chosen array is established by expressing the governing expressions in finite difference form. Using the calculus of finite differences,

first and second order differentials may be expanded by the following good approximations

$$\begin{aligned}\left(\frac{\partial \psi}{\partial r}\right)_{ij} &= \frac{1}{2a} (\psi_{i+1,j} - \psi_{i-1,j}) \\ \left(\frac{\partial^2 \psi}{\partial r^2}\right)_{ij} &= \frac{1}{a^2} (\psi_{i+1,j} + \psi_{i-1,j} - 2\psi_{i,j})\end{aligned}\tag{187}$$

where a is the grid spacing.

Working equations can now be set up embodying the stress functions, ψ and x , which will be representative of each category of points in the system. Since we are dealing with two functions, we have in general two equations to be solved simultaneously at array points. By introducing Eqs. (187) into Eqs. (183) governing the interior region there results the following two expressions which are suitable for numerical analysis

$$\begin{aligned}Q_{ij} = x_{i,j+1} + \left(\frac{2i-3}{2i-2}\right) x_{i+1,j} + x_{i,j-1} \\ + \left(\frac{2i-1}{2i-2}\right) x_{i-1,j} - 4x_{i,j} = 0\end{aligned}\tag{188}$$

$$\begin{aligned}R_{ij} = \psi_{i,j+1} + \left(\frac{2i-3}{2i-2}\right) \psi_{i+1,j} + \psi_{i,j-1} \\ + \left(\frac{2i-1}{2i-2}\right) \psi_{i-1,j} - 4\psi_{i,j} - x_{i,j+1} - x_{i,j-1} - 2x_{i,j} \\ + \frac{E\alpha a^2}{2(1-\nu)} (i-1)(T_{i+1,j} - T_{i-1,j}) = 0\end{aligned}\tag{189}$$

Points which are located along the horizontal curved boundary must obey formulas (188) and (189) and satisfy boundary conditions (186) as well. Also, the fact that positions $i+1,j$ lying above the boundary plane are fictitious requires suitable substitution for the variables at these points. By solving Eq. (188) for $x_{i+1,j}$ and (189) for $\psi_{i+1,j}$ and writing a third equation from (184a) at the cylindrical surface, ρ ,

as

$$\sigma_r = \frac{\psi_{ij} + (1-\nu) x_{ij}}{\rho^2}$$

$$- \frac{1}{2ap} (\psi_{i+1,j} + x_{i+1,j} - \psi_{i-1,j} - x_{i-1,j}) - \frac{E\alpha T}{1-\nu} = 0 \quad (190)$$

we may combine Eqs. (188), (189) and (190) to eliminate $x_{i+1,j}$ and $\psi_{i+1,j}$ from the boundary equation. In addition, since $T_{i+1,j}$ is also a fictitious temperature, the temperature difference $(T_{i+1,j} - T_{i-1,j})$ appearing in Eq. (190) must be expressed in terms of real temperatures. For this purpose, a MacLaurin series expansion is used to expand the temperature differential about surface point, ij , in the following manner

$$\left(\frac{\partial T}{\partial r}\right)_{ij} = \left(\frac{\partial T}{\partial r}\right)_{i-1,j} + a \left(\frac{\partial^2 T}{\partial r^2}\right)_{i-1,j} + \dots$$

If we now express these terms as finite differences, we find the above reduces to

$$\left(\frac{\partial T}{\partial r}\right)_{ij} = \frac{1}{2a} (3T_{ij} + T_{i-2,j} - 4T_{i-1,j})$$

which is equivalent to

$$\frac{1}{2a} (T_{i+1,j} - T_{i-1,j})$$

By making this substitution and performing the indicated algebra, the boundary equation becomes in final form

$$Q_{ij} = 2 \left[\frac{2}{(i-1)} (1-\nu) - \frac{(1-\nu)}{(i-1)^2} - 2 \right] x_{ij}$$

$$+ 4x_{i-1,j} + 4\psi_{i-1,j} + 2\psi_{i,j+1} + 2\psi_{i,j-1}$$

$$+ 2 \frac{E\alpha a}{(1-\nu)} \left[\left(a - \frac{\rho}{2}\right) T_{ij} + \frac{\rho}{2} T_{i-2,j} - 2\rho T_{i-1,j} \right] = 0 \quad (191)$$

$$R_{ij} = 0$$

For points along the vertical boundary we find from condition (186) that the axial stress goes to zero and may therefore write from (184b)

$$\sigma_z = \frac{1}{2ra} (\psi_{i+1,j} - \psi_{i-1,j}) = 0 \quad (192)$$

This requires that $\psi_{i+1,j}$ equal $\psi_{i-1,j}$ and implies that ψ_{ij} be a constant on the boundary. Hence, by combining Eqs. (188), (189) and (192) to eliminate $x_{i,j+1}$ and ψ_{i-j+1} , the final version of the boundary equation appears as

$$\begin{aligned} Q_{ij} = 2 \left[2\psi_{i,j-1} - 4\psi_{ij} + \left(\frac{2i-3}{2i-2} \right) (\psi_{i+1,j} + x_{i+1,j}) \right. \\ \left. + \left(\frac{2i-1}{2i-2} \right) (\psi_{i-1,j} + x_{i-1,j}) - 2x_{ij} \right. \\ \left. + \frac{arE\alpha}{2(1-\nu)} (T_{i+1,j} - T_{i-1,j}) \right] = 0 \end{aligned} \quad (193)$$

$$R_{ij} = 0$$

For points lying on an interior bound of symmetry, additional conditions will hold and the applicable equations above would be modified where possible. Thereby, at the left radial bound,

$$x_{i,j-1} = x_{i,j+1}; \quad \psi_{i,j-1} = \psi_{i,j+1}$$

For the cylinder axis, where $i = 1$, it results that equations (188) and (189) become indeterminate because of a division by zero in the second and fourth terms. Therefore, at axial boundary positions a somewhat specialized mathematical formulation is required. Beginning with the first of the equilibrium Eqs.(185), we find for $r = 0$ this reduces to

$$\sigma_r - \sigma_\theta = 0$$

observing that

$$\frac{\partial \sigma_r}{\partial r} = 0 \cdot \tau_{rz} = 0$$

on the axis.

By combining with Eqs. (184a,d) and performing the necessary algebra, the above expression becomes

$$\left(\frac{2}{r^2} - \frac{1}{r} \frac{\partial}{\partial r}\right) [\psi + (1-\nu)x] = 0$$

where, for the equation to be satisfied when $r = 0$,

$$[\psi_{1,j} + (1-\nu) x_{1,j}] = 0.$$

From the system of interdependent equations now defined, the values of x_{ij} and ψ_{ij} for each point is, in principle, determined knowing specifically only the temperature distribution imposed on the network. The solution, however, demands that the equations become simultaneously satisfied which, in effect, requires that residual quantities Q_{ij} and R_{ij} be reduced to identically zero in all equations.

Solving this problem by hand relaxation methods would be prohibitive, even for a small array, because of the tedious and lengthy computation involved. Therefore, a considerable portion of the task was devoted to preparing a computer program which would perform the relaxation operation automatically.

A brief description of the reduction technique developed follows. Handling up to a 300 point array, the program computes and stores the magnitude of the residual quantities, Q_{ij} , and R_{ij} , for all points based on selected values of x_{ij} and ψ_{ij} which are initially guessed. The relaxation procedure involves scanning the stored arrays for the highest value (positive or negative) of Q or R which exists and modifying the x and ψ values for the corresponding point by a computed increment according to

$$\begin{aligned} x'_{ij} &= x_{ij} + \lambda \left(\frac{Q_{ij}}{4} \right) \\ \psi'_{ij} &= \psi_{ij} + \phi \left(\frac{R_{ij}}{4} \right) \end{aligned} \quad (194)$$

where x'_{ij} and ψ'_{ij} become new values for the stress function associated with the point, ij . The relaxation control variables, λ and ϕ , may take on values between 0 and 2 as prescribed by the degree of under-relaxation or over-relaxation required. Upon altering values of x_{ij} and ψ_{ij} , it obviously necessitates re-computing the magnitude of residuals at neighboring points which

are affected. By this process of selection and correction, the iterative procedure is continued until all residuals are diminished to within a specified range from zero.

Using then the stress function values which have been found, the principal stresses are computed employing formulas (184). The corresponding thermally induced axial strain field is obtained using a three-dimensional stress strain relationship of the form

$$\epsilon_z = \frac{1}{E} [\sigma_z - \nu(\sigma_r + \sigma_\theta)] + \alpha T \quad (195)$$

And the axial displacement of the end face due to variation of the strain field over the end region is given by

$$w(r) = \int_0^{3\rho} \epsilon_z(r) dz$$

where the integration is performed over 1.5 diameters.

The change in optical pathlength for a ray of laser light traversing the cavity end region may now be calculated using the pertinent expressions developed by Quelle,⁴⁹ and modifying them slightly so as to include the axial variation of strain. The resulting expressions become for a ray polarized radially

$$\begin{aligned} \Delta P_r(r) = & (n-1) \int_0^{3\rho} \epsilon_z(r) dz \\ & - \int_0^{3\rho} [\sigma_r(r) B_{\parallel} + \sigma_z(r) B_{\perp} + \sigma_\theta(r) B_{\perp}] dz \\ & + 3\rho \Delta T \left[\left(\frac{\partial n}{\partial T} \right)_{\epsilon=0} - n_0 \alpha \left(\frac{2p}{v_0} + \frac{q}{v_0} \right) \right] \end{aligned} \quad (196)$$

and for one polarized tangentially

$$\begin{aligned} \Delta P_\theta(r) = & (n-1) \int_0^{3\rho} \epsilon_z(r) dz \\ & - \int_0^{3\rho} [\sigma_r(r) B_{\perp} + \sigma_z(r) B_{\perp} + \sigma_\theta(r) B_{\parallel}] dz \\ & + 3\rho \Delta T \left[\left(\frac{\partial n}{\partial T} \right)_{\epsilon=0} - n_0 \alpha \left(\frac{2p}{v_0} + \frac{q}{v_0} \right) \right] \end{aligned} \quad (197)$$

where n is the optical index of the glass; p and q , optical constants to be determined experimentally; V_0 , the velocity of light in the unstressed medium; and B_{\perp} and B_{\parallel} , the characteristic stress optic coefficients. To obtain the total change in pathlength for the optical cavity, requires that the above results be combined with additional results for the portion of the rod in which plane strain applies.

The computer provides the principal stresses and strains for each position in the relaxation array as superposed on the end portion of the rod. To determine the axial optical path change, then, through this region requires that a numerical point-by-point integration be made of the separate quantities defined in Eqs. (196) and (197). It was found expedient to perform this integration by hand using a desk calculator.

In the initial testing of the computer program, considerable difficulty was encountered in getting selected problems to converge. The principal source of difficulty was subsequently determined to be the result of choosing too few radial subdivisions in the array in an attempt to minimize computer operating time during the evaluation runs. When at least eight radial divisions were designated for an arbitrarily selected 2.54 cm diameter rod, the residual quantities, Q_{ij} and R_{ij} , would tend to zero and the problem converged properly. It occurred, similarly, that a higher limit also existed for the number of radial points chosen for which convergence could be assured. For the work done the number, n_r , of radial grid divisions fell within the limits

$$16 < \frac{n_r}{a} < 40$$

where a is the radius of the rod in inches. For a number of cases which fell outside these limits convergence was not obtained.

The relaxation coefficients, λ and ϕ , were found to play governing roles in the speed to which relaxation could be achieved. The most satisfactory value for both coefficients in this work seemed to be unity inasmuch as under-relaxation tended to make computing too slow, and over-relaxation caused the solution to diverge at certain stages due presumably to inherent limitations on the mathematical process.

To verify the accuracy of the computer solutions, it was sufficient to show that the results obtained compared favorably with known solutions in two limiting cases. Specifically, for the long rod, we know that the stress distribution through a cross section beyond about 1.5 diameters from the end must be given by

a plane strain solution. In addition, for the infinitely thin element, the disc, the results obtained must agree with the plane stress solution which is common to all radial sections. Figures 16 and 17 provide an illustration of how the computer results compare with hand-calculated results using plane strain and plane stress theory in these respective configurations. First, a 2.54 cm diameter AO 3835 neodymium glass rod, was considered with a 11.1°C linear temperature rise from center to edge. Figure 16 plots the principal stresses machine computed for a cross section 1.6 diameter from the end using a minimum network array of 9×27 points. Figure 17, similarly, plots the computed stress pattern at the midplane of a 2.40 cm diameter glass disc using a 21×3 array and a 2.22°C linear temperature rise between center and edge. Diameter to thickness ratio for the disc was 10 to 1. Negligible change was indicated in the stress distribution across the disc and axial stress remained essentially zero. Treating, in addition, the case of a short cylinder with a diameter to length ratio of 2, it was found that an intermediate solution to plane strain and plane stress occurred at the midplane.

Fairly good agreement, therefore, exists between the computed results and the exact theory for these cases. The gradual deviation indicated in the principal stresses with increasing proximity to the axis is due to small residual errors in the computed stress functions which magnify in turn as r^2 tends to zero in Eqs. (18⁴a,d). Since a finite error is introduced from the transition of differential Eq. (183) to finite difference form, small discrepancies between results cannot be removed completely. Error terms generated in using a square mesh array are generally of the order of a^2 where 'a' is the spacing of the points.⁵⁰ Thus, the magnitude of these terms can be reduced by going to more divisions and thereby decreasing the mesh size. The benefit of this is demonstrated in Fig. 17 where 21 radial points on the disc were chosen and considerably improved agreement was achieved near the axis.

Stress-strain patterns in the end region which contribute to an axial optical path variation are of interest. Accordingly, the simple arbitrary case described above using a 11.1°C linear temperature gradient in a 2.54 cm rod is treated further. Computed results showing the change in principal stresses and axial strain near the end are depicted in Figs. 18 and 19 for radial positions chosen at .477 and .954 cm, respectively, from the axis. Clearly, the solution agrees with the plane strain results beyond about 1 diameter from the end but changes significantly in the end region as predicted. Contrary to previous reasoning, though, the stress distribution at the end surface of the rod does not approach the

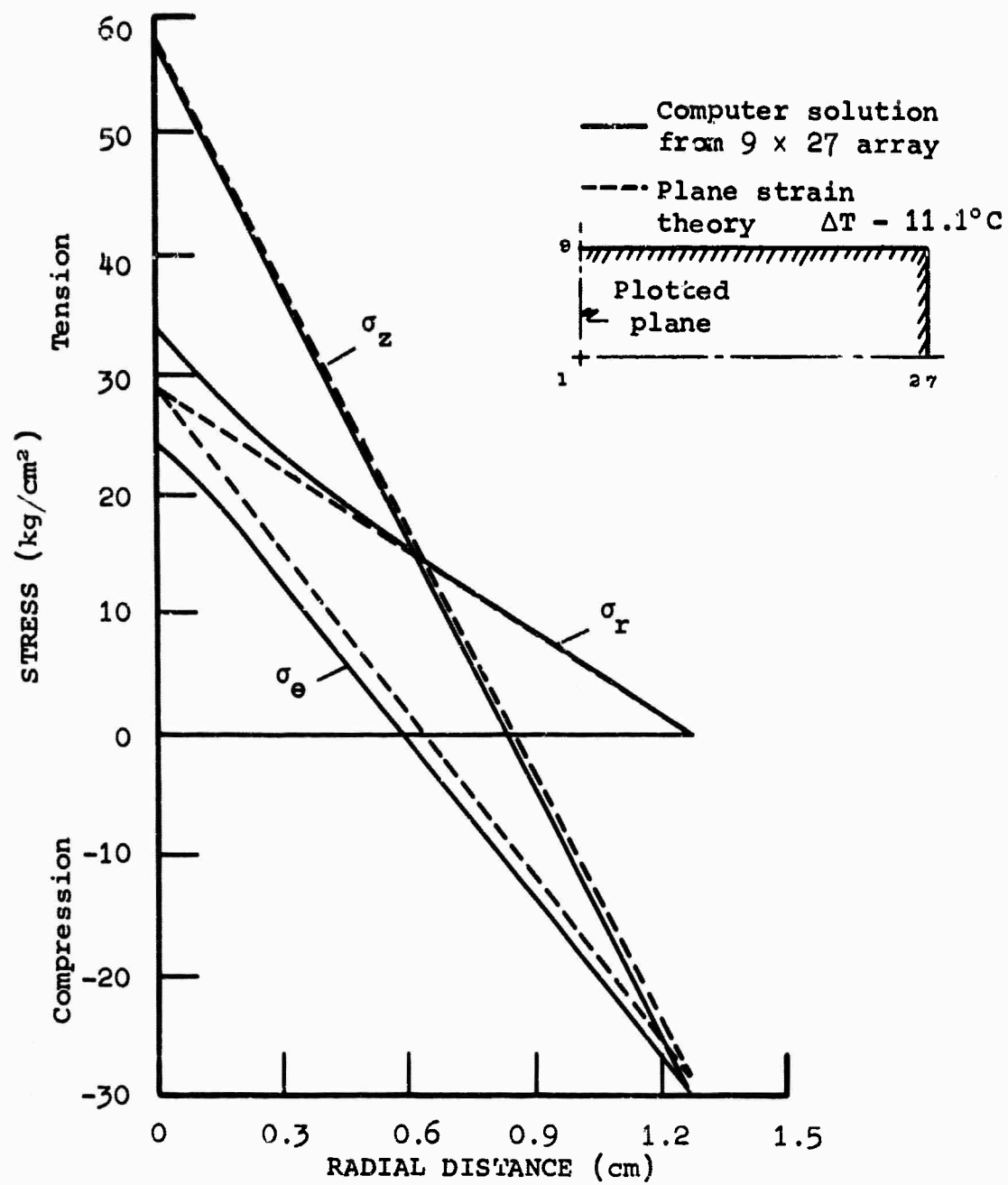


Figure 16. Comparison of computer solution and plane strain theory for a cross section about 1.6 diameters from end of rod.

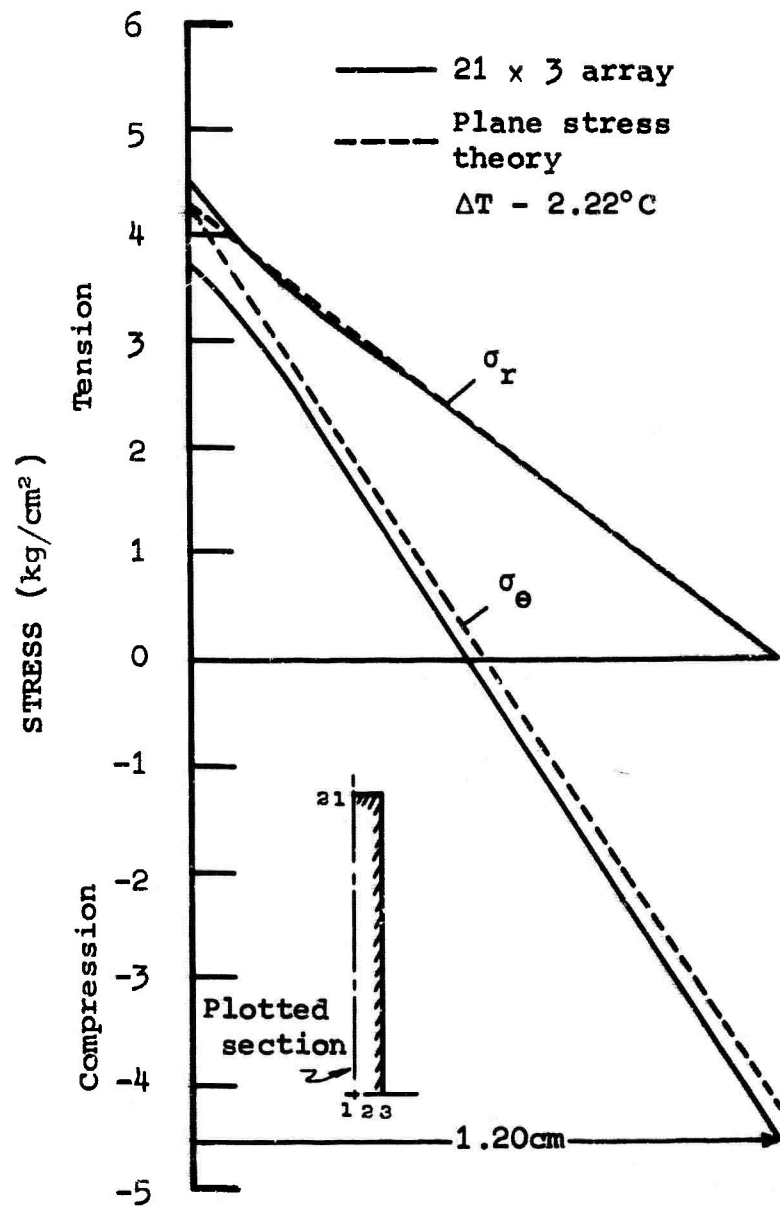


Figure 17. Comparison of computer solution and plane stress theory for midsection of disc.

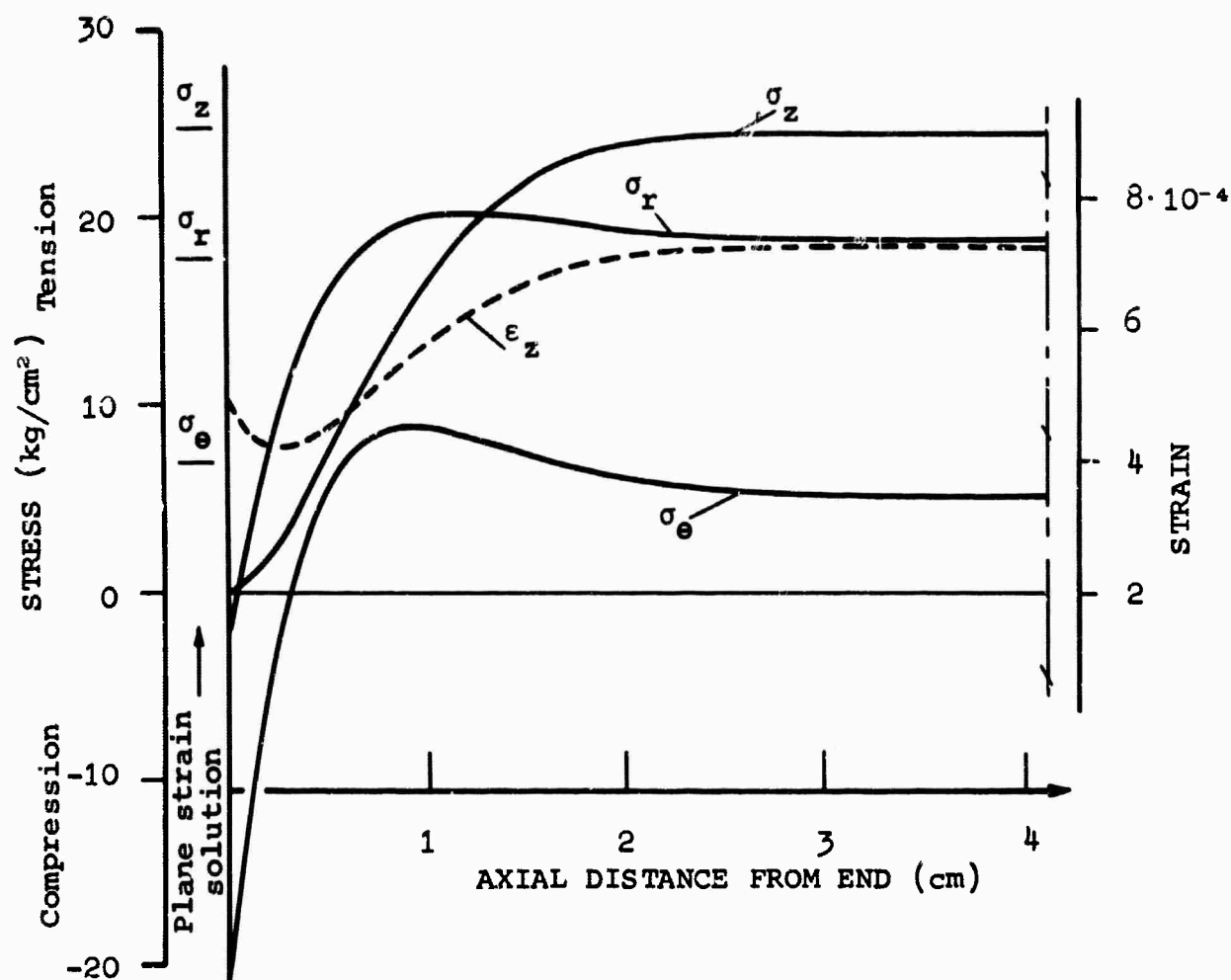


Figure 18. Stress-strain distribution at 0.477 cm. Radial distance from axis in a 2.54 cm diameter 0835 laser rod with 11.1°C temperature difference between center and edge.

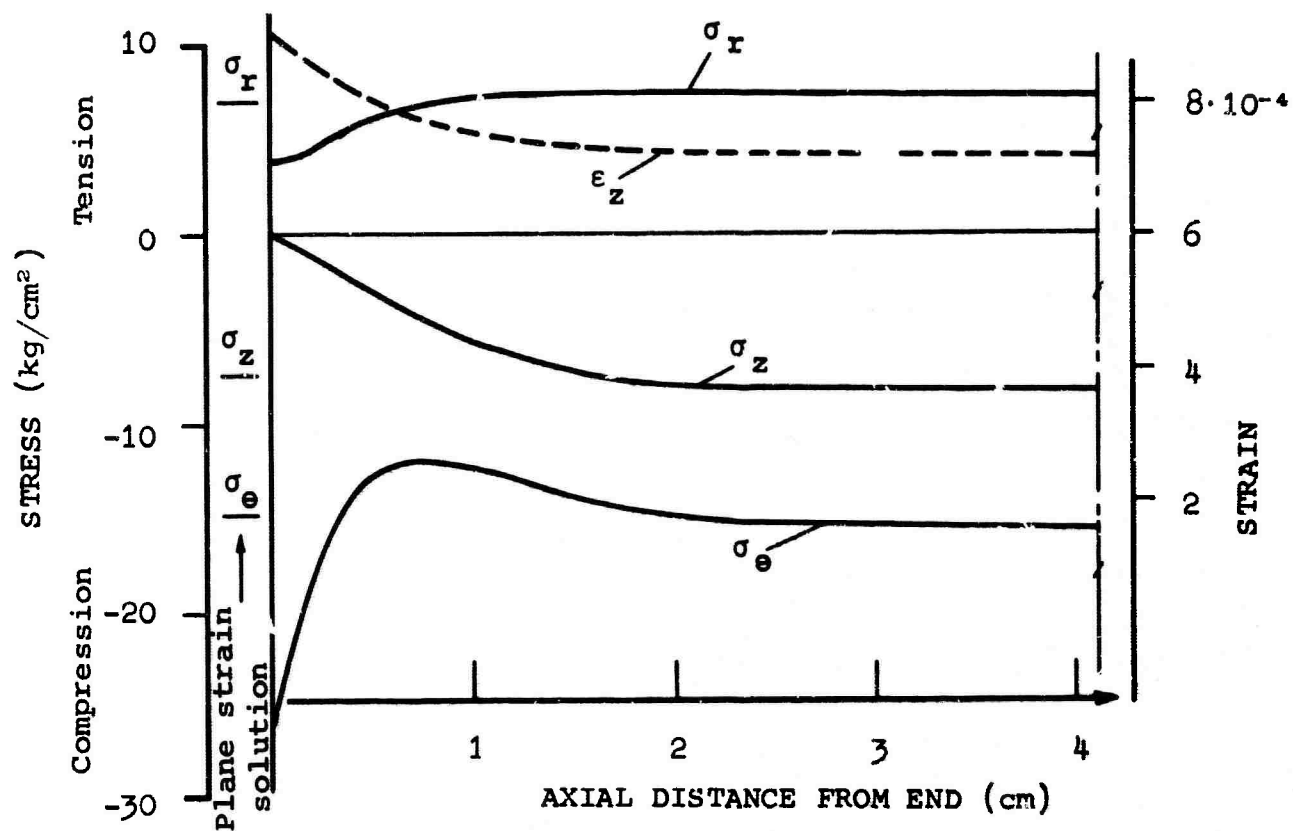


Figure 19. Stress-strain distribution at 0.954 cm. Radial distance from axis in a 2.54 cm diameter 0835 laser rod with 11.1°C temperature difference between center and edge.

radial and tangential results for the disc, which from theory would be approximately 4/5 of the plane strain results shown.

Using computed stress and strain results, the axial pathlength at various radial positions was calculated using Simpson's rule and integrating Eq. (196) above, for radially polarized light, over the end region. The equation accounts for three effects; namely, the stress optical change, the index change with temperature, and the elastic deformation or strain. The integrated result of the latter component, the axial strain, gives the physical displacement resulting in the end surface. Illustrating their relative contributions to the total path change in AO 3835 glass, these components are plotted separately in Fig. 20 along with their summated result. The path difference or distortion is expressed relative to the axial position. It is interesting to note that for a linear temperature gradient, a nearly linear relationship is preserved in all components. This suggests the possibility of compensating for differential path changes at the ends in such a specialized case by utilizing a glass having an appropriate thermal index coefficient value, α_n , for the rod length involved, where from above

$$\alpha_n = \frac{1}{n} \left[\left(\frac{\partial n}{\partial T} \right)_{\epsilon=0} - n_0 \alpha \left(\frac{2p}{v_0} + \frac{q}{v_0} \right) \right]$$

For comparison, the optical path change in the end region was computed also for this temperature distribution using plane strain theory and the results were higher by about 7% from the computer solution presented. In a 1 meter long rod, it turns out this error would amount to about 1%.

A similar optical path change can be determined for tangentially polarized light by evaluating the various components in accordance with Eq. (197) above. For AO 3835 laser glass, the optical coefficients $B_{||}$ and B_{\perp} , were measured to be 6.1 and 8.2 Brewsters, respectively. The optical path for the radial polarization is calculated to be about 13% greater than that for the tangential polarization at the point of maximum deviation which occurs at the surface of the rod. Since radial and tangential stresses become equal at the center of the rod, it follows that differences here due to polarization diminish to zero.

In this study, attempts were made to assess end effects for two other radial temperature patterns which could be considered more typical of conditions set up during lasing. The first

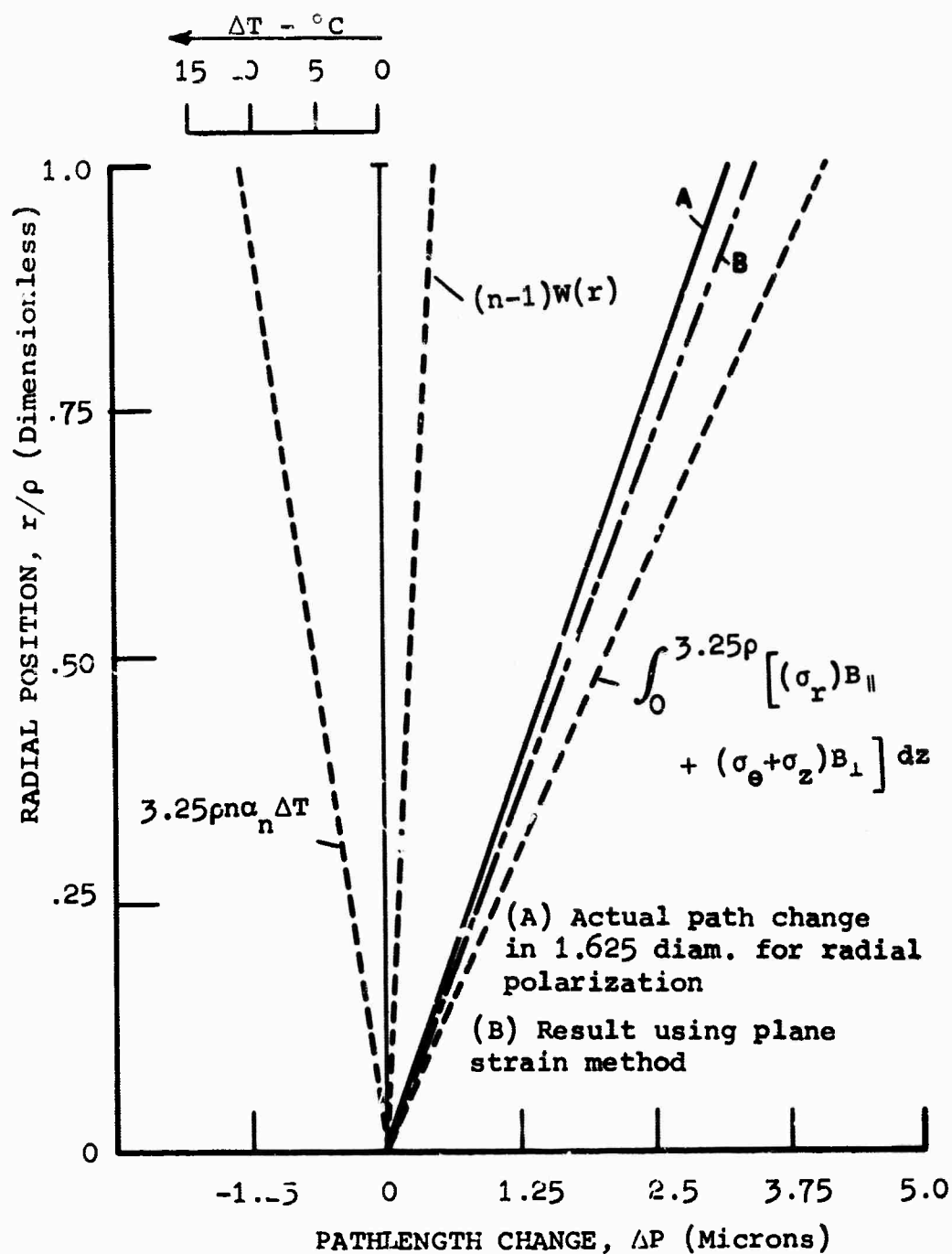


Figure 20. Optical path variation for the end region of a 2.54cm AO 3835 neodymium glass rod with a linear center to edge temperature gradient showing relative influence of the thermal index change, axial displacement and stress retardation effect.

temperature curve was derived from experimental gain distribution measurements, obtained under another program in using a 2.54 cm neodymium AO 3835 roughened surface rod pumped at 23.5 kj input. The profile of the second curve was established from the computer calculation performed on this contract for a polished 0.9 cm diameter rod of the same glass (Fig. 11, curve 2). Both temperature patterns represent significant non-linearity with radius.

In generating the first curve, temperature rise was considered to be proportional to the increase in gain coefficient, β , across the rod. This relationship proves basically valid since the inversion of ions in a four level laser material can be shown to be relatively linear with the absorption of incident photons per volume element. The specific equations become

$$\beta = \frac{\ln G}{L}$$

$$\Delta T \propto \beta$$

where G is the measured gain; L the length of the rod, and ΔT , the temperature rise of the corresponding position for which β is calculated. The proportionality between ΔT and β must be determined for the pumping geometry considered.

The fraction of electrical energy absorbed in the laser cavity as heat was actually investigated experimentally by making calorimetric measurements on 12.9 mm and 18 mm rods of AO 3835 glass. Each rod was fired at an input level of 9500 joules using two linear flashlamps close-coupled to the rod in a conventional reflector configuration without cooling. Immediately following the pulse, the rod was removed from the system and placed into a cylindrical Dewar flask where heat could be exchanged with a prescribed quantity of water contained within the flask. Heat production in the rod was then determined by making careful temperature measurements on the water initially and after equilibrium conditions were reached. A Leeds and Northrup precision potentiometer was employed to record temperature.

The results are described in Fig. 21. In one case, the flashlamps were jacketed with pyrex tubing which served to absorb selectively much of the incident UV and IR radiation; in the other case the flashtubes were non-jacketed, and this accounts for the greater heat production. One point is included also from earlier work in which the heat generated in a 2.54 cm rod was determined on a fully assembled system where cooling water was circulated

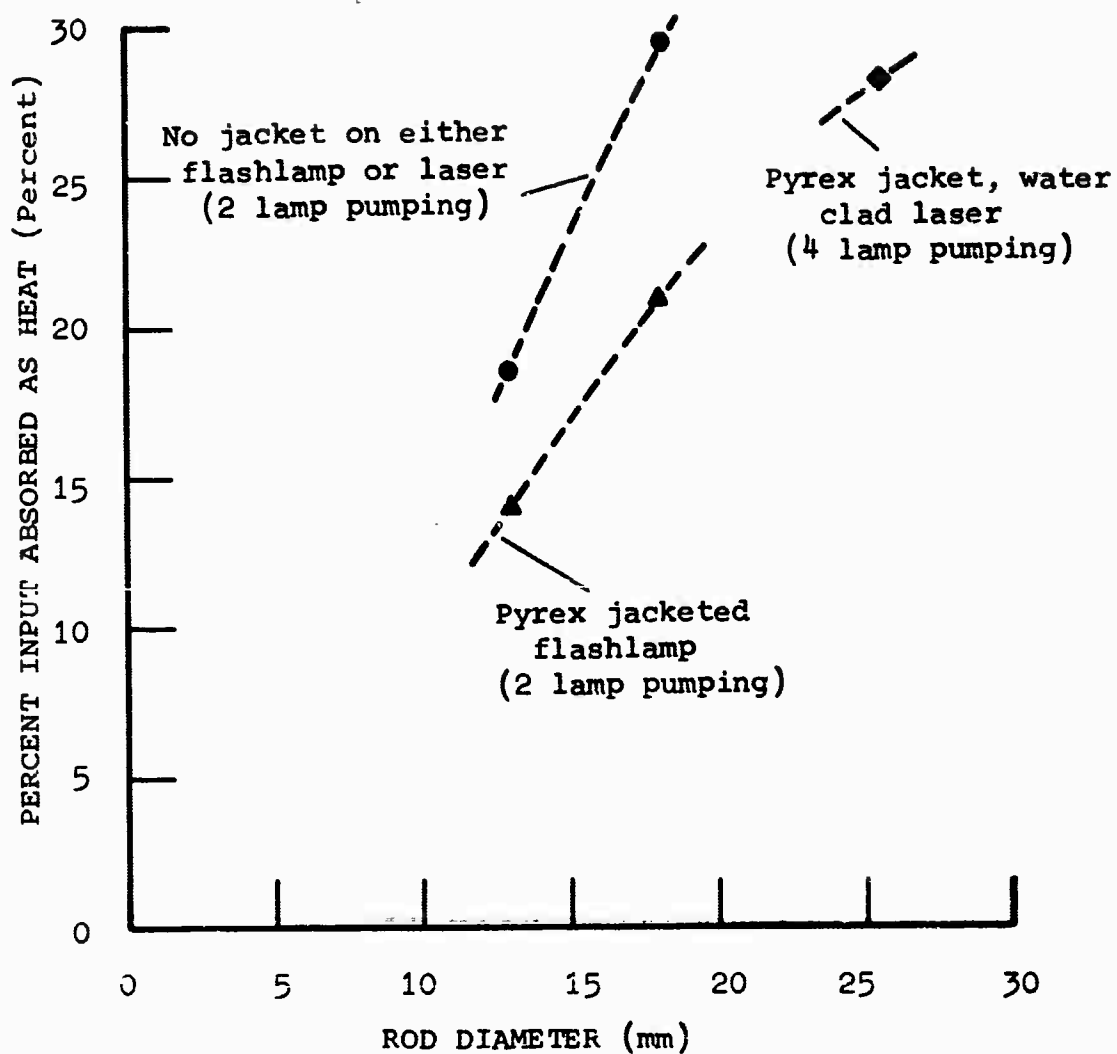


Figure 21. Experimental results for heat production in AO 3835 glass laser rods pumped in a cross-coupled silver reflector wrap.

over the rod within a pyrex jacket. In this investigation, differential water temperature measurements were recorded in time between the inlet and outlet positions to the cavity. The area represented by curve, then, was numerically integrated to establish the heat quantity released from the rod. Fairly good continuity of the data points was found. Therefore, it could be estimated with some certainty that between 25 and 30% of the energy appeared as heat in the 2.54 cm water clad rod under study. Using the 30% level and the gain information supplied on this rod, a temperature difference of about 2.8°C between center and edge is calculated.

Computed results for the optical path variation in the end region and surface contour change are plotted in Fig. 22 along with the temperature profile derived. The optical path, as illustrated, was averaged for the radial and tangential polarizations for purposes of comparing this curve with the athermalized case where temperature effects would be compensated for by proper regulation of α_n . As suggested in section 3, to obtain athermalization in birefringent glasses in a practical way, the light must pass first through the laser in one polarization and return through the other. α_n , then, must be averaged from the stress optical effects in the two orientations. The theory presumes, however, that the stress distribution will be axially uniform between the cavity bounds. In a rod of finite length, the stress distribution changes considerably from plane strain near the ends, which may warrant that conditions for athermalization be re-examined.

The significance of the ends is apparent from Fig. 22. Actual path changes over this region obtained by the computer method is represented by curve C and the results from another calculation invoking plane strain analysis throughout is shown by curve D. Since the expression for curve A, is a member of the composite expression for both curves C and D, changes can be implemented in the latter curves simply through control of the temperature coefficient of index values, α_n , in A. There is a proportionality evidenced here between curves D and A and this makes it possible to compensate for the temperature effect completely in a long rod by making α_n sufficiently negative as described earlier. Curve D would then coincide with the vertical axis of the graph. The difference between curves C and D, however, would remain essentially fixed; this being the finite optical path distortion remaining in an "athermalized" glass rod due to the ends. For the present temperature distribution, the path difference between center and edge is about 0.3 microns (for two ends) when athermalized. This results in very slight negative power for the

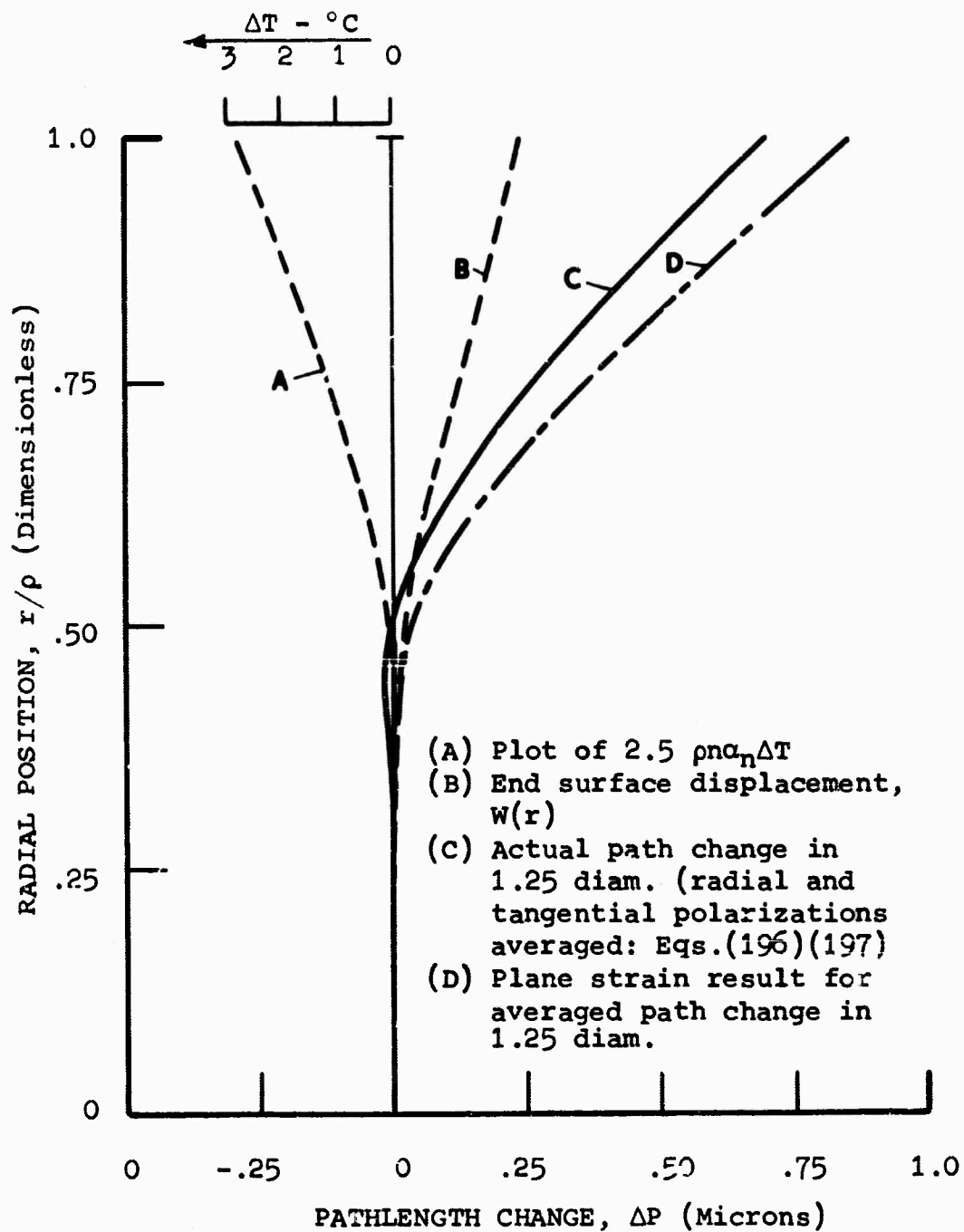


Figure 22. Relative temperature change, end face distortion, and optical path variation for the end region of a 2.54 cm diam. \times 1m 3835 glass laser rod pumped at 23.5 kj input.

overall rod under these athermalized conditions. The variation in surface contour is described by curve E.

To correct for end effects, the value of α_n should be chosen to be less negative, so that curve C rather than curve D lies along the axis. For the length shown (i.e., 1.25 diameters) the corrected value α'_n should have the approximate value $\alpha'_n = .72 \alpha_n$. Here α_n is the value which will bring curve D to the axis. The value of α'_n is that which will bring curve C to the axis at $rp = .75$.

However, for a longer length rod the end effect becomes relatively less important. At a length of 1 m, the corrected value α'_n , will be

$$\alpha'_n = \left[\frac{1.25 \cdot 2.54}{50} .72 + \frac{50 - 1.25 \cdot 2.54}{50} .1 \right] \alpha_n = .98 \alpha_n$$

A slightly more complex temperature distribution is treated by the second example. Figure 23 depicts the results of the computer solution for this case and shows somewhat more perturbation due to the ends. Plane strain results and actual optical path change were plotted here for the average of radial and tangential polarizations. It may be observed that as much as 1-1/4 microns path difference exists between the actual and the plane strain curves at about 60% of the radial distance to the edge. As with the previous case, this amounts to residual distortion that would be present having employed an athermalized glass. For this case, however, the end face displacement, represented by curve B, shows considerably greater irregularity.

In conclusion, it was demonstrated that for laser glasses which are not designed to compensate for thermal stress effects, the differences in optical pathlength near the ends could become virtually obscured when considering the cumulative pathlength variation generated within the long rod. The ends would account for a few percent change, at most, from the analytical result based on plane strain calculation for the full length. On the other hand, though, it was shown for athermalized glasses that end effects in the rod could be the principal source of distortion left. Since path changes in the end region are not, in general, related directly to the temperature distribution, compensation for these effects would require special modifications beyond regulation of the glass properties alone.

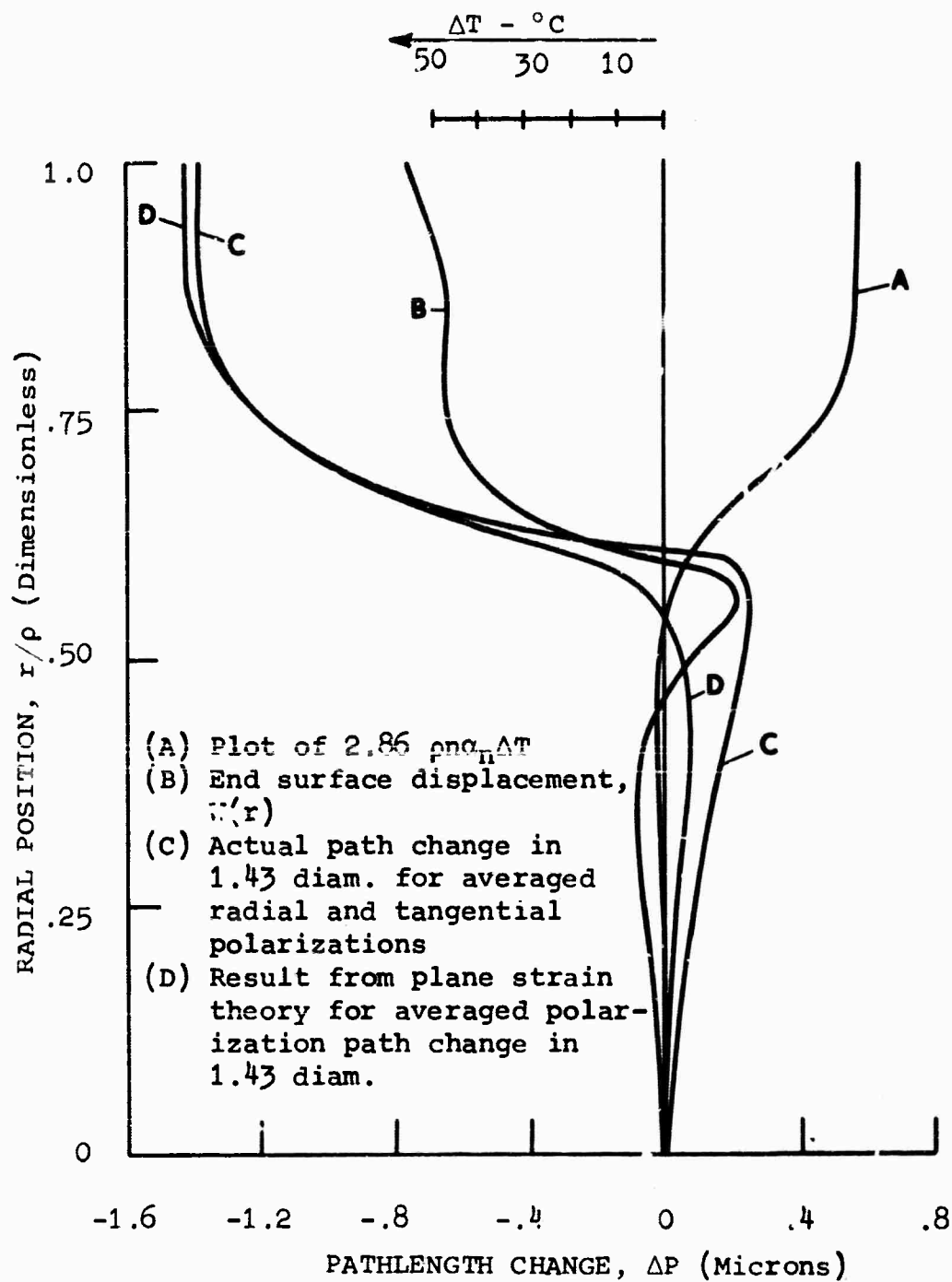


Figure 23. Relative temperature change, end face distortion, and optical path variation for the end region of an 0.9 cm diam. 3835 glass laser rod pumped at 153 j/cm^2 .

The most suitable scheme to use would depend to some degree on geometry employed and temperature pattern imposed. Theoretically, only the thin disc configuration has axially uniform stress. Effective athermalization of a series of these elements would then be achieved by utilizing a glass with the appropriate α_n value and correcting for the axial surface displacement in use by immersion in a suitable index matching fluid. For the rod configuration, where a significant temperature structure occurs, the addition of properly designed correction optics to the output system may substantially reduce the end problem.

REFERENCES


1. F. W. Quelle, Appl. Optics 5, 633 (1966).
2. E. Snitzer, Appl. Optics 5, 1487 (1966).
3. American Optical Company Technical Proposal AOQ 4-007 to Office of Naval Research, submitted April 1964.
4. American Optical Company Technical Proposal AOQ 4-014 to Office of Naval Research, submitted October 1964.
5. J. L. Walsh, unpublished manuscript.
6. F. W. Quelle, Memos 23 October, 29 October, and 8 December 1964, summarized in Ref. 1.
7. J. McKenna, Appl. Optics 2, 303 (1963).
8. W. R. Sooy and M. L. Stitch, J. Appl. Phys. 34, 1719 (1963).
9. J. R. Skinner, Appl. Optics 3, 963 (1964).
10. N. F. Borrelli and M. L. Charters, J. Appl. Phys. 36, 2172, (1965).
11. H. Welling and C. J. Bickart, J. Opt. Soc. Am. 56, 611 (1966); and H. Welling, C. J. Bickart, and H. G. Andresen, IEEE J. Quantum Electronics 1, 233 (1965).
12. J. G. Skinner and J. E. Geusic, J. Opt. Soc. Am. 52, 1319 (1962).
13. G. W. Morey, "The Properties of Glass," (Reinhold Publishing Corp., New York, 1938) p. 423.
14. B. A. Boley and J. H. Weiner, "Theory of Thermal Stresses," (John Wiley & Sons, New York, 1960) p. 244.
15. B. A. Boley and J. H. Weiner, Ibid. p. 291.
16. B. A. Boley and J. H. Weiner, Ibid, pp. 259, 290.
17. F. Pockels, Ann. Physik 9, 220 (1902); 11, 651 (1903).
18. P. W. Bridgman, Am. J. Sci. 10, 359 (1925); Proc. Am. Acad. Arts Sci. 63, 401 (1929).

19. G. W. Morey, Ibid, p. 428.
20. F. A. Molby, J. Opt. Soc. Am. 39, 600 (1949).
21. L. Prod'homme, Phys. Chem. Glasses 1, 119 (1960).
22. E. Snitzer, Appl. Optics 5, 121 (1966).
23. G. W. Morey, "The Properties of Glass," (Reinhold Publishing Corp., New York, 1954) 2nd ed., pp. 210-216.
24. C. F. Lucks, H. W. Deem, and W. D. Wood, Am. Ceram. Soc. Bull. 39, 313 (1960).
25. "The Science of Color" by the Committee on Colorimetry, Optical Society of America, (Thos. Y. Crowell Company, New York, 1953).
26. F. E. Nicodemus, Am. J. Phys. 31, 368 (1963).
27. J. H. Goncz and P. B. Newell, "The Spectra of Pulsed and Continuous Xenon Discharges," Tech. Memo No. B-471 (July 1965), Systems Division, EG&G, Bedford, Mass.
28. Landolt-Börnstein Tables and Functions; Vol. 2 (Properties of Bulk Materials) part 8 (Optical Constants), (Springer-Verlag, Berlin, 1962) p. 5-565.
29. International Critical Tables, (McGraw-Hill Book Co., Inc., New York, 1926) Vol. 7, p. 13.
30. W. R. Sooy and M. L. Stitch, J. Appl. Phys. 34, 1719 (1963).
31. N. F. Borrelli and M. L. Charters, J. Appl. Phys. 36, 2172 (1965).
32. H. Welling and C. J. Bickart, J. Opt. Soc. Am. 56, 611 (1966).
33. C. H. Cooke, J. McKenna, and J. G. Skinner, Appl. Optics 3, 957 (1964).
34. J. McKenna, Appl. Optics 2, 303 (1963).
35. J. A. Stratton, "Electromagnetic Theory," (McGraw-Hill Book Co., Inc., New York and London, 1941) p. 139.
36. L. Brillouin, "Wave Propagation and Group Velocity," (Academic Press, New York and London, 1960) p. 88.

37. Max Born, "Optik," (Springer, Berlin, 1933) p. 366.
38. G. W. More, "The Properties of Glass," (Reinhold Publishing Corp., New York, 1954), 2nd ed., p. 302.
39. O. D. Tauern, Ann. Physik 32, 1064 (1910).
40. F. Pockels, Ann. Physik 7, 767 (1902).
41. L. H. Adams and E. D. Williamson, J. Wash. Acad. Sci. 2, 609 (1919).
42. A.E.H. Love, "A Treatise on the Mathematical Theory of Elasticity," (Cambridge University Press, 1927).
43. G. Horvay, I. Giaever, and J. A. Mirabal, Ingenieur-Archiv 27, 179 (1959).
44. E. Sternberg, R. A. Eubanks, and M. A. Sadowsky, J. Appl. Phys. 22, 1121 (1951).
45. G. M. Valov, Translated in J. Appl. Math. Mech. 26, 975 (1963).
46. G. N. Polozhy and A. A. Kapshivy, "On the Solution of the Axisymmetrical Problems of the Theory of Elasticity for a Finite Cylinder," (in Russian) Prikladna Mekhanika (USSR) 7, 616 (1961).
47. C. J. Bellamy, Australian J. Appl. Sci. 11, 217 (1960).
48. R. D. Hoyle, Nature 167, 30 (1951).
49. F. W. Quelle, Appl. Optics 5, 633 (1966).
50. D. G. Christopherson, Brit. J. Appl. Phys. 3, 65 (1952).

DOCUMENT CONTROL DATA - R&D

(Security classification of title, body of abstract and indexing annotation must be entered when the overall report is classified)

1. ORIGINATING ACTIVITY (Corporate author) American Optical Company Research Division Southbridge, Massachusetts 01550		2a. REPORT SECURITY CLASSIFICATION Unclassified*	
		2b. GROUP	
3. REPORT TITLE Optical Inhomogeneities in Pumped Lasers			
4. DESCRIPTIVE NOTES (Type of report and inclusive dates) Final Report, 1 May 1965 - 31 October 1966			
5. AUTHOR(S) (Last name, first name, initial) Koester, C. J., Snitzer, E., Smith, L. W., Bergmann, S. M., Cuff, D.W.			
6. REPORT DATE May 1967		7a. TOTAL NO. OF PAGES 99 + vi	7b. NO. OF REFS 50
8a. CONTRACT OR GRANT NO. Nonr 4875(00)		9a. ORIGINATOR'S REPORT NUMBER(S) 	
b. PROJECT NO. 4730		9b. OTHER REPORT NO(S) (Any other numbers that may be assigned this report) N/A	
c. ARPA No. 306			
d.			

10. AVAILABILITY/LIMITATION NOTICES
Reproduction in whole or in part is permitted for any purpose of the United States Government. Available from DDC

11. SUPPLEMENTARY NOTES *A supplementary volume is published in conjunction with this report. The classification of that document is Secret.	12. SPONSORING MILITARY ACTIVITY Office of Naval Research Department of the Navy (Part of Washington, D.C. (Project DEFENDER)
--	---

13. ABSTRACT
This report delineates efforts expended during the one year period of contract Nonr 4875(00), entitled Optical Inhomogeneities in Pumped Lasers, which required an analysis in depth of thermal distortion of wavefronts in large laser rods and discs. Two approaches for elimination of this distortion were considered: (1) Establishment of a uniform temperature throughout the laser during pumping and (2) Development of athermal glass parameters. Elements of both approaches were found necessary to solve the problem. In separate sections of the report detailed treatments are given to Thermal Stable Cavities, Temperature Profile Calculations, the Effect of the Laser Field on Index of Refraction of the Laser Rod, and finally an Analysis of End Region Stress.

A classified supplement published separately as Volume II of this report completes the research findings under this project.

